Spectroscopic Characterization of Sol-gel Thin Films: Properties of Immobilization Matrix and Immobilized Proteins

by

Dominik Lukas Jürgen-Lohmann

A thesis
presented to the University of Waterloo
in fulfillment of the
thesis requirement for the degree of
Doctor of Philosophy
in
Chemical Engineering

Waterloo, Ontario, Canada, 2008

AUTHOR'S DECLARATION

I hereby declare that I am the sole author of this thesis. This is a true copy of the thesis, including any required final revisions, as accepted by my examiners.
I understand that my thesis may be made electronically available to the public.

Dominik Jürgen-Lohmann

Abstract

Although enzymes show great potential for use in industrial applications, their implementation from a practical perspective is still somewhat limited by various shortcomings in the area of enzyme immobilization. The use of silica sol-gels for protein entrapment has been studied extensively over the past 15 years or so. However, our understanding of the interactions between the immobilization matrix and the entrapped biomolecules is still relatively poor. Non-invasive *in situ* spectroscopic characterization is a promising approach to gain a better understanding of the fundamentals governing sol-gel immobilization. This thesis describes the application of Fourier transform infrared (FTIR) microscopy, two dimensional (2D) FTIR and fluorescence spectroscopy to characterize the immobilization matrix, entrapped model proteins and their interactions.

Hydroperoxide lyase (HPL [E.C. 4.1.2.]) was chosen as a potential model protein for sol-gel entrapment. HPL activity was evaluated by use of factorial experimental design investigating the effects of KCl and Triton X-100 on HPL activity with 13-hydroperoxy-octadecadienoic acid (LA-OOH) and the novel water soluble 13-hydroperoxy-octadienoyl sulfate (LS-OOH) as substrates. The highest HPL activity was achieved under aqueous conditions with high salt and low surfactant concentrations and LA-OOH as the substrate. A significant interaction between salt and surfactant as well as salt and substrate was identified and a hypothesis to explain the basis of the interaction phenomena is presented.

To analyze sol-gels with spectroscopic techniques, a sample format amenable to these techniques was needed. Therefore, a spin-coating technique for the preparation of aluminum or glass supported sol-gel thin films containing immobilized protein and a varying degree of the organically modified precursor propyltrimethoxysilane (PTMS) was developed. This approach produced samples that were suitable for chemical mapping using FTIR microscopy or fluorescence spectroscopic investigations.

A data analysis method was developed to extract information on chemical speciation and distribution from FTIR data matrices obtained through FTIR microscopy. Results indicate that sol-gel thin films are not homogeneous on the microscopic level. Instead, they are

heterogeneous with a clustering in the distribution of the model proteins studied (lysozyme [E.C. 3.2.1.17], lipase [E.C. 3.1.1.3] and bovine serum albumin (BSA)) at the scale investigated. The appearance of these clusters was found to depend on the type of protein entrapped, as well in some cases on the composition of the sol-gel. Moreover, the PTMS distribution was positively correlated with the protein distribution in the case of lipase and negatively correlated in the case of lysozyme and BSA. Additionally, sol-gels with a higher PTMS content appeared to conserve protein structure in areas where lipase clustered. Lysozyme and BSA, on the other hand, seemed to retain their structures in high concentration clusters better at lower PTMS content. A hypothesis taking into account the surface hydrophobicity of the proteins and the sol-gel composition as the basis for these phenomena is proposed.

Fluorescence spectroscopy revealed that the PTMS content of the sol-gels had a direct effect on the physical properties of the immobilized proteins as evidenced by a blue shift of the intrinsic tryptophan (TRP) fluorescence. Temperature-dependent fluorescence spectroscopy revealed that the amount of TRP quenching was inversely proportional to the PTMS content of the sol-gel, suggesting that there were varying amounts of water available for quenching for the different immobilized enzyme systems. Analysis of the sol-gels by 2D FTIR spectroscopy with a focus on the amide A region using Gaussian peak deconvolution revealed two different species of water for the 50 % PTMS thin film sol-gels with BSA that could be described as fully and not fully H-bonded. It was also found that these species of water showed different removal profiles during thermal treatment. 2D FTIR of the amide I region followed by absorbance difference spectrum evaluation revealed that the temperature stability of the three model proteins was also sol-gel composition dependent. A hypothesis that the surface characteristics of the proteins determine the nature of the composition dependence is presented.

Acknowledgements

First and foremost, I would like to express my most sincere thanks to my supervisor Dr. Raymond Legge. Ray has been a wonderful advisor and is simply a wonderful person to know and to work with.

I am grateful to my thesis committee members Dr. Amarjeet Bassi (University of Western Ontario), Dr. Christine Moresoli, Dr. Leonardo Simon and Dr. Elizabeth Meiering for their evaluation. I express my special thanks to Dr. Meiering for joining my committee on such a short notice.

NSERC funding of this project is gratefully acknowledged.

I would like to thank Dr. Kenji Matsui (Yamaguchi University) for kindly providing the *E. coli* transformants and Dr. Jérôme Delcarte (Walloon Agricultural Research Centre) for his help with the HPL expression system.

Thank you Christoph Nacke, for being an invaluable help with getting the FTIR work on track. Your contribution to the early stages of spin coating and FTIR analysis are gratefully acknowledged. I am also indebted to Dr. Leonardo Simon and Dr. James Forrest for sharing their equipment, to James Chang for his help with the spin coater and to John Potzold for a lot of help in the machine shop. I would also like to thank the staff of the Chemical Engineering department, especially Liz and Pat for being so helpful.

To all my labmates who made my time at Waterloo so enjoyable: Thank you so much for all the good times. There's too many of you so I'll thank you in person and keep this short: Joe, Maja, Jana and Kela, thanks for the company and friendship and congratulations on/best luck for your graduation!

Mein besonderer Dank gilt meinen Eltern, Barbara und Peter, und meinen Brüdern, Valentin und Severin. Vielen Dank für Eure Unterstützung.

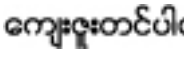
Chaw Su for all your love and support.

Für meine Eltern

Table of Contents

List of Figures

List of Tables

List of Acronyms

2D	Two dimensional
3D	Three dimensional
A	Enzymatic activity
ANOVA	Analysis of variance
AU	Arbitrary unit
BCA	Bicinchonic acid
BSA	Bovine serum albumin
CD	Circular dichroism
CMC	Critical micelle concentration
EPR	Electron paramagnetic resonance
FTIR	Fourier transform infrared
GFP	Green fluorescent protein
HPL	Hydroperoxide lyase
HSA	Human serum albumin
IBTMS	Isobutyl tetramethoxysilane
IPTG	Isopropyl β-D-1-thiogalactopyranoside
IR	Infrared
K_M	Michaelis constant
LA-OOH	13-hydroperoxy-octadecadienoic acid
LOX	Lipoxygenase
LS-OOH	13-hydroperoxy-octadienoyl sulfate
NAE	N-acyl(ethanol)amine
Ni-NTA	Nickel-nitrilotriacetic acid
NIR	Near infrared
OD	Optical density
P	Probability value
PA	Polyacetate
PAGE	Polyacrylamide gel electrophoresis

PE	Polyethylene
PET	Polyethylene terephthalate
PMSF	Phenylmethanesulphonylfluoride
PP	Polypropylene
PTFE	Polytetrafluoroethylene
PTMS	Propyltrimethoxysilane
R	Signal ratio
rel.	Relative
R_f	Retention factor
R_{MEDIAN}	Median signal ratio
SDS	Sodium dodecyl sulfate
TB	Terrific broth
TEOS	Tetraethoxysilane
TLC	Thin layer chromatography
TMOS	Tetramethoxysilane
TRIS	2-Amino-2-(hydroxymethyl)propane-1,3-diol
TRP	Tryptophan
UV	Ultraviolet
vis	Visible
v_{max}	Maximum rate/velocity
$\phi(\nu_i, \nu_{i+1})$	Synchronous 2D spectrum
$\Psi(\nu_i, \nu_{i+1})$	Asynchronous 2D spectrum
ν_i	$Wavenumber_i$
t	External perturbation variable
$y(\nu_i,t)$	Dynamic spectrum
$Y^*_1(\omega)$	Conjugate Fourier transform
$Y_1(\omega)$	Forward Fourier transform

Chapter 1
Introduction and Literature Review

Enzymes are essential for most chemical reactions occurring in biological systems. Because of their diversity and specificity they are of special interest to biochemists and biochemical engineers who seek to use them as catalysts for the production of valuable products or the destruction of harmful substances.

The production and purification of enzymes is a costly process. An efficient and economical way of using enzymes can be accomplished by creating an artificially heterogeneous catalyst through immobilization. Immobilized enzymes offer a number of advantages, including increased stability, ease of separation from the reaction medium and reuse of the biocatalyst [1,2]. Immobilization, however, is often a trial and error process that suffers from many drawbacks. The motivation behind this work is to use novel immobilization supports as well as novel analysis techniques, to contribute to the better understanding of immobilized enzyme systems that will ultimately aid in the creation of better biocatalysts. The concept of designing an immobilization support specifically to a given enzyme was well summarized in 1994 in a statement from D. Clark, which still holds true today:

"Shortly after the inception of immobilized enzymes, there was great enthusiasm about developing the knowledge-base to design and prepare immobilized enzyme catalysts with 'tailor-made' properties. Such efforts have been largely abandoned, as conventional enzyme engineering has been increasingly overshadowed by more-recent advances in biocatalysis; for example, the advent and/or discovery of protein engineering, catalytic antibodies, ribozymes and new enzymes from unusual organisms. However, our understanding of protein structure and function is expanding at an unprecedented rate, as is the development of new materials with predefined properties. Therefore, perhaps it is time to re-examine the potential of enzyme immobilization as a means to modify enzyme properties in a rational manner and thereby improve the utility of enzymes for specific applications."[3]

In this work, sol-gels were used as an immobilization support, as their physical properties can be easily modulated. It was expected that the physical properties of the sol-gels influence the

immobilized species directly, in a manner that is governed by the nature of the immobilized enzyme and the support. Spectroscopic techniques such as fluorescence and Fourier transform infrared (FTIR) spectroscopy were used to characterize samples *in situ*. Thin film technology was developed to open up the possibility to use certain spectroscopic techniques that were not applicable for bulk materials.

The fundamental understanding of immobilized enzyme systems and the possibility to design them in a rational manner is of great importance, industrially, ecologically and societal. Better biocatalysts may result in new industrial processes, greener production and a cleaner environment.

1.1 Hypotheses and Research Objectives

The general underlying hypothesis of this work can be summarized as follows:

It is expected that proteins and enzymes, immobilized in sol-gel thin films of varying composition, will be influenced by the properties of the immobilization matrix.

The main objective of this work was to use new materials and analysis methods to gain a better understanding of the interactions between immobilization support and immobilized species for improved engineering of immobilized enzyme systems. More specifically, the research objectives of this work included:

- Investigate the enzyme hydroperoxide lyase to gain a better understanding of the enzyme and the factors governing the activity of this enzyme with the view of developing a coupled immobilized enzyme system for the production of novel lipid derivatives.
- Develop a suitable format and methodology for non-invasive *in situ* spectroscopic characterization of sol-gel immobilized enzymes/biomolecules.
- Develop FTIR spectroscopic methods to determine the chemical homo-/heterogeneity of sol-gel thin film systems in terms of matrix and immobilized model species and the interrelationship between sol-gel composition and the nature of the immobilized protein.
- Determine the effect of sol-gel composition and destabilizing influences, such as temperature, on proteins immobilized in sol-gels using non-invasive approaches.

1.2 Enzymes as Biocatalysts – Enzyme Immobilization

Bioengineering can be defined as the "biological or medical application of engineering principles or engineering equipment" [4]. This rather broad definition comprises, amongst other areas, the use of whole cells or cell components, such as enzymes, for the synthesis of desired bulk or fine chemicals or the destruction of harmful toxins. The introduction of biological systems into classical chemical engineering domains has benefits in terms of reducing energy demand and the production of waste. Hence, the term "Green Chemistry" is often used synonymously for bioengineering. In addition to being an environmentally friendly approach, bioengineering opens up the possibility of synthesizing compounds, e.g. certain pharmaceuticals that could not be produced via classical chemical synthetic routes.

Enzymes are catalytically active proteins. Their application has particular advantages over the use of whole cell systems in certain scenarios. For instance, separation of the biocatalyst from its natural environment, e.g. the cytoplasm of a bacterial cell, removes the need for cell growth and maintenance and often facilitates product purification. Moreover, enzymes can be used in novel reaction media, such as organic solvents, to yield novel reactions and possibly eliminate problems associated with substrate solubility and other application issues. Usually, enzymes are preferred over whole cell systems in single reaction steps or short reaction cascades, whereas more complicated syntheses are largely carried out using the latter [1].

The production and purification of enzymes is a complex process. Despite the advances in recombinant protein expression, which allows relatively easy production of larger quantities of protein, enzymes are still a costly resource, making reusable biocatalysts and continuous processes desirable. In their native form most enzymes are colloidally dissolved and act as a homogeneous catalyst, thereby aggravating the use of simple separation techniques, such as filtration or centrifugation. The concept of enzyme immobilization aims at overcoming this drawback by artificially creating a heterogeneous catalyst which can be separated from the reaction medium and reused more easily. By definition, immobilized enzymes are "restricted in their mobility by physical or chemical means" [2]. Reusability, however, is not the only benefit of

enzyme immobilization. Immobilized biocatalysts often show improved stability towards elevated temperatures and harsh reaction conditions [2].

Intentional enzyme immobilization was carried out by Nelson and Griffin as early as 1916 through adsorption of invertase on charcoal [5]. Since this first report a large number of protocols and strategies for immobilization have been pursued and established. In an attempt to categorize different preparations, an international body at the First Enzyme Engineering Conference, Henniker, NH, USA (1971), introduced the following classification, depicted in Fig. 1.

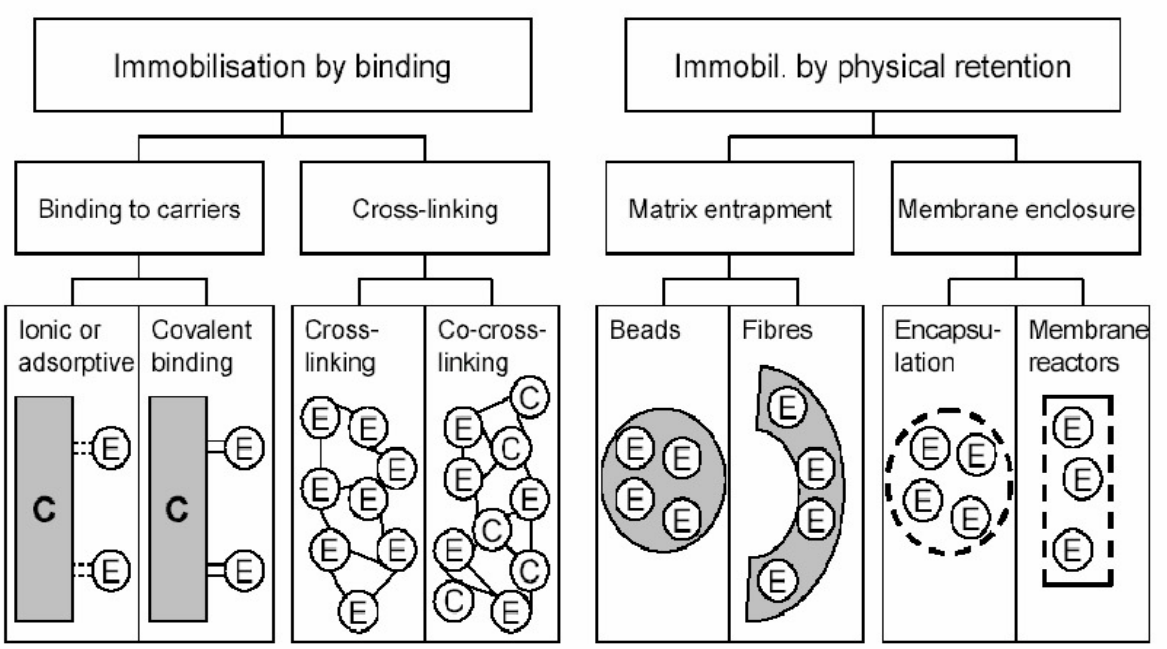

Fig. 1: Classification of Immobilized Enzymes

The schematic shows the classification of immobilized enzymes in groups and subgroups as suggested by the First Enzyme Engineering Conference, Henniker, NH, USA (1971). Adapted from [2].

As can be seen in Fig. 1, there are two basic approaches for immobilization: immobilization by binding and immobilization by physical retention. Binding techniques generally feature relatively easy protocols and the large variety of available carriers include natural and synthetic as well as organic and inorganic materials. In cross-linking techniques, the enzyme itself can serve as a carrier material. The nature of the bond can be either adsorptive or covalent with their

respective advantages. Generally (with exceptions), an adsorptive interaction leads to a higher retained activity with lower stability, whereas a covalent interaction yields a more stable biocatalyst with lower activity [2].

Immobilization by physical retention can be subdivided into matrix entrapment and membrane enclosure techniques. The major advantage of using physical retention lies in the absence of a relatively strong interaction between matrix and enzyme. In an ideal scenario, the enzyme is kept entirely in its native state, e.g. within a polymer such as alginate (matrix entrapment) or an ultrafiltration membrane reactor (membrane enclosure). Matrix effects on the enzyme, however, can occur and might even be beneficial as discussed later. A major disadvantage of immobilization by physical retention is the presence of mass transfer limitations in the form of internal diffusion resistance, which can be more or less significant depending on the given system. Similar to immobilization by binding techniques, method development aims at a compromise between activity and stability of the immobilized enzyme preparation.

A comprehensive review of the methodologies and materials available for enzyme immobilization is beyond the scope of this document. The interested reader is referred to the many excellent review articles and textbooks on the subject [1,2,6-8]. The following section will give an introduction on the use of sol-gel technology for enzyme immobilization.

1.3 Silica Sol-gels – Materials for Enzyme Immobilization

As the name implies, the sol-gel process describes the formation of a gel from a sol. A sol is a stable dispersion of colloidal particles in a liquid, while a gel is a biphasic network where a solid surrounds a liquid. The sol-gel process has been known for over a century as a method to produce inorganic glasses [9]. It wasn't until the early 1990s that it was developed as an immobilization method for biological species [10,11].

Sols can be formed by precursors (e.g. tetraalkoxysilanes or functional di- and tri-alkoxysilanes) that readily undergo hydrolysis. The hydrolysis equilibrium reaction, which is usually acid or base catalyzed, proceeds as follows. Tetraalkoxysilanes are taken as an example:

$$Si(OR)_4 + H_2O \leftrightarrow HO - Si(OR)_3 + ROH$$

where R depicts an alkyl residue, usually a methyl or ethyl group. The degree of hydrolysis depends on the water to silane ratio, catalyst type and concentration and the type of silane, but does not proceed to completion even with high water to silane ratios. This ratio was also found to have an influence on the pore characteristics of the resulting sol-gel material [12]. The resulting structures are partially hydrolyzed silanes:

$$Si(OR)_{4-n}(OH)_n \qquad n \geq 1$$

These partially hydrolyzed silanes undergo polycondensation in the second step of the process to yield soluble hydroxylated oligomers of the following general structure:

$$(Si-(O-Si-R_3)_x(OH)_y(OR)_z)_n \qquad x+y+z=4$$

During polycondensation, the reaction mixture can be doped with a suitable buffered solution containing the biomolecule of interest. As the network becomes more complex, the biomolecule is embedded in the interstitial space of the resulting matrix. It is generally believed that the embedded species acts as a template around which polymerization occurs [12]. Particles are formed and aggregate, raising the solution viscosity to a point where the sol-gel transition takes place and bulk gelation occurs. At this time, the solution can be used to form the desired shape, which can be for example, a monolith or a thin film.

Aging of the gel is accompanied by further cross-linking and expelling of water and the corresponding alcohol. During this period, a pore network is formed and shrinkage occurs. The result of this process is a so called hydrogel that typically has an aging related shrinkage of 5-20 % (v/v), pore volumes of 0.6-3.1 mL g^{-1}, pore sizes of 3-100 nm and surface areas of 600-1700 m^2 g^{-1} [12].

As an optional step, drying of the hydrogel leads to dehydration and a xerogel is formed. Silica xerogels typically have pore volumes of 0.4-2.7 mL g^{-1}, pore sizes of 0.5-20 nm, surface areas of 400-1300 m^2 g^{-1} and bulk shrinkages of 15-85 % (v/v) [12]. A schematic summary of the sol-gel process is given in Fig. 2.

The precursors used in this work are tetraethoxysilane (TEOS), tetramethoxysilane (TMOS) and propyltrimethoxysilane (PTMS). The use of sol-gel biocomposite materials has a number of advantages over traditional immobilized enzyme preparations. These advantages include:

- Simplicity of preparation
- Ability to manipulate chemical composition and physical properties
- Mild processing conditions
- Thermal and mechanical stability
- Potential optical transparency
- Ability to form different shapes and coat surfaces

Information on the spectroscopic properties and analysis of sol-gels will be given in the next sections. The significant literature on bioimmobilization in sol-gels spans whole cells to antibodies and enzymes to ribozymes and is well summarized in several current review articles [10,12-17].

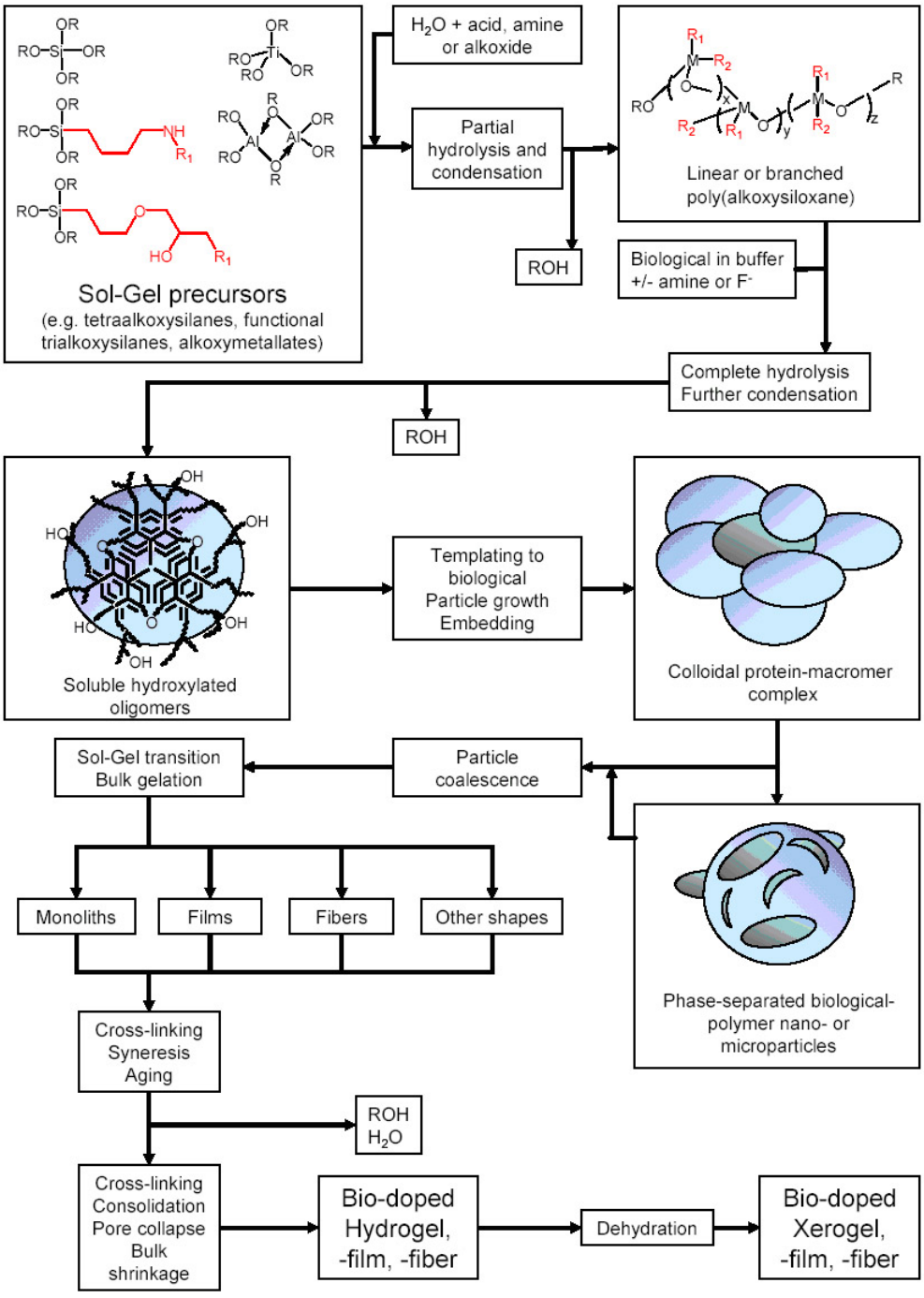

Fig. 2: Summary of the Sol-gel Process

The schematic shows the evolution of a sol-gel from precursors. The main steps are hydrolysis, condensation, sol-gel transition, aging and drying (R=alkyl group, R_1=special functionality (aminoacyl, ferrrocenyl, gluconyl, etc.))[12].

1.4 Sol-gel Thin Films

Sol-gel thin film coatings are well established in material science. The improved characteristics of coated surfaces cover a broad spectrum and, for instance, include altered color, reflection, conduction, or scratch resistance properties of the coated material. Industrial protocols almost exclusively feature a high temperature sintering step following the deposition of the sol-gel film on the solid support, which is often referred to as the substrate. This curing measure leads to homogeneous structures of high stability, but is inapplicable for bioimmobilization due to the temperature sensitivity of biological molecules. Therefore, the creation of a stable adherent film under mild processing conditions is a major challenge of sol-gel thin film enzyme immobilization and of this work [18,19].

Thin films can be applied to a support by several coating techniques, such as dip coating, spin coating, spray coating or solvent evaporation coating. In this project, dip coating was chosen first for reasons of availability of the apparatus, but was dismissed later in favor of spin coating.

Thin film technology has certain advantages over entrapment in bulk materials, which typically produce particle sizes > 20 μm. As mentioned earlier, matrix entrapment techniques often exhibit mass transfer problems due to internal diffusion resistance. Sol-gel thin films are fabricated at sub-micron thickness, thereby reducing the average diffusion path length, facilitating mass transfer through the inorganic entrapment matrix and increasing the overall efficiency of the immobilized biocatalyst. Moreover, sol-gel coated static mixers could be used in reactor setups, resulting in presumably improved mixing properties compared to packed bed or slurry reactors. Additionally, sol-gel thin films represent an ideal material for spectroscopic techniques involving light due to their potential optical transparency. UV/vis spectroscopy has been applied to enzymes entrapped in thin films and thin monoliths in some examples [20-22], but the information that can be obtained with this technique is somewhat limited. Fluorescence and FTIR spectroscopic techniques are introduced in the following sections as these were developed in this project to characterize the immobilized enzyme systems.

1.5 Spectroscopic Characterization of Sol-gels

A major advantage of thin film technology, besides the potential reduction of mass transfer resistance in biocatalysis, is the potential optical transparency of the material. This allows for the use of non-invasive optical techniques, such as fluorescence or FTIR spectroscopy for the study of these materials. Optical transparency has some limitations in terms of incorporation of organically modified precursors such as PTMS. Sols with a content of organically modified precursors of 50 % or more usually lead to opaque materials, which are not suitable for UV/vis, but might still have sufficient transparency for fluorescence or FTIR spectroscopy. Regardless, the use of submicron films, as in this project, presents a significant step forward in terms of suitability of the sol-gel material for spectroscopic characterization compared to bulk materials or monoliths.

1.5.1 Fluorescence Spectroscopy

Fluorescence spectroscopy has proven to be a valuable technique to characterize protein properties [23]. A major advantage of this technique compared to UV/vis spectroscopy is the vastly increased sensitivity. Fluorescence measurements, therefore, are especially suitable for sol-gel thin films that might present low protein quantities.

Fluorescence spectroscopy has been widely used to characterize sol-gel materials. It allows the examination of a number of sol-gel properties and can also be used as a signal in biosensor applications. Fluorescence spectroscopy can give insight into structure, function, rotational mobility, accessibility and stability of the entrapped species [13]. A large body of literature is available on the application of this technique to sol-gel materials. A good overview of the subject can be obtained from several review articles by Brennan, Gill and Gupta [16,17,24]. In the following, selected examples of fluorescence spectroscopy in the characterization of sol-gel entrapped fluorescent dyes, labeled proteins and intrinsically fluorescent proteins are presented.

The use of small reporter molecules, such as fluorescent dyes, is an elegant solution to characterize sol-gel materials through relatively stable and small molecules. Rhodamine 6G served as a reporter dye entrapped in TEOS derived sol-gel monoliths [25]. The dye was found to be dispersed on a molecular level as indicated by fluorescence results. Flora *et al.* entrapped 7-

azaindole and pyranine in a similar material [26]. The dyes were present in different environments during sol-gel aging and the final material showed a distribution of microenvironments, in which the dyes were embedded. Similarly, the heterogeneity of TEOS sol-gel monoliths in terms of alcohol/water presence in microenvironments was shown by Gupta *et al.* through fluorescence studies on entrapped Hoechst 33258 [27,28]. Nile red was used as a reporter dye in studies by Bardo *et al.* [29] and Fu *et al.* [30]. Bardo reports on the influence of matrix composition on the distribution of Nile red through the sol-gel material. It was concluded that its distribution in organically modified thin films is more homogeneous at higher contents of modified precursors. Moreover, Fu reported on the mobility of dye molecules in a surfactant templated sol-gel thin film.

The global rotational mobility of labeled proteins in TMOS sol-gels was studied by Jordan as early as 1995 [31]. Acrylodan labeled BSA and HSA retained their global rotational mobility in the sol-gel matrix. Similar results were obtained in 2002 by Chirico *et al.* who used GFP, which carries a strong intrinsic fluorescence, making labeling unnecessary [32]. However, recent studies on lysozyme in TEOS derived monoliths showed a significant reduction in enzyme rotational mobility upon entrapment [33]. Pastor *et al.* attribute the decrease in lysozyme mobility to an electrostatic interaction between charged domains of the enzyme and the sol-gel. These results indicate that the mobility of a sol-gel entrapped species is dependent on the matrix composition as well as on the properties of the entrapped species itself.

In addition to distribution and mobility of the entrapped species, fluorescence spectroscopy can also determine stabilizing effects of the sol-gel matrix on e.g. entrapped proteins and enzymes. While it was reported that glucose oxidase partially unfolds and denatures upon entrapment in TEOS monoliths [34], sol-gel immobilized myoglobin was shown to be protected from unfolding through the sol-gel matrix [35].

As described by Cruz-Aguado *et al.*, the fluorometric detection of luciferase activity revealed that a sol-gel entrapped enzyme can retain a high degree of activity, when sugar modified precursors are used [36]. These precursors do not release alcohol during hydrolysis and their use might therefore be a promising route to immobilize sensitive biomolecules [15].

The examples presented illustrate the versatility of fluorescence spectroscopy in the analysis of sol-gel entrapped species. A large number of contributions to the understanding of the phenomena governing sol-gel immobilization can be expected from the use fluorescence spectroscopy in the future.

1.5.2 FTIR Spectroscopy

FTIR spectroscopy has potential in the investigation of enzyme immobilization in sol-gels because it can provide information with respect to the immobilized enzyme as well as the immobilization support itself. In fluorescence spectroscopy, high energy radiation (e.g. UV light) results in a change of the electron distribution of the excited molecule. FTIR spectroscopy, on the other hand, uses lower energy IR radiation [37]. This results in a change of configuration of the bonds in an IR active molecule, if the absorption frequency is met. From the characteristic IR absorption frequencies, information of the chemical groups in a molecule can be obtained [37]. In the case of sol-gels and immobilized proteins/enzymes the main chemical groups of interest are silicate/silanol related, amide related, alkyl related or water related. The signals generated by these groups can be identified and quantified in the FTIR spectrum. The use of FTIR spectroscopy in protein science is especially interesting. The peak shape of the so called amide I signal, generated by the C=O stretching vibration of the amide bond, is sensitive to the secondary structure of the protein. FTIR spectroscopy can, therefore, be used to a limited extent to investigate protein structure [38].

Three different FTIR techniques were used in this study: FTIR spectroscopy, FTIR microscopy and 2D FTIR spectroscopy. The three techniques are introduced in the following and their application to sol-gels and immobilized enzyme systems in general is reviewed with selected examples from the literature.

FTIR spectroscopy was used to examine the chemical nature of polymerized sol-gels. In a number of studies, several precursor molecules were identified as being successfully incorporated into the final sol-gel network, such as TEOS/TMOS, PTMS, ethyltrimethoxysilane, methyltriethoxysilane, 3-mercaptopropyltrimethoxysilane, 3-aminopropyltriethoxysilane, 3-glycidoxypropyltrimethoxysilane and 3-

isocyanatopropyltriethoxysilane [39-41]. These results confirm the value of FTIR in chemical composition analyses, as the incorporation of modified precursors into the sol-gel material can be verified. In addition to information about the immobilization matrix, FTIR spectroscopy was used to characterize immobilized proteins and enzymes in sol-gels and other immobilization matrices. Sun *et al.* [42] and Jia *et al.* [43] both reported on the detection of immobilized horseradish peroxidase in a poly(N-isopropylacylamide-co-3-methacryloxy-propyltrimethoxysilane) and tin oxide sol-gel film, respectively using FTIR. No changes in secondary structure of the enzyme could be found in either case, as indicated by comparison of peak shape of the amide signal for free and immobilized enzyme. In a similar work, Wang *et al.* reported the retention of myoglobin secondary structure upon entrapment in a TEOS derived sol-gel [44].

1.5.3 FTIR Microscopy

The second FTIR technique used in this study was FTIR microscopy. It is also known as FTIR microspectroscopy, FTIR chemical mapping or FTIR imaging [45]. The terms will be used synonymously throughout this document. FTIR microscopy combines the advantages of FTIR spectroscopy in terms of broad analytical information with the ability to analyze a sample with spatial resolution. This is particularly interesting in the analysis of sol-gel samples, given the indication of sample heterogeneities as described earlier. Although not as widely used as FTIR spectroscopy, FTIR microscopy has been gaining attention mainly due to improvements in instrumentation. Computer controlled microscope stages and improvements in detector sensitivity allow for reliable mapping of samples using a small aperture and step size (e.g. 20 μm) [45]. However, the technique is somewhat limited by requiring suitable samples. Most FTIR microscopes can operate either in transmission or reflectance mode requiring a sufficiently transmissive or reflective sample, respectively. FTIR microscopy has been applied to both sol-gels and immobilized protein/enzyme systems; however, the literature does not contain reference with regards to the application to sol-gel thin film immobilized proteins.

The distribution of the organically modified precursor IBTMS in sol-gel thin films was assessed by Wetzel *et al.* in 2004 [46]. Using a synchrotron radiation source and a 7 x 7 μm

aperture, it was found that the thin films were chemically heterogeneous in terms of IBTMS localization. The applicability of FTIR microscopy in immobilized protein systems was demonstrated by Xu *et al.* in the same year [47]. Through FTIR mapping experiments, the diffusion coefficient of BSA could be measured upon adsorption into porous polymeric membranes. The experimental findings were in good agreement with diffusion coefficient estimates from theory.

In an attempt to characterize commercially available immobilized biocatalysts, Gross and coworkers were able to employ synchrotron FTIR microscopy to investigate the distribution and secondary structure of lipase adsorbed on poly(methyl(methacrylate)) (Novozyme 435) [48]. FTIR images recorded at a step size of 10 μm revealed that the enzyme is primarily distributed unevenly in the outer shell of the carrier beads. Moreover, the immobilized protein did not show any alterations in structure upon immobilization as indicated by conservation of the amide I peak shape. Recently, the same group reported on the adsorption of lipase on polystyrene resins of varying diameter and pore size distribution. Similar to their first study, FTIR microscopy indicated that the bulk of the enzyme concentration was localized on the outer shell of the polystyrene beads [49-51]. Therefore, smaller beads had a higher percentage of resin occupied with respect to the total amount of matrix available. These results show the direct applicability of FTIR microscopy to immobilized enzyme analysis, since it allows an assessment of distribution in order to optimize matrix support bead size to achieve a maximum catalyst density.

Although no literature is available on FTIR microscopy of sol-gel immobilized proteins or enzymes, the distribution and conformation of BSA in TMOS monoliths has been investigated by Tran *et al.* by means of near IR multispectral imaging [52]. It was found that BSA was heterogeneously distributed throughout the sol-gel matrix and that changes in BSA conformation occurred during gelation.

1.5.4 2D FTIR Spectroscopy

Two dimensional Fourier transform infrared (2D FTIR) spectroscopy is a relatively new approach to FTIR and was first described by Noda in 1990 [53]. In this analysis method, a series of FTIR spectra are collected over a range of an external perturbation to the system. The

perturbation to the system could be time, concentration, temperature, mechanical stress, and so forth. Through mathematical correlation analysis, a synchronous and an asynchronous 2D spectrum with two independent cross-correlated wavenumbers can be created. The most striking advantages of this approach are, according to Noda, the deconvolution of complex spectra with overlapping peaks, a spectral resolution enhancement due to the introduction of a second dimension and the identification of molecular interactions as seen in the cross correlation of peaks [53]. Noda has published a few key reviews over the last 15 years or so and they provide an excellent summary of the technique as well as current developments [53-55]. In the following, a brief introduction on the generation of 2D FTIR spectra and their interpretation will be given alongside selected relevant applications from the literature.

The first step in 2D FTIR analysis is the creation of dynamic FTIR spectra. A dynamic spectrum can be created by subtracting a spectrum that was recorded under perturbed conditions from the original spectrum. Originally, 2D correlation could only be calculated, if the perturbation was of a sinusoidal nature. However, Noda published a general formula in 1993 that allows the calculation of the 2D correlation for any arbitrary form of perturbation [55]:

$$\Phi(\nu_1, \nu_2) + i\Psi(\nu_1, \nu_2) = \frac{1}{\pi(T_{\max} - T_{\min})} \int_0^{\infty} \tilde{Y}_1(\omega) \cdot \tilde{Y}_2^*(\omega)\, \mathrm{d}\omega$$

where the synchronous and asynchronous 2D spectrum, $\phi(\nu_1,\nu_2)$ and $\Psi(\nu_1,\nu_2)$ are obtained from the forward Fourier transform $Y_1(\omega)$ of a dynamic spectrum $y(\nu_1,t)$ measured at a wavenumber$_1$ ν_1 and the conjugate Fourier transform $Y^*_1(\omega)$ of another dynamic spectrum $y(\nu_2,t)$ measured at wavenumber$_2$ ν_2, both calculated along the external perturbation variable t over the interval between T_{min} and T_{max}.

The advances in computational software now allow for the convenient calculation of synchronous and asynchronous 2D FTIR spectra directly from the acquired data through built in mathematical functions. The two generated 2D spectra (synchronous and asynchronous) have different properties and can reveal information not readily available from the original FTIR

spectra. The general interpretation of synchronous and asynchronous 2D FTIR spectra is explained in the following [54].

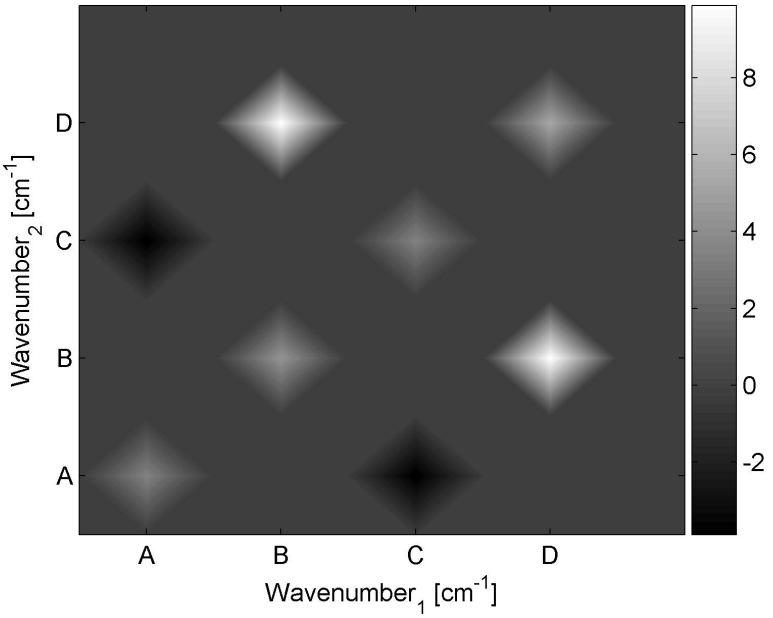

Fig. 3: Illustration of a Synchronous 2D FTIR Spectrum

A synchronous 2D FTIR spectrum typically shows positive (light) autopeaks at (A,A), (B,B), (C,C) and (D,D), also known as diagonal peaks. Cross peaks (C,A), (A,C), (D,B) and (B,D) are located off-diagonally and can be positive (light) and negative (dark). The spectrum is symmetric with respect to the diagonal [54].

Peaks in the synchronous 2D FTIR spectrum (Fig. 3) appear if the change in a spectrum at a given wavenumber$_1$ is coherent with the change at a second wavenumber$_2$, such as, e.g. (A,A) or (C,A) in Fig. 3. Therefore only synchronous changes in the spectrum at different wavenumbers can be detected. The intensity of the autopeaks, located on the diagonal, when both wavenumbers are equal, is representative of the magnitude of change over the range of the external perturbation. More interestingly, cross peaks, such as (C,A) and (D,B) (Fig. 3), reveal the nature of synchronized change in the spectrum at wavenumber$_1$ and wavenumber$_2$. If the cross peak intensity is positive, the intensities at wavenumber$_1$ and wavenumber$_2$ simultaneously change in the same direction over the range of the perturbation. If the cross peak intensity is negative, the intensities at wavenumber$_1$ and wavenumber$_2$ simultaneously change in opposite

directions over the range of the perturbation. In Fig. 3, for instance, A and C change in opposite directions, while D and B change in the same direction over the perturbation range. Also, the change in A is not correlated with the change in D and B. Similarly, the change in B is not correlated with the change in A and C, and so forth.

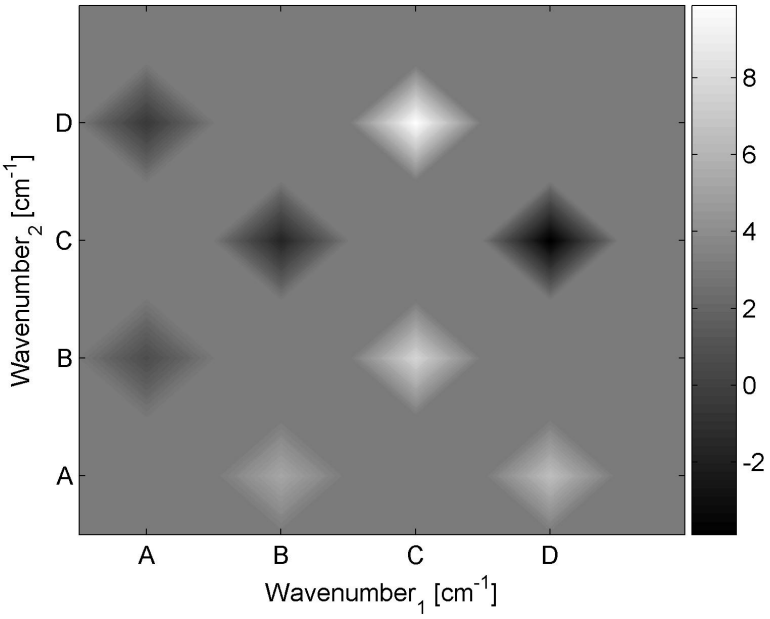

Fig. 4: Illustration of an Asynchronous 2D FTIR Spectrum

An asynchronous 2D FTIR spectrum typically shows no autopeaks. Correlated cross peaks (B,A)-(A,B), (D,A)-(A,D), (C,B)-(B,C) and (D,C)-(C,D) are located off-diagonally. The spectrum is antisymmetric with respect to the diagonal [54].

Peaks in the asynchronous 2D FTIR spectrum (Fig. 4) appear if the change at a given wavenumber$_1$ is uncoordinated with the change at a given wavenumber$_2$. The peaks suggest that the structures responsible for IR absorption at the given wavenumbers do not strongly interact with each other. Fig. 4 reveals that A is not correlated with B (peak at (A,B)) nor with D (peak at (A,D)).

Additionally, the order of the change at wavenumber$_1$ and wavenumber$_2$ can be resolved from the asynchronous 2D FTIR spectrum. If the intensity of an asynchronous peak is positive, the change at wavenumber$_1$ occurs before the change at wavenumber$_2$. Similarly, if the asynchronous

peak is negative, the change at wavenumber$_2$ occurs before the change at wavenumber$_1$. In Fig. 4, the change at B occurs before the change at A, while the change at D occurs after the change at C. It should be noted that this order has to be reversed if the intensity of the synchronous spectrum at the same coordinates is negative. Usually, peaks in the synchronous and asynchronous spectrum are significantly larger than shown in the illustrations of Fig. 3 and Fig. 4, so that an asynchronous peak can fall within the coordinates of a negative synchronous peak.

2D FTIR spectroscopy has been used as a valuable tool in protein science. As mentioned earlier, the shape of the amide I signal in the FTIR spectrum can be taken as an indication for protein conformation [38]. The amide I signal is really a superposition of a number of peaks that account for different structural features, such as β-sheets. The contribution of superimposed peaks to the overall amide I peak can be deconvoluted by asynchronous 2D FTIR spectroscopy. Yan *et al.*, for instance, could gain better insight into the heat induced unfolding and aggregation of myoglobin, by using this technique [56]. The temperature, at which an unfolding of helical structures in the protein started, could be identified. This information was not available from regular temperature dependent FTIR spectroscopy.

Application of this technique to immobilized systems is fairly novel. Pechkova *et al.* report on the heat treatment of lysozyme immobilized in Langmuir-Schaefer films [57]. The *in situ* 2D FTIR spectroscopy of this system revealed that there is no protein decomposition up to 200 ^{o}C. Additionally, different molecular species of water, fully H-bonded and not fully H-bonded could be identified in the system alongside with their respective temperature removal profiles.

The *in situ* application of 2D FTIR spectroscopy provides an improved analysis over conventional FTIR spectroscopy. The revelation of structural features of the immobilized enzyme is particularly interesting as this information is usually very difficult to obtain in immobilized systems. Additionally, the correlation analysis may allow for the determination of protein matrix interaction. A significant advancement in the understanding of immobilized enzyme systems can be expected from this application in the future. Especially in the area of sol-gel immobilized enzymes which are well suited for FTIR analysis.

1.6 Hydroperoxide Lyase as a Model Enzyme

Many enzymatic reactions yield products of commercial interest. Volatile short chain aldehydes - some of which are termed "green note" volatiles due to their characteristic organoleptic character - are such compounds. Their major application lies in the field of food processing, where flavor compounds are used to restore and maintain characteristic aroma properties of food preparations following sterilization.

In vivo, short chain aldehydes are synthesized by plants as part of a wound induced defense mechanism. An enzyme cascade termed lipoxygenase or octadecanoic acid pathway is responsible for the conversion of free fatty acids, namely linoleic and linolenic acid, to C6 and C9 aldehydes, such as hexanal, hexenal or nonenal [58]. The two main enzymes of this pathway are lipoxygenase (LOX) and hydroperoxide lyase (HPL). The volatile compounds that are synthesized are responsible for the characteristic smell of fresh cut fruit, leaves or grass, display antimicrobial and antifungal properties, and are also involved in the upregulation of wound response related genes [58,59]. An overview of the lipoxygenase pathway is depicted in Fig. 5.

One objective of the research group with which this research is associated is to establish a sol-gel immobilized multi-enzyme system that can convert fat molecules from natural sources, such as seed oil, to volatile aldehydes or other lipid derivatives. Lipase will be used to release free linoleic or linolenic acid from fat to provide substrates for the lipoxygenase pathway.

Hydroperoxide lyase is most likely a membrane associated tri- or tetramer of about 55-60 kDa per subunit and was classified as a member of the cytochrome P450 family [58,60-63], carrying a heme molecule in its active site. It is available from different sources through extraction from plant material [64-67] or by recombinant expression in *E. coli* [58,68-70]. As a model enzyme system, HPL offers a variety of advantages. It is a good test case for the immobilization of a membrane associated protein, where hydrophobicity of the support may play an important role in activity, stability and selectivity.

Hydroperoxide lyase was first described in the mid 1970s [71] and much of the work is based on HPL extracted and purified from plant sources. Although some current work on HPL still follows this approach, most of the recent literature relies on heterologous HPL, recombinantly

expressed in *E. coli*. Several HPLs from different sources, such as bell pepper, alfalfa, cucumber, tomato and guava fruit have been reported [58]. Depending on its source the enzyme can act on 9- or 13-hydroperoxylinoleic and -linolenic acid or both. In this work, 13-HPL from bell pepper, recombinantly expressed in *E. coli*, was used.

The reaction mechanism of HPL still remains unclear. There are two alternatives reported in the literature. One involves heterolytic decomposition of the fatty acid hydroperoxide to yield the volatile aldehyde [58]. An alternative to that mechanism was recently suggested by Grechkin and Hamberg [72]. Their work gives evidence for a short lived fatty acid hemiacetal as the "true" reaction product that is subsequently decomposed non-enzymatically. Both alternatives are being acknowledged but are of minor importance to this work.

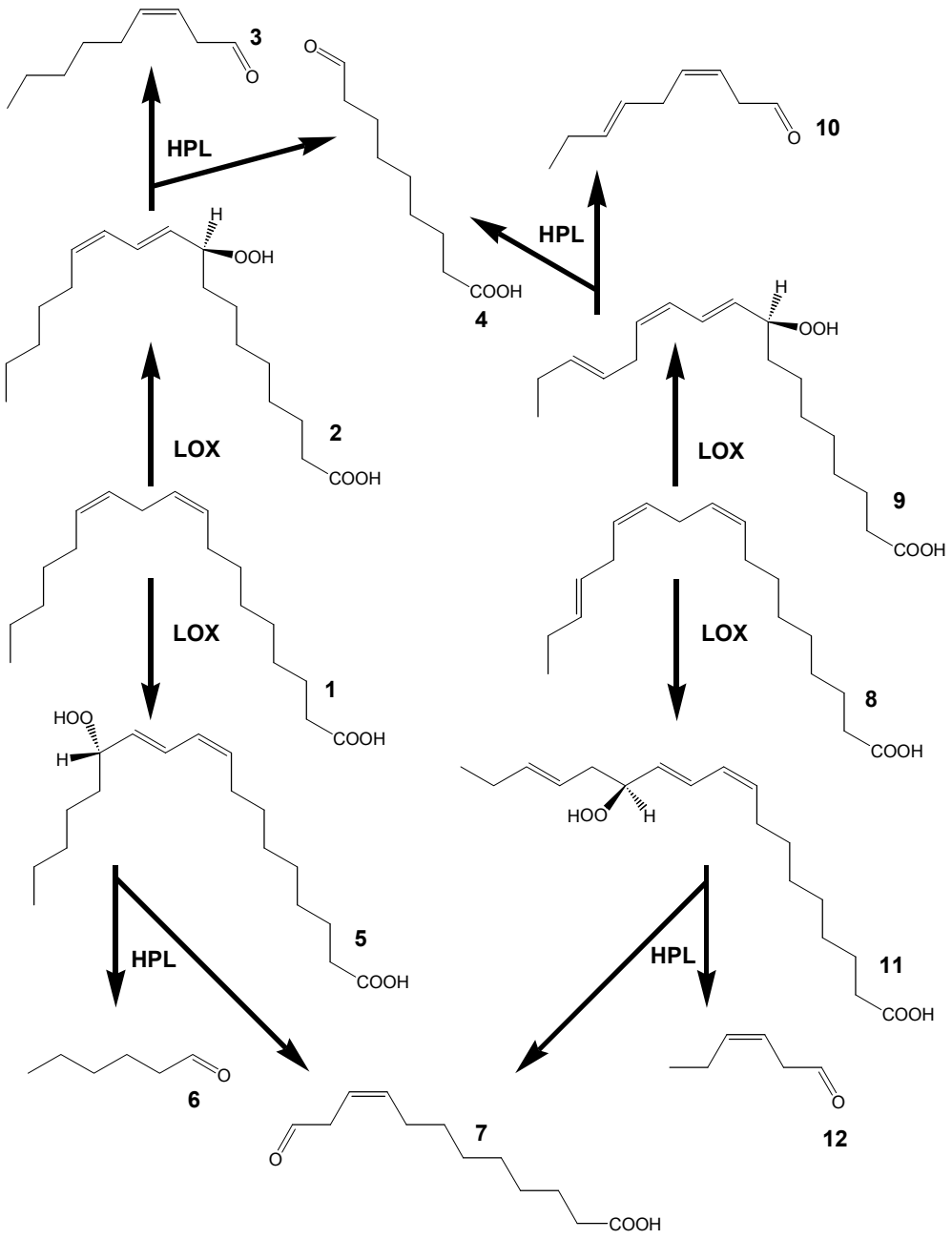

Fig. 5: Lipoxygenase Pathway

The schematic shows the biosynthesis of volatile aldehydes from linoleic acid (1) or linolenic acid (2). The first step is the LOX catalyzed hydroperoxide synthesis (9-HPOD (2), 13-HPOD (LA-OOH) (5), 9-HPOT (9) and 13-HPOT (11)). The intermediates are subsequently transformed to short chain aldehydes (nonenal (3), hexanal (6), nonadienal (10) and hexenal (12) by HPL. Byproducts of the HPL reaction are 9-oxononanoic acid (4) and 12-oxododecenoic acid (7) [58].

Two different research groups have observed activation phenomena for HPL. Noordermeer *et al.* [73] describe the transition of the heme Fe(III) from low to high spin state upon incubation of an alfalfa HPL preparation with the detergent Triton X-100. The change in spin state was detected by EPR spectroscopy, and CD measurements could identify a subtle conformational change associated with the phenomenon. Koeduka *et al.* investigated the effect of salt and detergent concentration on barley HPL [68,74]. Addition of 1.5 M KCl to the reaction buffer resulted in a 3 fold increase in V_{max} leaving the K_M nearly unaltered. Supplementary addition of the detergent Brij 99 led to a further increase in V_{max} of about 3 fold and roughly halved the K_M. The detergent concentration was 0.0008 % (v/v) and therefore below the CMC value, indicating that improved substrate solubility is not the cause of the increase in activity. Additionally, the influence of salt and detergent were found to be independent of one another [74].

Both groups suggest that the addition of salt and/or detergent results in a change in enzyme structure bringing it closer to its *in vivo* conformation. HPL is thought to be membrane associated, therefore embedded in a hydrophobic environment in the cell membrane. Because of the size of the detergents used, they presumably do not act on the enzyme's active site directly but rather alter the HPL through an indirect interaction with the enzyme surface [74].

The natural substrates of HPL are the 9- and 13- hydroperoxides of linoleic and linolenic acid. Enzymes from different sources show different preferences towards these substrates [75]. There are, however, reports that oxylipins from N-acyl(ethanol)amines (NAEs) could also be utilized as a HPL substrate. Van der Stelt *et al.* [76] describe hydroperoxy NAEs as a good substrate for HPL whereas hydroperoxy fatty acid methyl esters were found to be unsuitable for enzymatic conversion. It is speculated that the polarity of the fatty acid headgroup is the determining factor for activity rather than the size of it. The use of the novel water soluble HPL substrate 13-hydroperoxy-octadienoyl sulfate to examine this phenomenon further will be described in Chapter 2.

The information on successful immobilization of HPL is rather sparse. There are only a few publications available that describe the subject. The sources of HPL in these studies are mung beans [77] and *Chlorella* [78]. Generally, a good binding of the enzyme to the immobilization

support is described, yielding degrees of immobilization between 60-90 %. Also, Nunez *et al.* [77] report an increase in storage stability upon HPL immobilization. A formal characterization of the activity, e.g. in terms of comparing the Michaelis Menten kinetic parameters of free and immobilized enzyme, however, is not available. The lack of literature in this area could be seen as an indication of the problems associated with HPL immobilization. This is especially noticeable, if the industrial potential of the enzyme is taken into account. A need for a suitable immobilization procedure for HPL is, therefore, evident. Novel immobilization techniques that focus specifically on membrane proteins might provide a solution to this problem. The available literature on spectroscopy of cytochrome P450 enzymes [79-81], can help in the identification and interpretation of immobilization phenomena, which is expected to facilitate the design of an optimized immobilization support.

1.7 References

[1] *Enzyme Catalysis in Organic Synthesis*; Wiley-VCH: Weinheim, 2002.

[2] Hartmeier, W. *Immobilized Biocatalysts*; Springer-Verlag: 1986.

[3] Clark, D. S. Can Immobilization Be Exploited to Modify Enzyme-Activity. *Trends in Biotechnology* **1994**, *12*, 439-443.

[4] *Merriam-Webster Online*; 2007.

[5] Nelson, J. M.; Griffin, E. G. Adsortion of Invertase. *J.Am.Chem.Soc.* **1916**, *38*, 1109-1115.

[6] Liang, J. F.; Li, Y. T.; Yang, V. C. Biomedical Application of Immobilized Enzymes. *J.Pharm.Sci.* **2000**, *89*, 979-990.

[7] Liese, A.; Seelbach, K.; Wandrey, C. *Industrial Biotransformations*; Wiley-VCH: Weinheim, 2000.

[8] Tischer, W.; Wedekind, F. Immobilized Enzymes: Methods and Applications. *Biocatalysis - from Discovery to Application* **1999**, *200*, 95-126.

[9] Wright, J. D.; Sommerdjk, N. A. J. M. *Sol-Gel Materials*; Gordon and Breach Science Publishers: Amsterdam, 2001.

[10] Avnir, D.; Braun, S.; Lev, O.; Ottolenghi, M. Enzymes and Other Proteins Entrapped in Sol-Gel Materials. *Chem.Mater.* **1994**, *6*, 1605-1614.

[11] Braun, S.; Rappoport, S.; Zusman, R.; Avnir, D.; Ottolenghi, M. Biochemically Active Sol-Gel Glasses - the Trapping of Enzymes. *Mater.Lett.* **1990**, *10*, 1-5.

[12] Gill, I.; Ballesteros, A. Bioencapsulation Within Synthetic Polymers (Part 1): Sol-Gel Encapsulated Biologicals. *Trends in Biotechnology* **2000**, *18*, 282-296.

[13] Jin, W.; Brennan, J. D. Properties and Applications of Proteins Encapsulated Within Sol-Gel Derived Materials. *Anal.Chim.Acta* **2002**, *461*, 1-36.

[14] Pierre, A. C. The Sol-Gel Encapsulation of Enzymes. *Biocatalysis and Biotransformation* **2004**, *22*, 145-170.

[15] Brennan, J. D. Biofriendly Sol-Gel Processing for the Entrapment of Soluble and Membrane-Bound Proteins: Toward Novel Solid-Phase Assays for High-Throughput Screening. *Acc.Chem.Res.* **2007**, *40*, 827-835.

[16] Gill, I. Bio-Doped Nanocomposite Polymers: Sol-Gel Bioencapsulates. *Chem.Mater.* **2001**, *13*, 3404-3421.

[17] Gupta, R.; Chaudhury, N. K. Entrapment of Biomolecules in Sol-Gel Matrix for Applications in Biosensors: Problems and Future Prospects. *Biosensors & Bioelectronics* **2007**, *22*, 2387-2399.

[18] Goring, G. L. G.; Brennan, J. D. Fluorescence and Physical Characterization of Sol-Gel-Derived Nanocomposite Films Suitable for the Entrapment of Biomolecules. *J.Mater.Chem.* **2002**, *12*, 3400-3406.

[19] Dave, B. C.; Dunn, B.; Valentine, J. S.; Zink, J. I. Sol-Gel Encapsulation Methods for Biosensors. *Anal.Chem.* **1994**, *66*, A1120-A1127.

[20] Smith, K.; Silvernail, N. J.; Rodgers, K. R.; Elgren, T. E.; Castro, M.; Parker, R. M. Sol-Gel Encapsulated Horseradish Peroxidase: A Catalytic Material for Peroxidation. *J.Am.Chem.Soc.* **2002**, *124*, 4247-4252.

[21] Lloyd, C. R.; Eyring, E. M. Protecting Heme Enzyme Peroxidase Activity From H2O2 Inactivation by Sol-Gel Encapsulation. *Langmuir* **2000**, *16*, 9092-9094.

[22] Jürgen-Lohmann, D. L.; Legge, R. L. Immobilization of Bovine Catalase in Sol-Gels. *Enzyme Microb.Technol.* **2006**, *39*, 626-633.

[23] Ladokhin, A. S. Fluorescence Spectroscopy in Peptide and Protein Analysis; In *Encyclopedia of Analytical Chemistry*; Meyers, R. A., ed. John Wiley & Sons Ltd: Chichester, 2000; pp 5762-5779.

[24] Brennan, J. D. Using Intrinsic Fluorescence to Investigate Proteins Entrapped in Sol-Gel Derived Materials. *Appl.Spectrosc.* **1999**, *53*, 106A-121A.

[25] Costa, T. M. H.; Hoffmann, H. S.; Benvenutti, E. V.; Stefani, V.; Gallas, M. R. Pressure-Induced Changes on the Optical Properties and Microstructure of Silica-Gel Matrices Doped With Rhodamine 6G. *Optical Materials* **2005**, *27*, 1819-1824.

[26] Flora, K. K.; Dabrowski, M. A.; Musson, S. P.; Brennan, J. D. The Effect of Preparation and Aging Conditions on the Internal Environment of Sol-Gel Derived Materials As Probed by 7-Azaindole and Pyranine Fluorescence. *Canadian Journal of Chemistry-Revue Canadienne de Chimie* **1999**, *77*, 1617-1625.

[27] Gupta, R.; Mozumdar, S.; Chaudhury, N. K. Effect of Ethanol Variation on the Internal Environment of Sol-Gel Bulk and Thin Films With Aging. *Biosensors & Bioelectronics* **2005**, *21*, 549-556.

[28] Gupta, R.; Mozumdar, S.; Chaudhury, N. K. Fluorescence Spectroscopic Studies to Characterize the Internal Environment of Tetraethyl-Orthosilicate Derived Sol-Gel Bulk and Thin Films With Aging. *Biosensors & Bioelectronics* **2005**, *20*, 1358-1365.

[29] Bardo, A. M.; Collinson, M. M.; Higgins, D. A. Nanoscale Properties and Matrix-Dopant Interactions in Dye-Doped Organically Modified Silicate Thin Films. *Chem.Mater.* **2001**, *13*, 2713-2721.

[30] Fu, Y.; Ye, F. M.; Sanders, W. G.; Collinson, M. M.; Higgins, D. A. Single Molecule Spectroscopy Studies of Diffusion in Mesoporous Silica Thin Films. *Journal of Physical Chemistry B* **2006**, *110*, 9164-9170.

[31] Jordan, J. D.; Dunbar, R. A.; Bright, F. V. Dynamics of Acrylodan-Labeled Bovine and Human Serum-Albumin Entrapped in A Sol-Gel-Derived Biogel. *Anal.Chem.* **1995**, *67*, 2436-2443.

[32] Chirico, G.; Cannone, F.; Beretta, S.; Diaspro, A.; Campanini, B.; Bettati, S.; Ruotolo, R.; Mozzarelli, A. Dynamics of Green Fluorescent Protein Mutant2 in Solution, on Spin-Coated Glasses, and Encapsulated in Wet Silica Gels. *Protein Science* **2002**, *11*, 1152-1161.

[33] Pastor, I.; Ferrer, M. L.; Lillo, M. P.; Gomez, J.; Mateo, C. R. Structure and Dynamics of Lysozyme Encapsulated in a Silica Sol-Gel Matrix. *Journal of Physical Chemistry B* **2007**, *111*, 11603-11610.

[34] Przybyt, M. Behaviour of Glucose Oxidase During Formation and Ageing of Silica Gel Studied by Fluorescence Spectroscopy. *Materials Science-Poland* **2003**, *21*, 397-416.

[35] Bottini, M.; De Venere, A.; Lugli, P.; Rosato, N. Conformation and Stability of Myoglobin in Dilute and Crowded Organically Modified Media. *J.Non-Cryst.Solids* **2004**, *343*, 101-108.

[36] Cruz-Aguado, J. A.; Chen, Y.; Zhang, Z.; Elowe, N. H.; Brook, M. A.; Brennan, J. D. Ultrasensitive ATP Detection Using Firefly Luciferase Entrapped in Sugar-Modified Sol-Gel-Derived Silica. *J.Am.Chem.Soc.* **2004**, *126*, 6878-6879.

[37] Günzler, H.; Gremlich, H. U. *IR spectroscopy*; Wiley-VCH: Weinheim, 2002.

[38] Gremlich, H. U.; Yan, B. *Infrared and Raman spectroscopy of biological materials*; Marcel Dekker: New York, 2001.

[39] Chernev, G.; Samuneva, B.; Djambaski, P.; Kabaivanova, L.; Emanuilova, E.; Salvado, I. M. M.; Fernandes, M. H. V.; Wu, A. Synthesis and Structure of New Biomaterials Containing Silica and Chitosan. *Physics and Chemistry of Glasses-European Journal of Glass Science and Technology Part B* **2007**, *48*, 147-150.

[40] Mansur, H.; Orefice, R.; Pereira, M.; Lobato, Z.; Vasconcelos, W.; Machado, L. FTIR and UV-Vis Study of Chemically Engineered Biomaterial Surfaces for Protein Immobilization. *Spectroscopy-An International Journal* **2002**, *16*, 351-360.

[41] Soares, C. M. F.; dos Santos, O. A.; Olivo, J. E.; de Castro, H. F.; de Moraes, F. E.; Zanin, G. M. Influence of the Alkyl-Substituted Silane Precursor on Sol-Gel Encapsulated Lipase Activity. *Journal of Molecular Catalysis B-Enzymatic* **2004**, *29*, 69-79.

[42] Sun, Y. X.; Zhang, H. T.; Huang, S. W.; Wang, S. F. Hydrogen Peroxide Biosensor Based on the Bioelectrocatalysis of Horseradish Peroxidase Incorporated in a New Hydrogel Film. *Sensors and Actuators B-Chemical* **2007**, *124*, 494-500.

[43] Jia, N. Q.; Xu, J.; Sun, M. H.; Jiang, Z. Y. A Mediatorless Hydrogen Peroxide Biosensor Based on Horseradish Peroxidase Immobilized in Tin Oxide Sol-Gel Film. *Anal.Lett.* **2005**, *38*, 1237-1248.

[44] Wang, Q. L.; Lu, G. X.; Yang, B. J. Myoglobin/Sol-Gel Film Modified Electrode: Direct Electrochemistry and Electrochemical Catalysis. *Langmuir* **2004**, *20*, 1342-1347.

[45] Schultz, C. P. Precision Infrared Spectroscopic Imaging: The Future of FT-IR Spectroscopy. *Spectroscopy* **2001**, *16*, 24-+.

[46] Wetzel, D. L.; Striova, J.; Higgins, D. A.; Collinson, M. M. Synchrotron Infrared Micro Spectroscopy Reveals Localized Heterogeneities in an Organically Modified Silicate Film. *Vibrational Spectroscopy* **2004**, *35*, 153-158.

[47] Xu, T. W.; Fu, R. Q. Determination of Effective Diffusion Coefficient and Interfacial Mass Transfer Coefficient of Bovine Serum Albumin (BSA) Adsorption into Porous Polyethylene Membrane by Microscope FTIR-Mapping Study. *Chem.Eng.Sci.* **2004**, *59*, 4569-4574.

[48] Mei, Y.; Miller, L.; Gao, W.; Gross, R. A. Imaging the Distribution and Secondary Structure of Immobilized Enzymes Using Infrared Microspectroscopy. *Biomacromolecules* **2003**, *4*, 70-74.

[49] Chen, B.; Gross, R. A.; Miller, M. E.; Miller, L.; Maikner, J. Immobilization of Candida Antarctica Lipase B on Porous Polystyrene Resins: Protein Distribution and Activity. *Abstracts of Papers of the American Chemical Society* **2005**, *230*, U3784.

[50] Chen, B.; Miller, M. E.; Gross, R. A. Effects of Porous Polystyrene Resin Parameters on Candida Antarctica Lipase B Adsorption, Distribution, and Polyester Synthesis Activity. *Langmuir* **2007**, *23*, 6467-6474.

[51] Chen, B.; Miller, E. M.; Miller, L.; Maikner, J. J.; Gross, R. A. Effects of Macroporous Resin Size on Candida Antarctica Lipase B Adsorption, Fraction of Active Molecules, and Catalytic Activity for Polyester Synthesis. *Langmuir* **2007**, *23*, 1381-1387.

[52] Tran, C. D.; Ilieva, D.; Challa, S. Inhomogeneity in Distribution and Conformation of Bovine Serum Albumin in Sol-Gel: A Closer Look With a Near-Infrared Multispectral Imaging Technique. *Journal of Sol-Gel Science and Technology* **2004**, *32*, 207-217.

[53] Noda, I. 2-Dimensional Infrared (2D Ir) Spectroscopy - Theory and Applications. *Appl.Spectrosc.* **1990**, *44*, 550-561.

[54] Noda, I.; Dowrey, A. E.; Marcott, C. Recent Developments in 2-Dimensional Infrared (2D-Ir) Correlation Spectroscopy. *Appl.Spectrosc.* **1993**, *47*, 1317-1323.

[55] Noda, I. Progress in Two-Dimensional (2D) Correlation Spectroscopy. *J.Mol.Struct.* **2006**, *799*, 2-15.

[56] Yan, Y. B.; Wang, Q.; He, H. W.; Hu, X. Y.; Zhang, R. Q.; Zhou, H. M. Two-Dimensional Infrared Correlation Spectroscopy Study of Sequential Events in the Heat-Induced Unfolding and Aggregation Process of Myoglobin. *Biophys.J.* **2003**, *85*, 1959-1967.

[57] Pechkova, E.; Innocenzi, P.; Malfatti, L.; Kidchob, T.; Gaspa, L.; Nicolini, C. Thermal Stability of Lysozyme Langmuir-Schaefer Films by FTIR Spectroscopy. *Langmuir* **2007**, *23*, 1147-1151.

[58] Noordermeer, M. A.; Veldink, G. A.; Vliegenthart, J. F. G. Fatty Acid Hydroperoxide Lyase: A Plant Cytochrome P450 Enzyme Involved in Wound Healing and Pest Resistance. *Chembiochem* **2001**, *2*, 494-504.

[59] Hatanaka, A. The Fresh Green Odor Emitted by Plants. *Food Reviews International* **1996**, *12*, 303-350.

[60] Froehlich, J. E.; Itoh, A.; Howe, G. A. Tomato Allene Oxide Synthase and Fatty Acid Hydroperoxide Lyase, Two Cytochrome P450s Involved in Oxylipin Metabolism, Are Targeted to Different Membranes of Chloroplast Envelope. *Plant Physiol.* **2001**, *125*, 306-317.

[61] Howe, G. A.; Lee, G. I.; Itoh, A.; Li, L.; DeRocher, A. E. Cytochrome P450-Dependent Metabolism of Oxylipins in Tomato. Cloning and Expression of Allene Oxide Synthase and Fatty Acid Hydroperoxide Lyase. *Plant Physiol.* **2000**, *123*, 711-724.

[62] Itoh, A.; Vick, B. A. Fatty Acid Hydroperoxide Lyase From Sunflower Hypocotyl Is a Cytochrome P450-Type Enzyme. *Plant Physiol.* **1997**, *114*, 942.

[63] Matsui, K.; Shibutani, M.; Hase, T.; Kajiwara, T. Bell Pepper Fruit Fatty Acid Hydroperoxide Lyase Is a Cytochrome P450 (CYP74B). *FEBS Lett.* **1996**, *394*, 21-24.

[64] Cass, B. J.; Schade, F.; Robinson, C. W.; Thompson, J. E.; Legge, R. L. Production of Tomato Flavor Volatiles From a Crude Enzyme Preparation Using a Hollow-Fiber Reactor. *Biotechnol.Bioeng.* **2000**, *67*, 372-377.

[65] Fauconnier, M. L.; Delcarte, J.; Jaziri, M.; du Jardin, P.; Marlier, M. Fatty Acid Hydroperoxides Biotransformation by Potato Tuber Cell-Free Extracts. *J.Plant Physiol.* **2002**, *159*, 1055-1060.

[66] Gargouri, M.; Drouet, P.; Legoy, M. D. Hydroperoxide-Lyase Activity in Mint Leaves Volatile C6-Aldehyde Production From Hydroperoxy-Fatty Acids. *J.Biotechnol.* **2004**, *111*, 59-65.

[67] Nunez, A.; Foglia, T. A.; Piazza, G. J. Improved Method for Extraction of Hydroperoxide Lyase From Chorella. *Biotechnol.Tech.* **1995**, *9*, 613-616.

[68] Koeduka, T.; Stumpe, M.; Matsui, K.; Kajiwara, T.; Feussner, I. Kinetics of Barley FA Hydroperoxide Lyase Are Modulated by Salts and Detergents. *Lipids* **2003**, *38*, 1167-1172.

[69] Matsui, K.; Miyahara, C.; Wilkinson, J.; Hiatt, B.; Knauf, V.; Kajiwara, T. Fatty Acid Hydroperoxide Lyase in Tomato Fruits: Cloning and Properties of a Recombinant Enzyme Expressed in Escherichia Coli. *Bioscience Biotechnology and Biochemistry* **2000**, *64*, 1189-1196.

[70] Delcarte, J.; Fauconnier, M. L.; Jacques, P.; Matsui, K.; Thonart, P.; Marlier, M. Optimisation of Expression and Immobilized Metal Ion Affinity Chromatographic Purification of Recombinant (HiS)(6)-Tagged Cytochrome P450 Hydroperoxide Lyase in Escherichia Coli. *Journal of Chromatography B-Analytical Technologies in the Biomedical and Life Sciences* **2003**, *786*, 229-236.

[71] Vick, B.; Zimmerman, D. Identification of Linoleate Hydroperoxide Lyase in Germinating Watermelon Seedlings. *Plant Physiol.* **1975**, *56*, 84.

[72] Grechkin, A. N.; Hamberg, M. The "Heterolytic Hydroperoxide Lyase" Is an Isomerase Producing a Short-Lived Fatty Acid Hemiacetal. *Biochimica et Biophysica Acta-Molecular and Cell Biology of Lipids* **2004**, *1636*, 47-58.

[73] Noordermeer, M. A.; Veldink, G. A.; Vliegenthart, J. F. G. Spectroscopic Studies on the Active Site of Hydroperoxide Lyase; the Influence of Detergents on Its Conformation. *FEBS Lett.* **2001**, *489*, 229-232.

[74] Koeduka, T.; Matsui, K.; Kajiwara, T.; Stumpe, S.; Feussner, I. Cloning and Characterization of Barley Fatty Acid Hydroperoxide Lyase. *Plant Cell Physiol.* **2003**, *44*, S136.

[75] Shen, Y. T.; Mackey, G.; Rupcich, N.; Gloster, D.; Chiuman, W.; Li, Y. F.; Brennan, J. D. Entrapment of Fluorescence Signaling DNA Enzymes in Sol-Gel-Derived Materials for Metal Ion Sensing. *Anal.Chem.* **2007**, *79*, 3494-3503.

[76] van der Stelt, M.; Noordermeer, M. A.; Kiss, T.; van Zadelhoff, G.; Merghart, B.; Veldink, G. A.; Vliegenthart, J. F. G. Formation of a New Class of Oxylipins From N-Acyl(Ethanol)Amines by the Lipoxygenase Pathway. *Eur.J.Biochem.* **2000**, *267*, 2000-2007.

[77] Rehbock, B.; Berger, R. G. Covalent Immobilization of a Hydroperoxide Lyase From Mung Beans (Phaseolus Radiatus L.). *Biotechnol.Tech.* **1998**, *12*, 539-544.

[78] Nunez, A.; StArmand, G.; Foglia, T. A.; Piazza, G. J. Immobilization of Hydroperoxide Lyase From Chlorella. *Biotechnology and Applied Biochemistry* **1997**, *25*, 75-80.

[79] Jung, C. Insight into Protein Structure and Protein-Ligand Recognition by Fourier Transform Infrared Spectroscopy. *Journal of Molecular Recognition* **2000**, *13*, 325-351.

[80] Loew, G. Structure, Spectra, and Function of Heme Sites. *Int.J.Quantum Chem.* **2000**, *77*, 54-70.

[81] Gustafsson, M. C. U.; Roitel, O.; Marshall, K. R.; Noble, M. A.; Chapman, S. K.; Pessegueiro, A.; Fulco, A. J.; Cheesman, M. R.; von Wachenfeldt, C.; Munro, A. W. Expression, Purification, and Characterization of Bacillus Subtilis Cytochromes P450CYP102A2 and CYP102A3: Flavocytochronie Homologues of P450BM3 From Bacillus Megaterium. *Biochemistry* **2004**, *43*, 5474-5487.

Chapter 2

Activity of Hydroperoxide Lyase Under Aqueous and Micro-Aqueous Conditions[1]

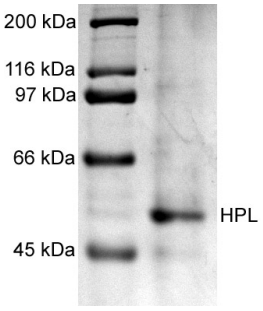

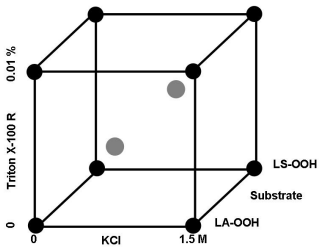

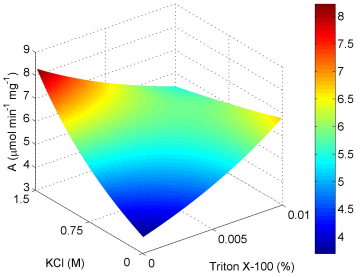

[1] With minor editorial changes, this chapter appeared as D.L. Jürgen-Lohmann and R.L. Legge, "Activity of Hydroperoxide Lyase Under Aqueous and Micro-Aqueous Conditions", Journal of Molecular Catalysis B: Enzymatic 44 (2007) 32-38

Preface

At the start of this project, hydroperoxide lyase (HPL) was identified as a possible model enzyme to probe the influence of different sol-gel support materials on immobilized enzyme properties using spectroscopic techniques. HPL is an interesting enzyme from a biotechnology perspective as it can be used to produce value-added products from fatty acid esters through a three step multienzyme cascade. Additionally, HPL can be investigated by UV-vis spectroscopy (heme centre), by fluorescence spectroscopy (intrinsic tryptophan fluorescence) and by FTIR (amide signal). These spectroscopic techniques could be used to provide insight into the state of the immobilized enzyme. Moreover, activity modulation of HPL had been described in the literature. HPL activity had been found to be greatly enhanced when subjected to high salt concentrations or certain detergents. The present working theory is that the presence of surfactant might mimic the membrane environment that HPL is exposed to *in vivo*. During the planning of this work, it was proposed that sol-gels could be developed to mimic these conditions. Higher PTMS-content in sol-gels could be used to modulate hydrophobicity and to provide the necessary template for activity enhancement. To facilitate the interpretation of the activity data for immobilized HPL preparations, it was necessary to characterize the activity of free HPL since the literature was inconclusive on the effects of salt and detergents.

During the course of this project, it was found that HPL, especially in immobilized systems, was more challenging than anticipated. Immobilized HPL was found to be inactive for all scenarios tested (aqueous, micro-aqueous and various PTMS content sol-gels). This was attributed to adsorption problems of the HPL substrates to the sol-gel matrix and to possible inactivation of the somewhat unstable enzyme during the course of immobilization. In light of these problems the thin film immobilization experiments were carried out using the more readily available and purified proteins/enzymes: lysozyme, lipase and BSA.

Summary

Hydroperoxide lyases (HPL [E.C. 4.1.2.]) are part of the lipoxygenase pathway in plants and catalyze the conversion of fatty acid hydroperoxide into oxo acids and short chain aldehydes. These aldehydes have desirable properties for the food and agricultural industry. HPL activity can be modulated by salts and surfactants, but the mechanisms governing the modulation are not fully understood. Recombinant HPL activity was evaluated by use of factorial experimental design investigating the effects of KCl and Triton X-100 on HPL activity with 13-hydroperoxy-octadecadienoic acid (LA-OOH) and 13-hydroperoxy-octadienoyl sulfate (LS-OOH) as substrates. To investigate solubility issues of the two different substrates, an aqueous and a two-phase micro-aqueous reaction medium was used. The highest HPL activity (8.7 μmol min^{-1} mg^{-1}) was achieved under aqueous conditions with high salt (1.5 M) and low surfactant (0%, v/v) concentrations and LA-OOH as a substrate. Maximal activity (2.4 μmol min^{-1} mg^{-1}) under micro-aqueous conditions was achieved with high salt (1.5 M) and high surfactant (0.01%, v/v) concentrations and LS-OOH as a substrate. A significant interaction between salt and surfactant as well as salt and substrate could be identified and a hypothesis for the interaction phenomena is presented.

2.1 Introduction

Hydroperoxide lyases (HPL) are part of the Cytochrome P450 family and catalyze the conversion of fatty acid hydroperoxides to oxo acids and volatile short chain aldehydes. HPL is a constituent of the octadecanoic acid or lipoxygenase pathway. This pathway is one of the most important inducible defense mechanisms in plants. Fatty acids, namely linoleic and linolenic acid, are released as a wound response by the plant and are subsequently converted to their corresponding 9- or 13-hydroperoxides by lipoxygenases of respective regio-selectivity. HPL then catalyzes the reaction to C6 or C9 short chain aldehydes and corresponding oxo acids (Fig. 6) [1].

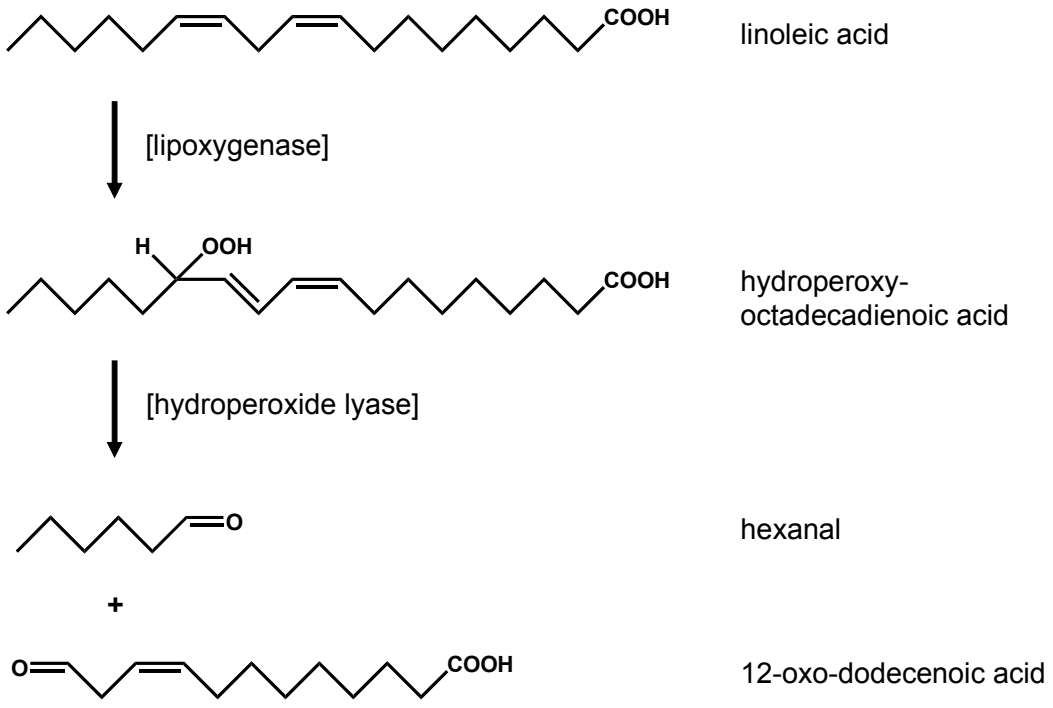

Fig. 6: Schematic of the Lipoxygenase Pathway [1]

HPL has received considerable attention since its first description by Vick *et al.* in 1975 [2]. Much HPL research was hampered by tedious extraction procedures of HPL from plant sources. Since 2000, recombinantly expressed versions of the enzyme from various sources have been described, resulting in much easier preparation and higher quantities of pure HPL [3,4]. There are several reasons why there is considerable interest in the enzyme. The enzyme represents a target for fundamental research because it is part of a multi-enzyme cascade in vivo and has a variety of interesting characteristics in terms of reaction mechanism, catalytic properties and activation phenomena. From a biotechnology perspective, the products of this enzyme, such as hexanal or (3Z)-hexenal, possess desirable organoleptic properties, which make them valuable for use as food flavor additives [1]. Additionally, these aldehydes were shown to increase pest resistance in plants, being potential natural, environmentally friendly agrichemicals [1].

Factors which modulate HPL activity and its spectroscopic properties have been described in the literature. HPL activity has been shown to be enhanced in the presence of non-ionic surfactants, such as Triton X-100, or monovalent salts, such as KCl [5]. Additionally, it was found that Triton X-100 caused a slight conformational change and a spin state transition of the catalytic iron centre of the enzyme [6]. These phenomena are believed to in part cause enhancement in enzymatic activity although this has not been fully elucidated.

The objective of this study was to garner a better understanding of HPL activation phenomena and to identify optimal conditions for HPL activity. To achieve this objective, a recombinant HPL from bell pepper expressed in *E. coli* was studied under aqueous and micro-aqueous conditions. Substrate effects were also probed by using a fatty acid hydroperoxide and a novel, water soluble fatty sulfate hydroperoxide. Salt and surfactant effects as well as their interactions were evaluated by means of appropriate experimental design.

2.2 Materials and Methods

2.2.1 Materials

Lysozyme, IPTG, Triton X-100, Triton X-100 R, δ-aminolevulenic acid, linoleic acid and linoleyl alcohol were purchased from Sigma (Oakville, ON, Canada). PMSF was obtained from Boehringer Mannheim (Mannheim, Germany) and soybean lipoxygenase was from Fluka (Oakville, ON, Canada). Ni-NTA agarose was purchased from Qiagen (Mississauga, ON, Canada). All other chemicals were of analytical grade or better. Transformant *E. coli* M15 carrying the cDNA for bell pepper HPL in pQE-31 (Qiagen, Mississauga, ON, Canada) were kindly provided by Prof. K. Matsui (Yamaguchi University, Japan).

2.2.2 HPL Expression and Purification

HPL expression and purification was carried out according to Delcarte *et al.* [7]. Briefly, cells were grown in 100 mL TB medium containing 100 mg L^{-1} ampicillin, 50 mg L^{-1} kanamycin and 2.5 mM δ-aminolevulenic acid. A 5% inoculum from a culture that had been grown overnight was used in 100 mL of culture media in a 500 mL shake flask at 37 °C and 250 rpm and grown to an OD of 0.9-1.1; expression was induced by adding IPTG to a final concentration of 0.1 mM. The cultures were incubated at 20 °C and 150 rpm for 48 h following induction.

Cells were harvested from the fermentation broth by centrifugation (10000 x g, 4 °C, 15 min) and the resulting pellet was resuspended in 50 mL phosphate buffer (50 mM, pH 7) and centrifuged (10,000 x g, 4 °C, 15 min). Cell lysis was carried out by the addition of 5 mL of lysis buffer (50 mM TRIS-HCl pH 8, 25 mg of lysozyme, 50 μL of 10 mg mL^{-1} PMSF (in ethanol), 25 μL of 1 M $MgCl_2$, 10 μL of DNAseI, 500 mM NaCl and 1 % (v/v) Triton X-100) and stirring for 30 min at 4 °C. Cell debris and other solid components were separated from the lysate by centrifugation (25,000 x g, 4 °C, 15 min) and the supernatant used for HPL purification.

Ni-NTA affinity chromatography was used for HPL purification. One mL of the affinity resin was packed into a column (0.5 cm inner diameter), washed with 5 mL of deionized water and equilibrated with 5 mL buffer 1 (50 mM TRIS-HCl, pH 8, 500 mM NaCl, 1 % (v/v) Triton X-100). The crude lysate was loaded onto the column, washed with 5 mL buffer 1, 15 mL buffer 2

(50 mM phosphate, pH 6, 500 mM NaCl, 1 % (v/v) Triton X-100) and eluted with 10 mL buffer 3 (50 mM acetate, pH 4, 500 mM NaCl, 1 % (v/v) Triton X-100 R). The flow rate was kept at about 0.5 mL min^{-1} during the isolation. The HPL containing fraction was identified visually by its brown color and collected in a microcentrifuge tube. The concentration of HPL was determined by the BCA method (Pierce, Rockford, IL) and HPL purity verified by standard SDS-PAGE (15 % polyacrylamide).

2.2.3 Substrate Synthesis

13-Hydroperoxy-octadecadienoic acid (LA-OOH) and 13-hydroperoxy-octadecadienoyl sulfate (LS-OOH) were synthesized as HPL substrates. LA-OOH was prepared according to Nunez *et al.* (1997) [8]. A mixture of 40 mg of linoleic acid and 50 mL borate buffer (50 mM, pH 9) were kept at 0 ^{o}C in a temperature controlled vessel and subjected to a constant flow of air (5 mL min^{-1}). Ten mg mL^{-1} of soybean lipoxygenase was added in 100 μL aliquots over 30 min intervals for a total reaction time of 2 h. The pH of the mixture was adjusted to pH 2 with 1 M HCl and the LA-OOH was extracted from the borate buffer with 10 mL aliquots of diethyl ether three times. The organic phase was subsequently dried over anhydrous sodium sulphate and evaporated under nitrogen; the LA-OOH was then reconstituted in a minimal amount of ethanol.

Linoleyl sulfate was prepared from linoleyl alcohol according to Mogul *et al.* (2000) [9]. 0.5 g linoleyl alcohol and 0.35 g sulfamic acid were dissolved in 3 mL dry pyridine. The reaction was carried out at 95 ^{o}C for 1.5 h under nitrogen and the reaction stopped by the addition of 15 mL methanol and 1 mL of saturated sodium carbonate. After filtering off waste solids, the methanol was removed *in vacuo* and the residue recrystalized from hot methanol to yield purified linoleyl sulfate. LS-OOH was prepared in the same manner as LA-OOH, using linoleyl sulfate as the substrate for the lipoxygenase reaction.

Substrates were analyzed by TLC (aluminum sheets, silica gel 60 F_{254}, Merck, Darmstadt, Germany) developed in hexane:diethyl ether:acetic acid (60:39:1) mobile phase with iodine detection. Substrate quantification was carried out spectrophotometrically (Cary Bio 1, Varian,

Mississauga, ON, Canada) at a wavelength of 234 nm according to Lambert-Beer with a molar extinction coefficient of 25000 M^{-1} cm^{-1} [10].

2.2.4 Enzyme Assay

HPL activity was monitored spectrophotometrically (Cary Bio 1, Varian, Mississauga, ON, Canada) at a wavelength of 234 nm, corresponding to the conjugated double bond of the substrates. Assays were carried out under temperature controlled conditions at 25 °C with mixing. A typical reaction mixture consisted of phosphate buffer (50 mM, pH 7) or hexane, 0-0.01 (w/w) % Triton X-100 R, 0-1.5 M KCl (in the case of phosphate buffer), 24 μM LA-OOH or LS-OOH and X μg of purified HPL. The enzyme was added in 20 μL aliquots, containing the appropriate concentration of KCl, resulting in a two phase system when hexane was used. The total reaction volume was 3 mL. The rate of decrease in absorbance at 234 nm was used to calculate the specific enzymatic activity A in μmol min^{-1} mg^{-1}.

2.2.5 Experimental Design

A full factorial design [11] was used for both aqueous and micro-aqueous conditions. The effects of the numerical factors (surfactant and salt concentration) as well as the categorical factor (substrate type) were assessed. Triton X-100 R concentrations ranged from 0 (-) to 0.01 % (w/w) (+) and KCl concentrations from 0 (-) to 1.5 M (+). Design points were assayed in triplicate, center points were replicated twice for each substrate, resulting in 28 runs for each design and 56 runs in total. The order of experiments was randomized. A schematic of the experimental design is shown in Fig. 7.

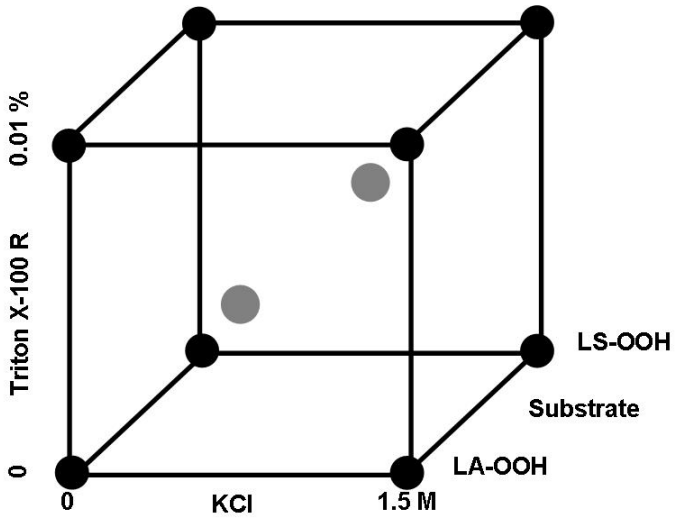

Fig. 7: Schematic Representation of the Experimental Design

Two full factorial designs were used for aqueous and micro-aqueous conditions. Triton X-100 R concentration ranged from 0 to 0.1% (w/w) and KCl concentration from 0 to 1.5 M. LA-OOH and LS-OOH were used as substrates. Design points (black) were assayed in triplicate; center points (grey) in duplicate [11].

2.3 Results and Discussion

2.3.1 HPL Expression and Purification

Expression and purification procedures for HPL from bell pepper, recombinantly expressed in *E. coli*, were used as described by Delcarte *et al.* [7] without further modification. Results in terms of yield and purity were in accord with the literature. Shake flask cultures (100 mL) yielded 20 mg L^{-1} of purified HPL. HPL purity was assessed by SDS-PAGE (Fig. 8). Under denaturing conditions, the gel showed a single band at about 50 kDa, which is expected for a single HPL subunit. Other protein impurities were below detection limits. The integrity of the heme centre of the enzyme was verified by UV-vis-spectroscopy, yielding a strong Soret peak with a maximum at 390 nm (data not shown).

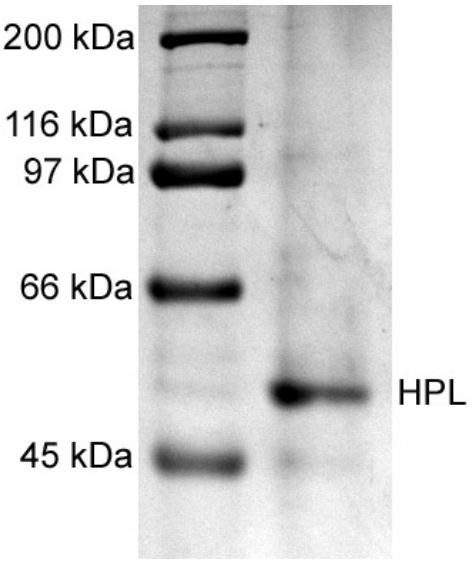

Fig. 8: SDS-PAGE of HPL

Molecular weight standards are shown in the left lane and the HPL preparation (right lane) shows a single band at about 50-55 kDa.

2.3.2 Substrate Synthesis

To date HPL activity has been assayed with two different classes of substrates: fatty acid hydroperoxides (e.g. LA-OOH) [1] and hydroperoxy fatty acid (ethanol)amides (e.g. LA-OOH ethanol amide) [12]. Both classes of substrate have little to no water solubility and so the influence of substrate dispersion and effect of surfactants on enzyme activity has not been studied and is not clearly understood. To gain a better understanding of the fundamentals governing HPL activity, and the role that the substrate plays in HPL activity, an alternative, water soluble substrate, as well as enzyme activity under micro-aqueous conditions was investigated.

LA-OOH synthesis was conducted according to the literature producing the anticipated yields, purity and level of conversion. LS-OOH was synthesized enzymatically from linoleyl sulfate. Both substrates were analyzed by UV-vis-spectroscopy as reported in Fig. 9 and TLC. The sharp peak centered at 234 nm for both substrates in Fig. 9 verifies the presence of the conjugated double bond introduced through the lipoxygenase reaction. Single spots in the TLC were observed for both substrates at $R_f = 0.73$ for LA-OOH and $R_f = 0.37$ for LS-OOH indicating the difference in substrate properties and their purity.

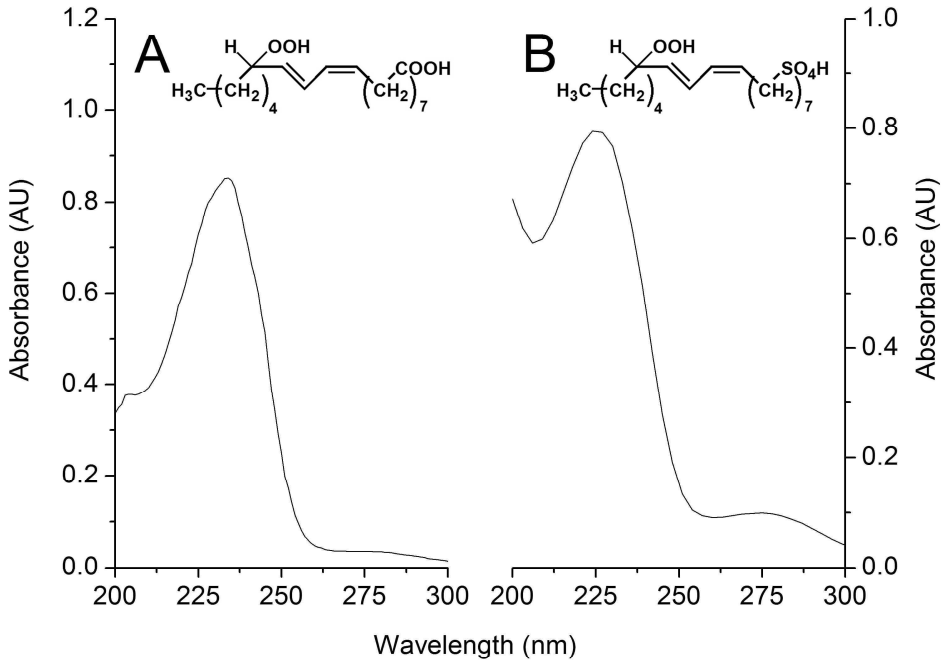

Fig. 9: UV-vis Spectra of (A) LA-OOH and (B) LS-OOH

2.3.3 HPL Activity Assay and Solvent Selection

HPL activity was assayed spectrophotometrically therefore the choice of solvent for the micro-aqueous conditions was limited to solvents with a UV-cutoff of about 220 nm or lower to avoid interference problems with the signal of the conjugated double bond. Another key parameter in the selection of solvents for enzymatic conversions is the octanol/water partition coefficient or Log P value. Generally, solvents with a Log P value of 4 or larger are considered to be suitable media for enzymatic conversions [13]. The selection of a solvent for any given system, however, depends largely on the properties of the specific enzyme and substrate and is, therefore, often made on an empirical basis. In this study, three different solvents were evaluated: hexane (Log P 3.944), methyl tert-butyl ether (1.147) and acetonitrile (-0.447), resulting in a two phase system for hexane and methyl tert-butyl ether and a one phase system for acetonitrile. HPL activity was observed in hexane and methyl tert-butyl ether but not in

acetonitrile (Fig. 10). The lack of activity in the acetonitrile may be attributed to the removal of bound water from the enzyme resulting in its inactivation. To our knowledge this is the first report on HPL activity under micro-aqueous conditions in solvents. For practical purposes, the remaining experiments for micro-aqueous conditions were carried out in hexane.

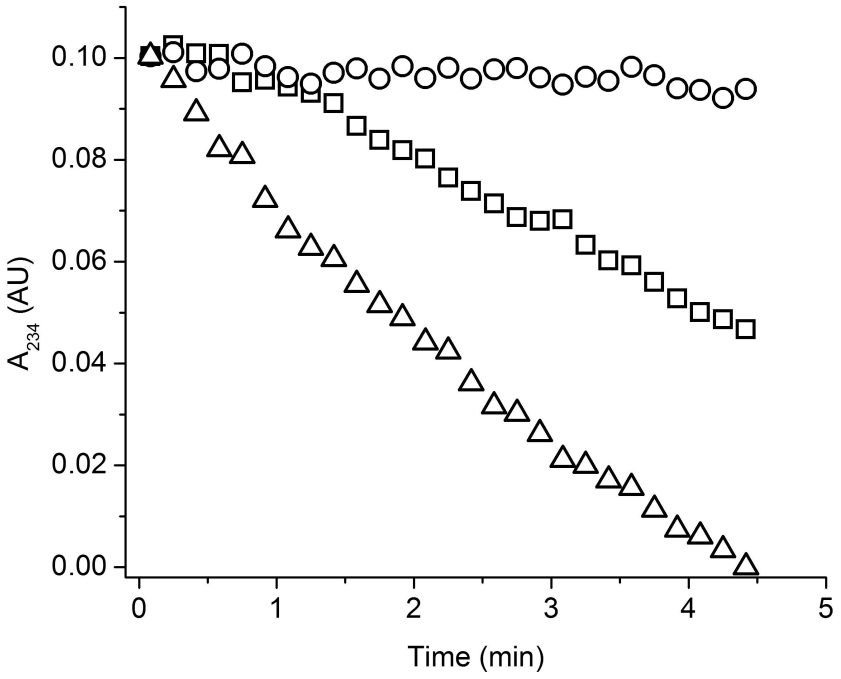

Fig. 10: Activity of HPL in Various Solvents

Time course of absorbance at 234 nm of LA-OOH in hexane (Δ), tert-methyl butyl ether (□) and acetonitrile (○). In all cases the LA-OOH concentration was 24 μM and HPL was added in 20 μL of phosphate buffer.

2.3.4 Experimental Design for HPL Activity

A factorial experimental design was used to quantify the effects of salt concentration, surfactant concentration, solvent and substrate on HPL activity. In addition to optimizing the number of required experiments, experimental design also reveals possible interactions between the selected factors, which to date with HPL hasn't been investigated. A Box Cox transformation of the activity data was performed [11]. The data of the aqueous design was transformed using the inverse square root, while the data of the micro-aqueous system was Log_{10} transformed. For both cases, a factorial model was set-up, using a half-normal probability plot to identify significant main effects and interactions. ANOVA showed the factorial model to be significant in both cases. Also, surfactant, salt, surfactant/salt interaction and salt/substrate interaction were identified as significant effects in both cases. The ANOVA results are summarized in Table 1.

Table 1: ANOVA for HPL Activity Model

	Aqueous				Micro-Aqueous			
Source	**DF**	**MS**	**Prob. > F**		**DF**	**MS**	**Prob. > F**	
Model	5	0.2558	< 0.0001	s.	5	0.5860	< 0.0001	s.
Surf.	1	0.0043	0.0319	s.	1	1.7522	< 0.0001	s.
Salt	1	0.3065	< 0.0001	s.	1	0.0850	0.0002	s.
Substr.	1	0.7313	< 0.0001	s.	1	0.9478	< 0.0001	s.
Surf. X Salt	1	0.0687	< 0.0001	s.	1	0.0229	0.0288	s.
Salt X Substr.	1	0.1594	< 0.0001	s.	1	0.1220	< 0.0001	s.
Curvature	1	0.0089	0.0036	s.	1	0.0118	0.1063	n.s.
Residual	20	0.0008			21	0.0042		
Lack of Fit	3	0.0015	0.1250	n.s.	3	0.0025	0.6505	n.s.
Pure Error	17	0.0007			18	0.0044		
Total	26				27			

Surf., surfactant; substr., substrate; DF, degrees of freedom; MS, mean squared; Prob., probablilty; F, F-statistics.

Only the aqueous scenario showed significant curvature but the lack of fit was not significant in either case. To further validate the model, predicted and actual values were plotted for both scenarios (Fig. 11). The predicted values were calculated from the model equations and show good correlation with the experimental values in both cases. The models that were developed can therefore be considered valid in describing the activity modulation of hydroperoxide lyase by salt, surfactant and substrate under aqueous and micro-aqueous conditions.

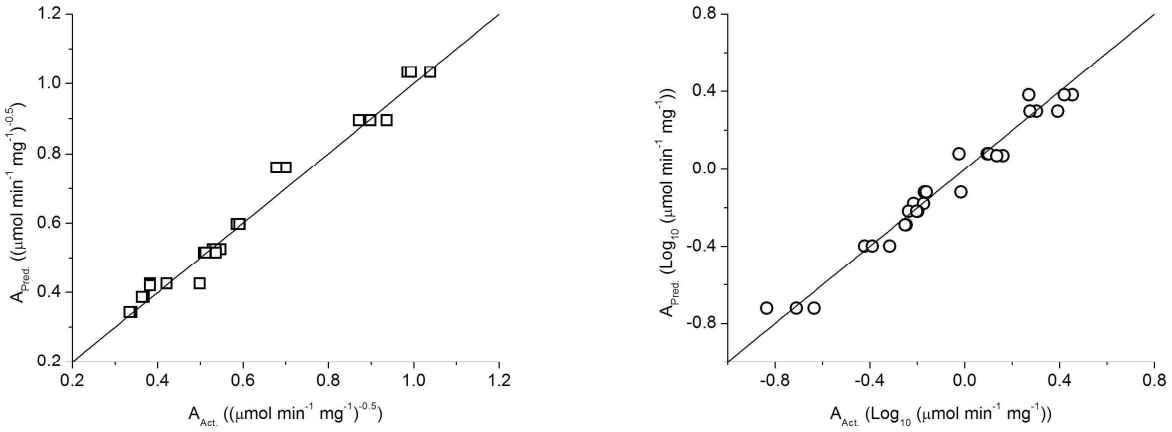

Fig. 11: Model Predictions for Aqueous and Micro-Aqueous Conditions

Plotted are the predicted and actual values for aqueous (□) and micro aqueous (○) conditions. The solid line (–) represents the ideal prediction.

To visualize and interpret the results, the data were split into four sets for the creation of response surface graphs: LA-OOH as substrate under aqueous conditions (A), LS-OOH under aqueous conditions (B), LA-OOH under micro-aqueous conditions (C) and LS-OOH under micro-aqueous conditions (D) (Fig. 12). The equations describing the four different scenarios are given below.

$$\left(\sqrt{A}\right)^{-1} = 0.52 - 13.75 \cdot Surf - 0.12 \cdot Salt + 14.65 \cdot Salt \cdot Surf \qquad \text{(A)}$$

$$\left(\sqrt{A}\right)^{-1} = 1.02 - 13.75 \cdot Surf - 0.34 \cdot Salt + 14.65 \cdot Salt \cdot Surf \qquad \text{(B)}$$

$$Log_{10} A = -0.4 + 47.87 \cdot Surf - 0.21 \cdot Salt + 8.23 \cdot Salt \cdot Surf \qquad \text{(C)}$$

$$Log_{10} A = -0.18 + 47.87 \cdot Surf - 0.03 \cdot Salt + 8.23 \cdot Salt \cdot Surf \qquad \text{(D)}$$

(A) to (D) show that salt concentration is the predominant effect in the aqueous system (A & B), whereas surfactant concentration is the predominant effect in the micro-aqueous system (C & D). Fig. 12 A depicts the scenario that has been previously described in the literature [5,6]. With increasing salt concentration from 0 to 1.5 M, HPL activity increases from 3.7 to 8.7 μmol min^{-1} mg^{-1}. Upon increasing the surfactant concentration (0 – 0.01 %) HPL activity increases from 3.7 to 6.8 μmol min^{-1} mg^{-1}. Both effects are, therefore, somewhat comparable in magnitude within the observed range of concentrations. However, due to the interaction of both phenomena, HPL activity is only 5.6 μmol min^{-1} mg^{-1} at high salt and surfactant concentrations. This interaction has not been previously described in the literature and is contradictory to the assumption that the salt and surfactant effects would be additive.

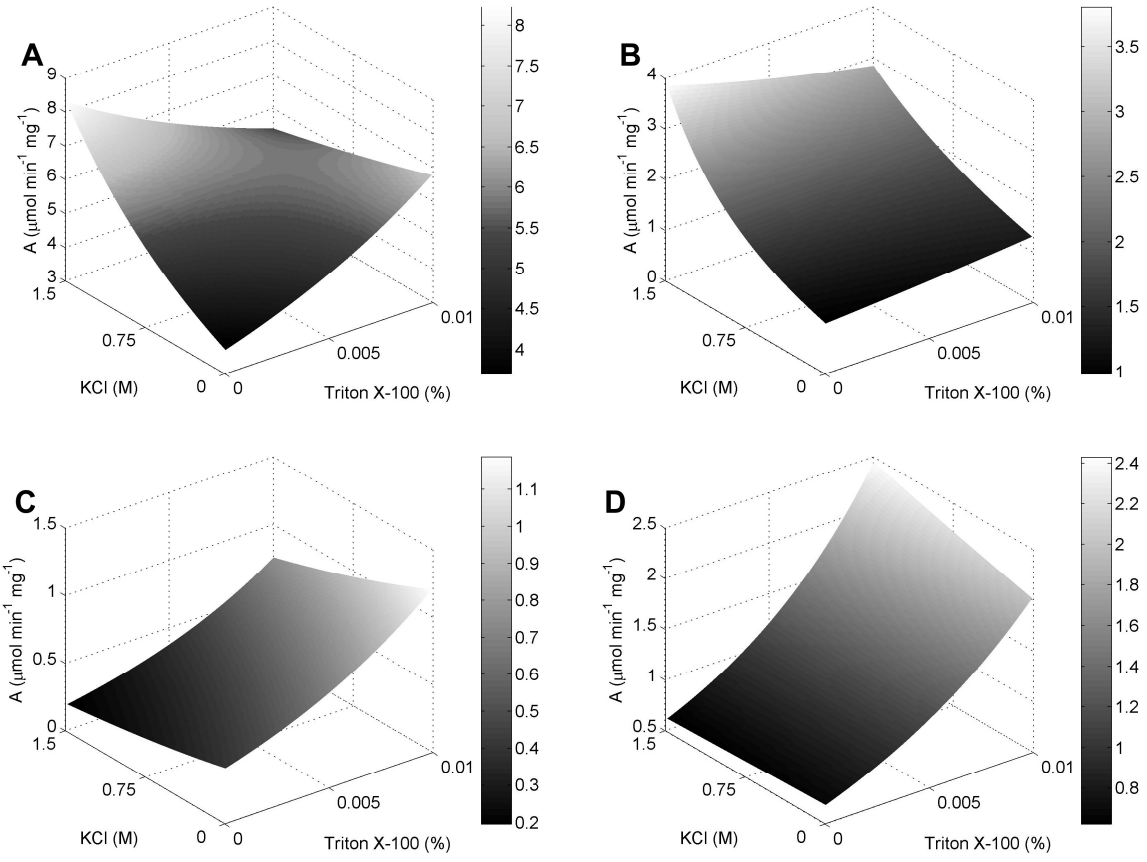

Fig. 12: Response Surface Plots for HPL Activity Under Various Conditions

The plots show HPL activity as calculated by the experimental design model under aqueous conditions with LA-OOH (A) and LS-OOH (B) as a substrate and under micro aqueous conditions with LA-OOH (C) and LS-OOH (D) as a substrate.

Fig. 12 B shows the HPL activity with the novel substrate LS-OOH under aqueous conditions. In absence of Triton X-100 R, HPL activity increases from 0.96 to 3.8 μmol min^{-1} mg^{-1} over the range of KCl concentrations used. The surfactant concentration on the other hand, shows only a slight effect on activity and only at higher salt concentrations.

Fig. 12 C and D show the activity response for HPL under micro-aqueous conditions. It can be clearly seen that, for both substrates, Triton X-100 R has the largest influence on enzyme activity. For LA-OOH activity increases from 0.39 to 1.2, for LS-OOH from 0.66 to 1.99 μmol min^{-1} mg^{-1}. A contrary salt-effect is visible for LA-OOH under micro-aqueous conditions. HPL

activity decreases with increasing salt concentration (e.g. from 0.4 to 0.19 μmol min^{-1} mg^{-1} at low Triton X-100 R concentrations) throughout the whole range of surfactant concentrations tested. For LS-OOH, the salt effect is only visible at higher surfactant concentrations and is consistent with the observations for LS-OOH under aqueous conditions, but much smaller: HPL activity increases from 1.99 to 2.38 μmol min^{-1} mg^{-1} at high Triton X-100 R concentrations. Maximal activity (8.7 μmol min^{-1} mg^{-1}) is achieved under aqueous conditions with high salt and low surfactant concentrations and LA-OOH as a substrate. Maximal activity (2.4 μmol min^{-1} mg^{-1}) under micro-aqueous conditions is achieved with high salt and surfactant concentrations and LS-OOH as a substrate.

Fig. 12 reveals the complexity of effects in this system. The influence of several factors has to be considered for interpretation. For example, the surfactant Triton X-100 R affects HPL directly, but also has an effect on the solubility of sparsely water soluble components such as LA-OOH. Under aqueous conditions (scenarios A & B) the predominant effect of salt can be attributed to a possible increase in HPL stability. HPL is believed to be a multimeric enzyme in its native state [1] and high salt concentrations are known to affect inter-subunit interaction [14]. HPL could therefore be kept in a stable native conformation resulting in a higher activity.

Under micro-aqueous conditions (scenario B & C), the presence of salt has less of an effect on HPL activity. Under micro-aqueous conditions the salt would remain exclusively in the aqueous phase; the enzyme will also likely be located in this phase or at the interface of the phases. The limited volume of available water could therefore be responsible for a more rigid conformation of HPL, so the presence of the salt would have a reduced effect on the enzyme. Another possible explanation is that the enzyme was located at the interface and that this interfacial positioning caused a more native and stable/active conformation. This is known to be the case for some membrane associated enzymes and enzymes involved in lipid transformations [15].

The effect of Triton X-100 R on HPL is different for scenarios A and B. For LA-OOH, a beneficial effect can be seen, whereas the effect of surfactant on the activity for the water soluble LS-OOH substrate is minimal at higher salt concentrations. It is reasonable that the predominant mode of action of surfactant in aqueous systems is an increase in substrate solubility. The direct activity modulation of HPL, in which the surfactant is believed to interact

with HPL, may still be in place, but does not show the same magnitude as the salt effect or the influence of Triton X-100 R on LA-OOH solubility.

The importance of Triton X-100 R in the two phase system can be seen in Fig. 12 C and D. Several modes of action could operate simultaneously. Triton X-100 R could increase the activity by increasing the interface surface area and/or it could be involved in facilitating mass transfer of substrate and products between the two phases. The salt/surfactant interaction is most prominent in scenario A (Fig. 12 A). Triton X-100 R is a non-ionic surfactant so a direct interaction of salt and surfactant molecules seems unlikely. It may be that both factors enhance HPL activity by non-compatible exclusive mechanisms. The salt/substrate interaction as identified by ANOVA (Table 1) can not be seen from Fig. 12, because the data was blocked by substrates. However, a direct interaction of anionic substrate molecules (carboxylates and sulfates) with K^+ ions at high salt concentrations seems likely. Polarity of the substrate head group was found to be a crucial feature for good HPL activity [12]. High salt concentrations could mask the head group charge, hence diminishing HPL activity to some extent.

2.4 Conclusion

The objective of the work presented here was to develop a better understanding of the factors which modulate HPL activity by using novel reaction media and substrates. HPL activities under micro-aqueous conditions and with the novel substrate LS-OOH are described for the first time. The effect of salt, surfactant, solvent and substrate on HPL activity was assessed by means of experimental design. It was found that HPL activity is maximal at high salt and low surfactant concentrations under aqueous conditions with LA-OOH as a substrate. Furthermore, an influence of the surfactant Triton X-100 on solubility properties of the system and resulting HPL activity were identified. The interaction of different effects was found to be significant, which is in contrast to previously reported findings [5]. Specifically, a salt/surfactant interaction under aqueous conditions with LA-OOH as a substrate revealed the complexity of the investigated effects, which do not combine additively.

This work represents a step towards the use of HPL for the production of value added compounds. The results obtained can aid in the choice of reaction conditions and in the design of a suitable immobilization supports, which will ultimately be needed for feasible biotransformation reactions[2].

[2]The Appendix (A) for this chapter contains *E. coli* growth curve data, 13-HPL kinetics, 13-HPOD calibration data and HPL-activity model data.

2.5 References

[1] Noordermeer, M. A.; Veldink, G. A.; Vliegenthart, J. F. G. Fatty Acid Hydroperoxide Lyase: A Plant Cytochrome P450 Enzyme Involved in Wound Healing and Pest Resistance. *Chembiochem* **2001**, *2*, 494-504.

[2] Vick, B.; Zimmerman, D. Identification of Linoleate Hydroperoxide Lyase in Germinating Watermelon Seedlings. *Plant Physiol.* **1975**, *56*, 84.

[3] Matsui, K.; Ujita, C.; Fujimoto, S.; Wilkinson, J.; Hiatt, B.; Knauf, V.; Kajiwara, T.; Feussner, I. Fatty Acid 9-and 13-Hydroperoxide Lyases From Cucumber. *FEBS Lett.* **2000**, *481*, 183-188.

[4] Matsui, K.; Miyahara, C.; Wilkinson, J.; Hiatt, B.; Knauf, V.; Kajiwara, T. Fatty Acid Hydroperoxide Lyase in Tomato Fruits: Cloning and Properties of a Recombinant Enzyme Expressed in Escherichia Coli. *Bioscience Biotechnology and Biochemistry* **2000**, *64*, 1189-1196.

[5] Koeduka, T.; Stumpe, M.; Matsui, K.; Kajiwara, T.; Feussner, I. Kinetics of Barley FA Hydroperoxide Lyase Are Modulated by Salts and Detergents. *Lipids* **2003**, *38*, 1167-1172.

[6] Noordermeer, M. A.; Veldink, G. A.; Vliegenthart, J. F. G. Spectroscopic Studies on the Active Site of Hydroperoxide Lyase; the Influence of Detergents on Its Conformation. *FEBS Lett.* **2001**, *489*, 229-232.

[7] Delcarte, J.; Fauconnier, M. L.; Jacques, P.; Matsui, K.; Thonart, P.; Marlier, M. Optimisation of Expression and Immobilized Metal Ion Affinity Chromatographic Purification of Recombinant (HiS)(6)-Tagged Cytochrome P450 Hydroperoxide Lyase in Escherichia Coli. *Journal of Chromatography B-Analytical Technologies in the Biomedical and Life Sciences* **2003**, *786*, 229-236.

[8] Nunez, A.; StArmand, G.; Foglia, T. A.; Piazza, G. J. Immobilization of Hydroperoxide Lyase From Chlorella. *Biotechnology and Applied Biochemistry* **1997**, *25*, 75-80.

[9] Mogul, R.; Johansen, E.; Holman, T. R. Oleyl Sulfate Reveals Allosteric Inhibition of Soybean Lipoxygenase-1 and Human 15-Lipoxygenase. *Biochemistry* **2000**, *39*, 4801-4807.

[10] Vick, B. A. A Spectrophotometric Assay for Hydroperoxide Lyase. *Lipids* **1991**, *26*, 315-320.

[11] Montgomery, D. C. *Design and Analysis of Experiments*; John Wiley & Sons, Inc.: New York, 2001.

[12] van der Stelt, M.; Noordermeer, M. A.; Kiss, T.; van Zadelhoff, G.; Merghart, B.; Veldink, G. A.; Vliegenthart, J. F. G. Formation of a New Class of Oxylipins From N-Acyl(Ethanol)Amines by the Lipoxygenase Pathway. *Eur.J.Biochem.* **2000**, *267*, 2000-2007.

[13] Laane, C.; Boeren, S.; Vos, K.; Veeger, C. Rules for Optimization of Biocatalysis in Organic-Solvents. *Biotechnol.Bioeng.* **1987**, *30*, 81-87.

[14] Chi, E. Y.; Krishnan, S.; Randolph, T. W.; Carpenter, J. F. Physical Stability of Proteins in Aqueous Solution: Mechanism and Driving Forces in Nonnative Protein Aggregation. *Pharm.Res.* **2003**, *20*, 1325-1336.

[15] Gelb, M. H.; Min, J. H.; Jain, M. K. Do Membrane-Bound Enzymes Access Their Substrates From the Membrane or Aqueous Phase: Interfacial Versus Non-Interfacial Enzymes. *Biochimica et Biophysica Acta-Molecular and Cell Biology of Lipids* **2000**, *1488*, 20-27.

Chapter 3

Preparation and Methodology for Chemical Mapping of Sol-gel Thin Films Containing Lysozyme[3]

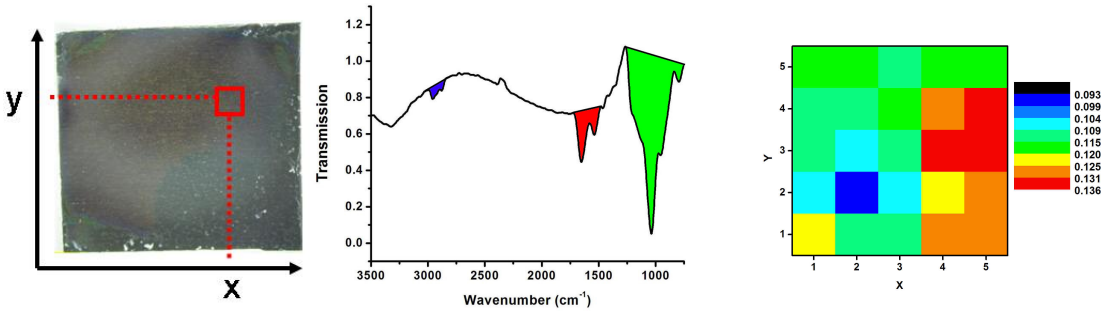

[3] This chapter is co-authored by Christoph Nacke and Dominik Jürgen-Lohmann. Christoph Nacke contributed in part to the planning, execution and interpretation of some of the work reported in this chapter.

Preface

The use of sol-gel thin films for the immobilization of biomolecules presents several potential advantages. The three most prominent advantages are 1) the opportunity to develop a relatively wide range of material properties through precursor choice and additives; 2) optical transparency, which allows for spectroscopic analysis or use in optical sensors and 3) sub micron thickness, which greatly improves substrate and product diffusion properties compared to bulk materials.

There were two main challenges associated with this aspect of the thesis. The first was the choice of a suitable carrier material that would lend itself to spectroscopic analysis and secondly the development of an appropriate biocompatible coating formulation. These challenges are not mutually exclusive as carrier material and coating formulation also have to be compatible with each other. The coating technique described in this chapter is the result of a thorough screening of several coating techniques, materials and formulations. Three coating techniques were originally evaluated: dip coating, spin coating and evaporation coating. Spin coating, the deposition of a small amount of coating solution on a rotating substrate, was found superior to dip coating (the withdrawal of a substrate from a coating solution reservoir at a controlled rate) because more films could be created with the same amount of coating solution. In the case of spin coating a quality apparatus was available allowing the production of superior films. Evaporation coating was dismissed as an appropriate approach as it requires a large amount of solvent and although it produces films of excellent quality, it is not suitable for biological applications due to sensitivity of most biomolecules to many of the necessary solvents.

A number of materials were examined as possible support materials including glass, various polymer sheets, NaCl discs and aluminum. Glass provided an excellent substrate for adhesion of the sol-gel thin films; however, because of the chemical similarities of glass and sol-gel, IR investigations are difficult. Nevertheless, glass slides proved to be suitable for fluorescence applications as discussed in Chapter 5. The polymers that were examined provided good adhesion for more hydrophobic films (polytetrafluoroethylene (PTFE)) and for more hydrophilic films (polyethylene (PE), polypropylene (PP), polyacetate (PA) and polyethylene terephthalate (PET)). However, none of these supports were suitable for IR

analysis as they display a strong background absorbance (PE, PP, PA and PET) or poor transmissive properties (PTFE). The use of NaCl discs was not pursued after initial exploratory work, since sol-gel adhesion was problematic and there were solubility issues associated with the NaCl. Aluminum was found to be the best of the carriers tested since good adhesion properties were displayed for a range of sol-gel materials and it possessed excellent IR reflectance properties with virtually no background signal.

Sol-gel thin film coatings are well established in material science. Sol-gel coated surfaces show improved characteristics and a broad spectrum of properties which include altered color, reflection, conduction or scratch resistance of the coated material. Industrial protocols almost exclusively feature a high temperature sintering step following the deposition of the sol-gel film on the solid support. This curing measure leads to homogeneous structures of high stability, but is inapplicable for bioimmobilization due to the temperature sensitivity of most biological molecules. Therefore, the creation of a stable adherent film under mild processing conditions is a major challenge of sol-gel thin film enzyme immobilization which needed to be addressed in this thesis. The protocol developed that was used in this work is the result of an extensive literature review and an effort to reduce the amount of alcohol to minimize adverse effects on the enzymes being considered.

The enzyme used for immobilization in these studies was chosen primarily for practical purposes. Lysozyme is available in large quantities at high purity and can be readily detected by FTIR spectroscopy.

Summary

Sol-gels are seeing widespread interest as suitable materials for the immobilization of biomolecules in applications ranging from optical coatings to specialty biocatalysts. Although there are numerous studies that have characterized these materials in terms of their macroscopic properties, few studies have examined and correlated these properties at the microscopic level. This study describes a spin-coating technique for the preparation of aluminum-supported sol-gel thin films containing immobilized lysozyme [E.C. 3.2.1.17] that are suitable for chemical mapping using FTIR microscopy operating in reflectance mode. This type of information can then be used to understand a variety of aspects of these materials which can be used for optimal engineering of these materials, as well as insightful design and modeling. A data analysis method was developed to extract information on chemical speciation and domain information on the materials from FTIR data matrices. Results from these studies indicated that, contrary to what might be expected, these sol-gels are not homogeneous on the microscopic level. Instead, they are heterogeneous in both the distribution of lysozyme and hydrophobic monomers at the scale investigated (20 μm resolution). The method described here has promise in terms of providing a non-invasive approach of chemically mapping concentrations of proteinaceous and related substances as well as chemical domains *in situ* in sol-gel thin films.

3.1 Introduction

Many enzymatic reactions yield products of commercial interest [1]. However, there is a large discrepancy between the biological diversity of enzymatic reactions and the relatively small number of enzyme-based processes established in industry. Some of this discrepancy can be attributed to the necessity to immobilize enzymes for efficient use and in the shortcomings associated with the current state of enzyme immobilization technology.

Common problems can include: inactivation of the immobilized species, e.g. caused by protein aggregation, or mass transfer limitations leading to low efficiency immobilized biocatalysts. Traditionally, macroscopic analyses were used to address these issues with limited success. However, progress in instrumentation now allows for a variety of microscopic techniques to be used to characterize immobilized enzyme systems. Similarly, advances in material science have led to a variety in novel materials, such as silica sol-gels, with predefined properties suitable for enzyme immobilization. Both these advances have resulted in a recent gain in the understanding of immobilized enzyme systems in these matrices [2].

Sol-gels can be made from siloxane precursors that readily undergo hydrolysis and polycondensation to form a porous matrix. Sol-gels are particularly interesting for enzyme immobilization as they combine mild processing conditions, a range of predefined material properties (e.g. hydrophobicity, pore size etc.) and are typically well suited for spectroscopic applications [3]. The ability to form sol-gel thin films is an advantage as this is an ideal sample format for the investigation of material properties since they can be fabricated in sub-micron thicknesses which are well suited for spectroscopic analysis. The field has been regularly reviewed and research related to immobilization of biologicals in sol-gel matrices has intensified significantly recently [4-6].

Fourier transform infrared (FTIR) spectroscopy is a well established and powerful tool for the identification of chemical groups within a molecule or mixtures of molecules [7]. By analyzing the features of a recorded infrared spectrum, the composition or the structure of chemical components can be determined [8]. FTIR spectra of pure compounds are generally so unique that they are referred to as a “molecular fingerprint". FTIR microscopy combines this detection power with spatial resolution to obtain localized data from a sample. Modern

detectors and precision motorized stages in combination with a microscope now make it possible to reliably map small areas [9]. Through automated scanning of grids chemical maps can be created at reasonable resolution for multiple components simultaneously. Synchrotron FTIR microscopy has been successfully implemented to determine lipase distribution in a commercially available lipase preparation [10]. An FTIR microscopy approach was used here to characterize the distribution of a model enzyme lysozyme in a silica sol-gel thin film. The focus of this chapter is the preparation of a suitable sol-gel thin film format for FTIR microscopy and an approach for the analysis of the acquired FTIR maps.

3.2 Materials and Methods

3.2.1 Materials

Lysozyme from chicken egg white [E.C. 3.2.1.17] (Sigma, Oakville, ON) was used without further purification (95 % purity with the remaining 5 % being primarily buffer salts; 46,200 U mg^{-1} solid). Tetraethoxysilane (TEOS) (98 %, Sigma, Oakville, ON), propyltrimethoxysilane (PTMS) (98 %, Fluka Chemicals, Oakville, ON) and 2-amino-2-(hydroxymethyl)propane-1,3-diol (TRIS) (Baker Chemicals, Phillipsburg, NJ) were used as received. Aluminum sheet metal (Alcan Inc., Montreal, QC) of 1 mm thickness was cut into 10 mm x 10 mm squares with a sheet metal notcher, ensuring a flat surface. After cutting, the carrier material was washed twice with Alconox detergent solution (Alconox Inc., White Plains, NY) on an orbital shaker and rinsed with deionized water followed by two washes with acetone. Two hours prior to spin coating, the aluminum carriers were surface treated in 2 N NaOH for 40 sec followed by consecutive rinses with deionized water. The carrier was dried under a stream of N_2 gas and any excess $NaAl(OH)_4$ was wiped from the carrier surface using a lint-free tissue paper (Kimwipes, VWR, Mississauga, ON). Carriers were stored in desiccators and any surface dust removed by purging with a stream of nitrogen gas prior to use.

3.2.2 Sol-gel Preparation

All liquid components were microfiltered using a 0.2 μm Pall Gelman Laboratories Aerodisc syringe filters (Sigma, Oakville, ON) for particle removal. TEOS and PTMS were hydrolyzed separately by sonication for 2 h (TEOS) or 4 h (PTMS) in 1.67 mM HCl using a stoichiometric water:monomer ratio of 4:1. Hydrolyzed monomer batches were stored at -20°C for a maximum of one week. Ethanol was added at a concentration of 20 % (v/v) 10 min prior to coating to improve the coating properties. Polycondensation was initiated by mixing equal volumes of the hydrolyzed monomers with a starting buffer consisting of 10 mM TRIS at pH 7.2, 100 mM KCl and the desired amount of lysozyme. Chemical structures of the monomers and sample polymer structure are given in Fig. 13.

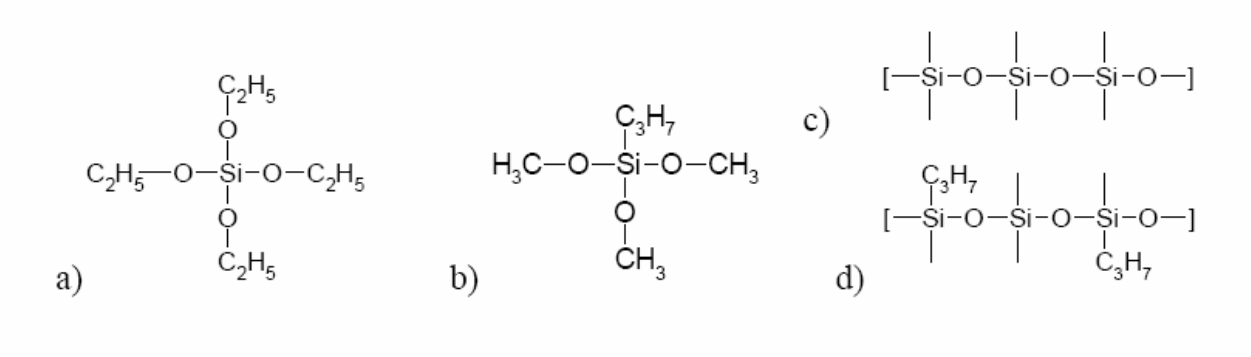

Fig. 13: Sol-gel Monomers and Sample Polymer Structures

The two types of monomers used in this study are tetraethoxysilane (TEOS) (a) and propyltrimethoxysilane (PTMS) (b). Possible polymer repeating units are displayed for a pure TEOS gel (c) and an organically modified gel consisting of a TEOS/PTMS mixture (d).

3.2.3 Spin Coating

Samples were coated on a custom-built spin coater with rotation speed control and vacuum chuck. Spin coating was conducted in a dust free environment to avoid contamination of the gel coat. Monomer hydrolysate and buffer solution were mixed directly before coating. The best results in terms of the coating process were achieved when the process was initiated 8-10 sec after mixing. Twenty μL of sample was applied in a single step to the centre of the carrier rotating at 3000 rpm and spun for 60 sec. Coated samples were stored in dust free containers at ambient temperature prior to analysis. Details on the experimental procedure can be found in the appendix.

3.2.4 FTIR Microscopic Mapping

FTIR microscopic mapping was conducted using a Hyperion 2000 microscope and a Tensor 27 FTIR spectrometer (Bruker Optics, Milton, ON). Spectra acquisition and evaluation were performed with OPUS 4.2 software using the 3D and MAP packages (Bruker Optics, Milton, ON). Spectra were recorded over a wavenumber range from 3500 cm^{-1} to 700 cm^{-1} at a resolution of 4 cm^{-1} in reflectance mode. Background spectra were averaged from 64 scans and each grid spectrum from 52 scans. A background spectrum was recorded after scanning the entire grid and compared to the initial background. All grid scans were conducted with an aperture of 20 μm x 20 μm and a step width of 20 μm. Below this aperture size the signal to noise ratio was too low. The grid position was automatically

controlled by a motorized stage with 1 μm resolution. All samples were analyzed in randomized order. No sol-gel aging effects were observed for samples stored up to 2 weeks.

3.3 Results and Discussion

3.3.1 Properties of Lysozyme Doped Thin Films

Three main factors influence the formation of thin films during spin coating: surface characteristics of the carrier, revolution speed and the viscosity of the liquid [11-13]. Although doped sol-gel thin films have already been described on different substrates (primarily glass), some substrates are incompatible with FTIR analysis. Moreover, a suitable carrier material has to be compatible with the desired sol-gel composition. In this study, the viscosity of the liquid rapidly changed during the coating process because the polycondensation of the sol was initiated before coating. The quality of the thin film was therefore highly dependent on the elapsed time between mixing and coating. The best results were achieved when the sol was applied 8-10 sec after mixing the hydrolysate with the lysozyme/buffer solution. Periods longer than 8-10 sec resulted in uneven coatings and incomplete coverage of the carrier. In order to ensure similar surface features, all carriers were pretreated in 2 N NaOH for 40 sec. This base treatment significantly improved coating results. In addition, base treatment roughened the surface resulting in stronger adhesion of the gel layer to the carrier. The reflective properties of aluminum in the infrared range were good and the signal intensities achieved were roughly three times higher than those obtained with samples prepared on 4 mm thick NaCl crystal windows. Additionally, the surface properties of NaCl did not permit acceptable coverage or film formation.

One of the most likely applications of doped sol-gel thin films are biosensors, in which metals are often used as support to enable amperometric measurements. Therefore aluminum also represents a carrier with some potential of practical application.

The properties of the sol-gel thin films changed significantly in the presence of enzyme or organically modified precursors. Table 2 qualitatively summarizes the gelation time and adhesion to the aluminum carrier of doped and blank sol-gel thin films. The range of enzyme loads investigated was from 0 to 100 mg mL^{-1} of lysozyme in the sol/buffer mix, a typical range found in literature [6]. The presence of lysozyme resulted in a significantly

shorter gelation time. As soon as amounts as small as 1 mg mL^{-1} of enzyme were incorporated, the bulk gelation time dropped from approximately 20 min to 2 min, regardless of the presence and concentration of modified precursors. No differences were observed between low and high enzyme concentrations. Shortened gelation times were also observed with bovine serum albumin (BSA) as an immobilized species (data not shown). It could therefore be inferred that the macromolecules might serve as nucleation cores for the hydrolytically labile sol-gel precursors and that the effect was not related to the enzyme's catalytic properties.

Table 2: Coating Properties of Lysozyme Doped Sol-gels in Relation to the Proportion (% (v/v)) of Hydrophobic Monomer PTMS in the Gel.

Property	**Lysozyme doped (50-100 mg mL^{-1})**		**Without lysozyme**	
	≤ 40 % (v/v) PTMS	**>40 % (v/v) PTMS**	**≤ 40 % (v/v) PTMS**	**>40 % (v/v) PTMS**
Gelation time	~2 min	~2 min	~20 min	~20 min
Adhesion to carrier in liquid state	Good, even surface formed	Poor, formation of gel drops on carrier surface	Good, even surface formed	Poor, formation of gel drops on carrier surface
Adhesion to carrier in solid state	Good, no exfoliation	Poor, exfoliation under light mechanical stress	Good, no exfoliation	Mediocre, exfoliation under medium mechanical stress

Note: For all gels the molar ratio of water to monomer for hydrolysis was 4:1, which is the required stoichiometric ratio. All aluminum carriers were base treated and coated under identical conditions.

The PTMS fractions investigated in this study ranged from 0 to 40 % (v/v). Above a PTMS content of 40 % the aluminum carrier could not be properly coated with the sol-gel thin film. Two phenomena were observed above 40 % PTMS. The sol no longer formed an even layer during spin coating, but rather formed drops or patches of gel. Additionally, the adhesion to the carrier material decreased significantly with increasing PTMS content. While thin films of low PTMS content were mechanically stable, those with high PTMS content

tended to curl off the carrier under light mechanical stress. Drop formation and patchy coverage can be attributed to a decrease in substrate wettability. The maximum content of organically modified precursors of 40 % reported here is relatively low compared to studies carried out with sol-gel monoliths or powders, where organically modified precursors can be incorporated in ratios as high as 90 % [14].

3.3.2 Chemical Analysis and Characterization

Fig. 14 shows three sample spectra for sol-gel thin films which contain (a) no lysozyme and only TEOS precursors, (b) a typical lysozyme load of 75 mg mL^{-1} and only TEOS precursors and (c) a typical lysozyme load of 75 mg mL^{-1} with 40 % (v/v) PTMS. Three regions of the FTIR spectra were used to characterize the sol-gel thin films: amide region (1710-1490 cm^{-1}), aliphatic region (2980 -2830 cm^{-1}) and silicon region (1250-790 cm^{-1}). The amide region consists of an amide I and amide II band. The amide I band represents a C=O stretching vibration occurring at every amide bond within the protein backbone. The amide II band is the result of the combined C-N stretching and C-H bending vibrations within the methyl group and the C-H stretching vibration in the methylene group as well as degenerate carbon-hydrogen vibrations within the aliphatic chain [7,8]. Fig. 13 shows that PTMS can be easily identified in this system by its aliphatic group. The silicon region is visible in all three sample spectra and consists of three main peaks arising from Si-O-Si and Si-O-H stretching vibrations [7]. The Si-O-H band is present due to incompletely polymerized sol-gel [15]. Table 3 summarizes the absorption wavenumbers and the associated vibrations.

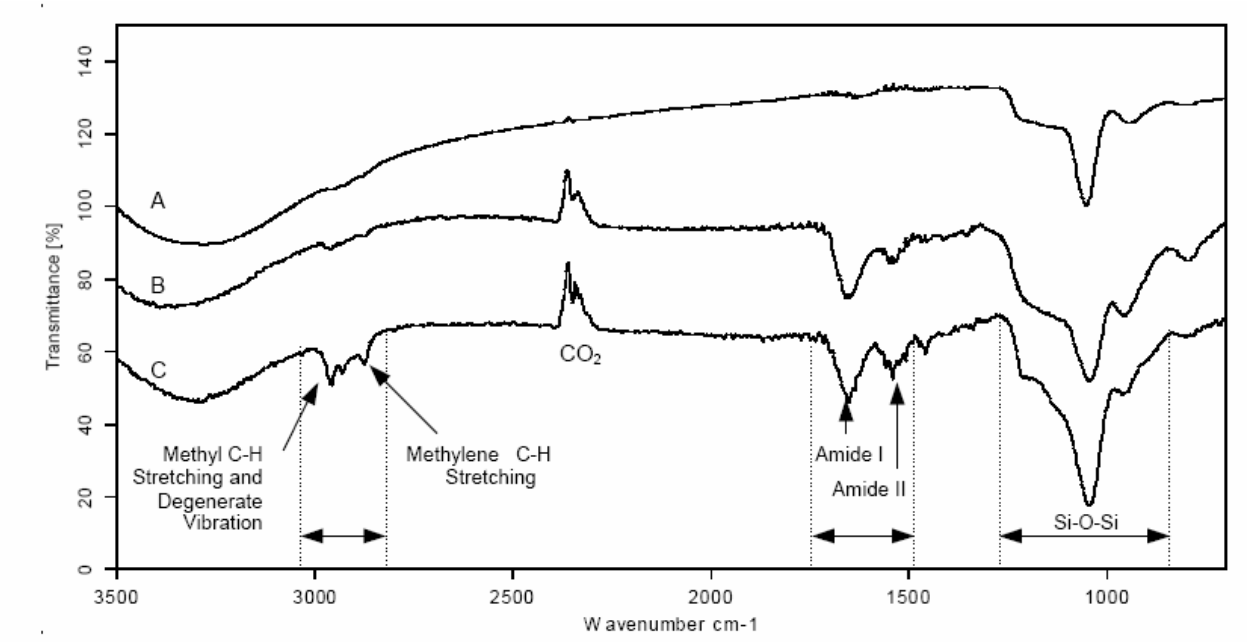

Fig. 14: Sample FTIR Spectra of the Three Peak Groups Used in Chemical Mapping

(A) Sol-gel thin film containing 0 % (v/v) PTMS and 0 mg mL^{-1} L lysozyme; (B) Sol-gel thin film containing 0 % (v/v) PTMS and 75 mg mL^{-1} lysozyme; and (C) Sol-gel thin film containing 40 % (v/v) PTMS and 75 mg mL^{-1} lysozyme [7].

The signals of all three characteristic regions consisted of several overlapping peaks. Therefore, the peak region was integrated for quantification with a straight baseline method. The baseline was defined by the transmission values at the start and at the end points of each region. To minimize noise influence, the transmittance values at the start and end points were determined by calculation of the mean transmittance of two data points at each respective position in the spectrum. The two data points at each end of the baseline were the first point of the respective wavenumber range and a second point 10 cm^{-1} towards the centre of the peak group. The wavenumber ranges used in the automatic integration were 1710-1490 cm^{-1} for the amide peak group, 2980-2830 cm^{-1} for the aliphatic peak group and 1250-790 cm^{-1} for the silicon peak group. No spectra corrections such as baseline straightening were conducted before the integration.

The peak area is proportional to the amount of a given chemical species according to Lambert-Beer's law [10]. The relative concentration of the respective chemical groups was obtained using the ratio of the area of the chemical group to the area of the silicon group for each individual position scanned in the sample. This approach compensates for variations in

the film thickness, because according to Lambert-Beer's law, the area of the silicon peak group is proportional to the film thickness. Division of the amide or aliphatic area by the silicon area lead to a dimensionless value representing the relative concentration of the respective component in the sol-gel layer at each specific position. The approach also compensated for variations in the reflectance of the carrier material, because amide, aliphatic and silicon peak areas were affected equally by variations in signal intensity.

Table 3: Peak Assignment for Amide, Aliphatic and Silicon Chemical Groups [7]

Wavenumber (cm^{-1})	Assignment
2930, 2850	Methylene C-H stretching (two modes)
2900, 2870	Methyl C-H stretching (two modes) and C-H degenerate vibration
1650	Amide I for secondary amides in solid state
1540	Amide II for secondary amides in solid state
1050	Si-O-Si stretching
850	Si-OH stretching

Since most amino acids contain aliphatic chains, the aliphatic signal cannot be attributed exclusively to the modified precursor PTMS. However, compared to the signal intensity of PTMS, the aliphatic signal due to amino acids in the lysozyme was small (Fig. 14). In a gel containing the highest lysozyme load (100 mg mL^{-1}) and the lowest PTMS content (10 % (v/v)) the share of the aliphatic peak caused by lysozyme was 5.5 %. Since the influence of lysozyme on the aliphatic signal is proportional to the area of the amide peak group, an empirical correlation was used to compensate for the contribution of those groups when PTMS was present.

3.3.3 Chemical Mapping

Fig. 15 is a flow diagram that illustrates the sequence of steps from scanning the grid to converting the data in the matrix to a chemical map. The first step in the method involved scanning the area of interest on the aluminum carrier with an appropriate aperture necessary to provide reasonable resolution. Each position in the grid, or pixel, corresponds to one FTIR spectrum. The location of each pixel is determined by a motorized computer-controlled stage used to move the sample. After acquisition of all spectra, the areas of each characteristic group in the spectrum were integrated and the ratios between the areas were used to calculate the relative concentrations of the chemical groups in each pixel. The chemical map was constructed by calculation of the relative concentration of each characteristic group for every pixel. Finally, a threshold limit was set for the relative concentration in order to produce a binary distribution of chemical composition that could be used for evaluation of chemical clusters.

The relative concentration data can be visualized as a surface plot. Typical raw data for a grid scan in the form of surface plots of the amide and aliphatic groups is shown in Fig. 16. The 500 μm x 500 μm area was scanned with a 20 μm x 20μm aperture and a step width of 20 μm to give a grid of 625 pixels. Both surface plots show that the distribution of functionalities was not homogenous throughout the region scanned. The relative concentrations of amide and aliphatic groups were used to indicate the relative concentrations of lysozyme and PTMS, respectively. By plotting the relative concentrations of PTMS and lysozyme, chemical maps of these components within sol-gel thin films can be generated. Variations in film thickness and carrier reflectance are compensated for if the relative concentration of a component is calculated by determining the ratio of the respective peak over the silicon peak.

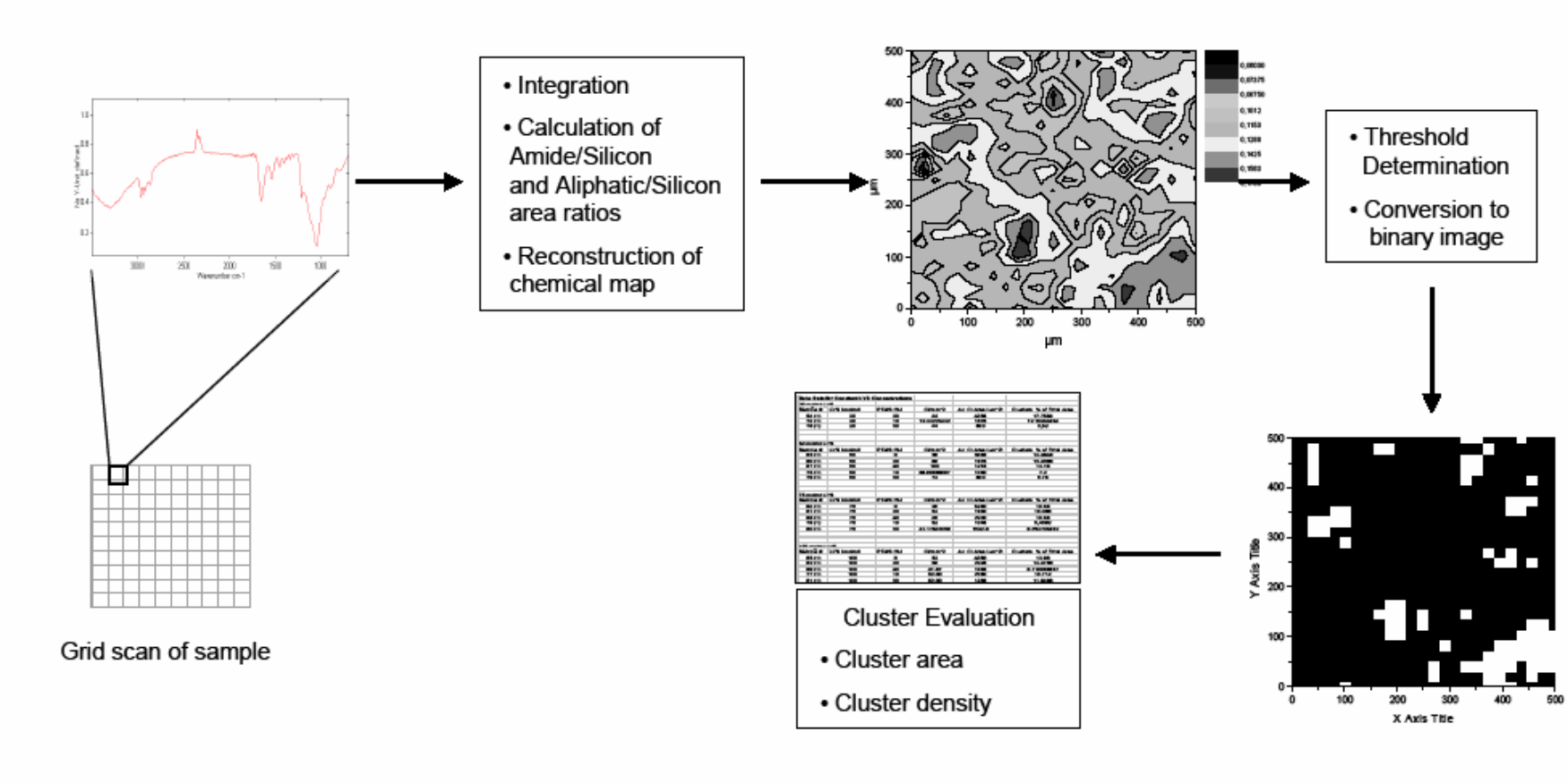

Fig. 15: Schematic of the Sequence of Steps for Chemical Mapping of Sol-gel Thin Films

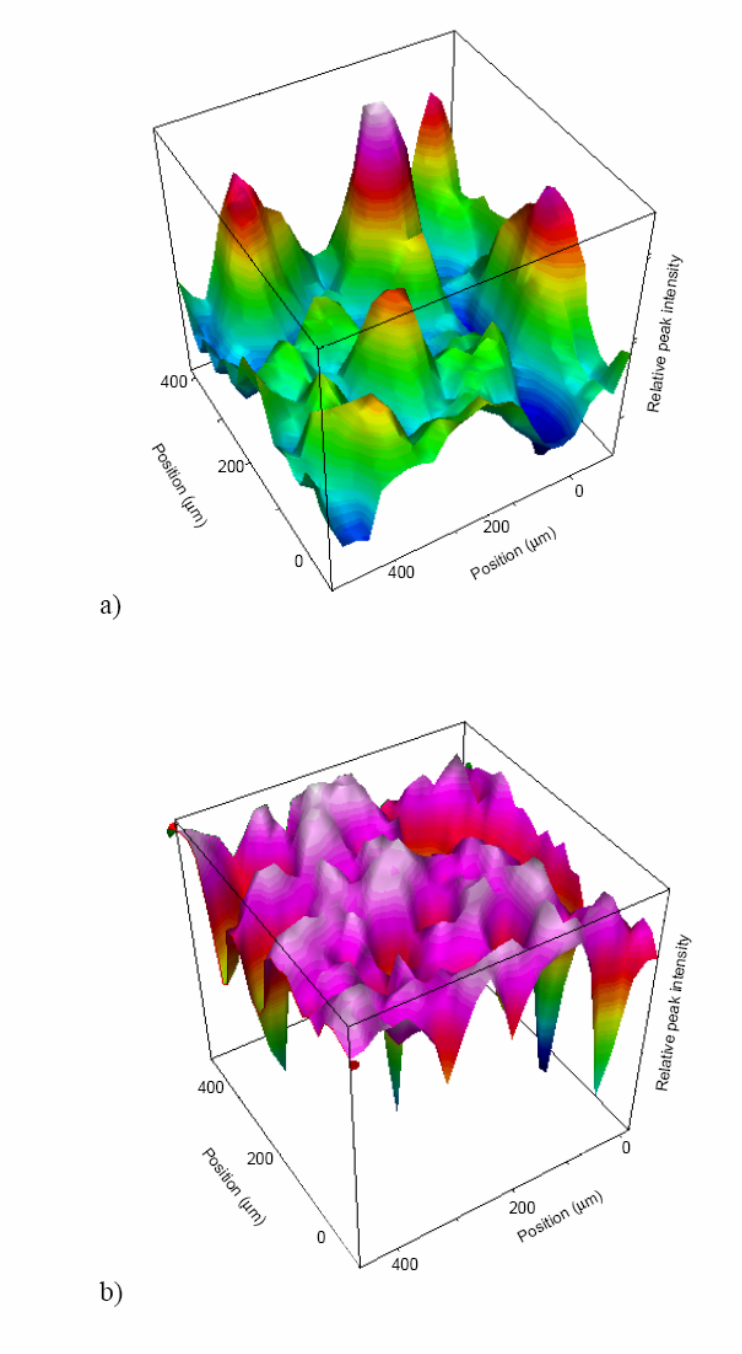

Fig. 16: Surface Plot of a Grid Scan

The figure shows the integrated areas of the amide (a) and the aliphatic (b) peak group. An area of 500 µm x 500 µm was scanned with an aperture of 20 µm x 20 µm at a step width of 20 µm. The surface consists of 625 pixels with interpolated transitions. The sample was a 30 % (v/v) PTMS sol-gel with a lysozyme load of 75 mg mL^{-1}.

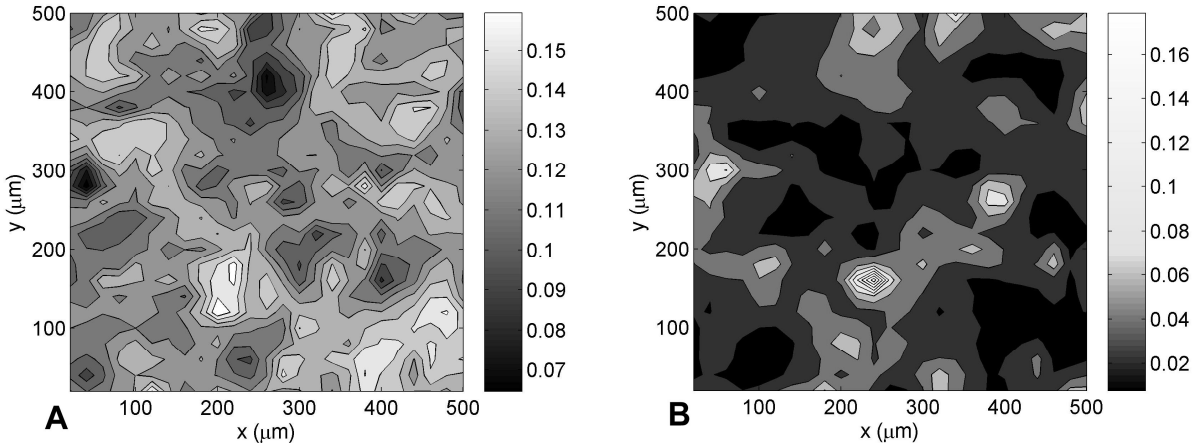

Fig. 17: Contour Plots of a Grid Scan

The figure shows contour plots of the amide/silicon signal ratio (a) and of the aliphatic/silicon signal ratio (b). The plots depict a 500 μm x 500 μm grid scan acquired using a 20 μm aperture and 20 μm step width for a 30 % (v/v) PTMS sol-gel with a lysozyme load of 75 mg mL^{-1}. Projection was obtained with interpolation of the transitions between data points.

Maps of the relative concentrations indicate that clustering occurs for both enzyme and organically modified monomer. Another visualization of the relative concentrations was obtained using contour plots. Fig. 17 shows the projected contour plots of the amide/silicon ratio (a) and the aliphatic/silicon ratio (b) in a sample containing 75 mg mL^{-1} of lysozyme and 30 % (v/v) PTMS. The contour plots for both lysozyme and PTMS show clear clustering of the components. The relative concentration of lysozyme was up to 2.4 times higher in the clusters compared to regions of low lysozyme concentration. The range of concentrations was even broader for the organically modified precursor. Within PTMS clusters, its concentration was up to 8 times greater than in regions of low relative PTMS concentration. Heterogeneities in organically modified sol-gels have been described in the literature [15,16]. For both lysozyme and PTMS, a base concentration of the component was present throughout the whole gel layer. The clusters of increased relative concentration occurred in an apparently random pattern across the scanned area. The clustering of lysozyme and PTMS can be attributed to surface interactions with the aluminum carrier, to interactions between lysozyme molecules, or heterogeneity of the sol components during coating, e.g. caused by phase separation [16]. Interpolation of the transitions between data points made it easier to recognize the clusters visually (Fig. 17).

However, if used for quantification of clustering, this type of plot would imply a level of resolution that cannot be achieved by using a 20 μm x 20 μm aperture. Therefore, pixel images without interpolation were used in the quantification steps.

To analyze the size and the density of lysozyme clusters within the sol-gel thin film, a concentration threshold was defined. The threshold determines the limit of relative concentration above which a pixel is counted as an area of increased lysozyme concentration. A lysozyme cluster was then defined as one or more of these positions of increased lysozyme concentration that were directly adjacent to each other. The choice of the threshold has significant influence on the quality of the quantitative analysis of enzyme clustering. If the threshold value was too low, the portion of the grid occupied by regions identified as enzyme clusters would be very high. As a result, the borders of individual clusters would be close to each other, sometimes making it impossible to distinguish reliably between individual clusters.

If the threshold value was high, only a few clusters were identified and the statistical significance of the results for cluster density and average cluster size decreased. A prerequisite for quantitative analysis was to set a threshold value that was a reasonable compromise between statistical significance and reliable distinction between individual clusters. The correlation between the threshold value and the percentage of occupancy in a sample with average PTMS and lysozyme contents used in this work were determined empirically. The best compromise between statistical significance and distinction between clusters is met at an occupancy of 15 % of the total grid area by regions identified as clusters of enzyme or modified monomer. The resulting threshold percentage is 25 %. The algorithm for the calculation of the actual threshold from this percentage value is described below. Fig. 18 shows the correlation between the degree of occupancy and the required threshold percentage.

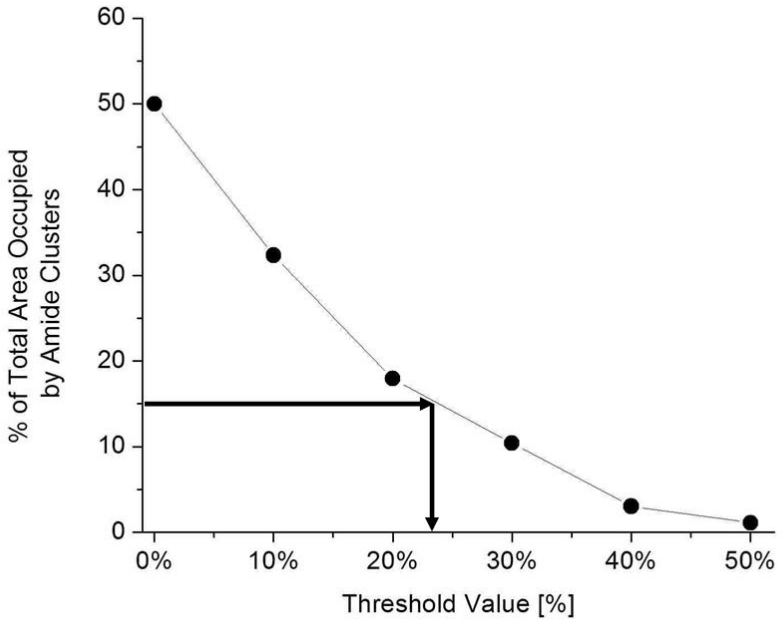

Fig. 18: Relation of Threshold Value and Lysozyme Cluster Area

Shown is the percentage of a sol-gel thin film occupied by lysozyme clusters as a function of the set threshold value.

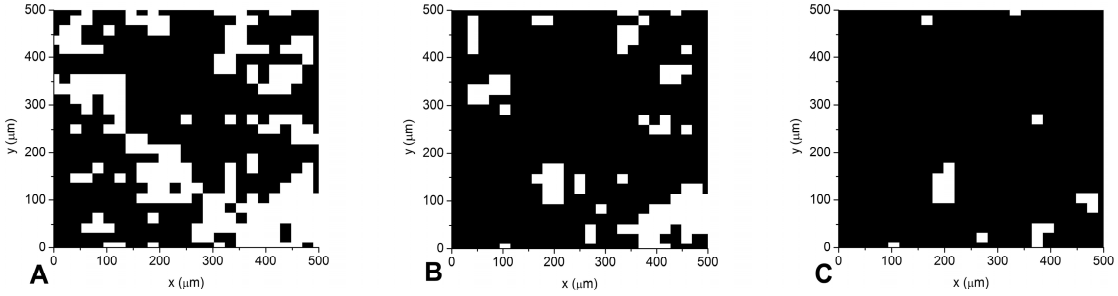

Fig. 19: Sample Binary Maps of Lysozyme Clusters

The maps are showing the influence of different threshold values on lysozyme cluster analysis (indicated by white regions). A sample of medium hydrophobic monomer content (20 % (v/v) PTMS) and medium lysozyme load (50 mg mL^{-1}) was analyzed with threshold values of mean +10 % (a) mean +25 % (b) and mean +40 % (c).

Since lysozyme concentrations vary over a wide range, it is necessary to define the threshold value in relation to the range of amide/silicon ratios found in a particular sample configuration. The following definition was used in cluster identification: a scanned position was considered a position of increased enzyme concentration if its amide/silicon ratio was higher than the median amide/silicon ratio plus the threshold percentage times the range between the 1 % percentile and the 99 % percentile of amide/silicon values in this sample configuration:

$$R > R_{MEDIAN} + \text{Threshold (\%)} \cdot (P0.99 - P0.01) \qquad (1)$$

where R is the measured amide peak area/silicon peak area ratio, R_{MEDIAN} is the median amide peak/silicon peak ratio for this sample configuration, P0.99 is the 99 % percentile of amide peak/silicon peak ratios in samples of this configuration, and P0.01 is the 1 % percentile of amide peak/silicon peak ratios in samples of this configuration. The range of amide/silicon ratios was reduced from the top and bottom by 1 % to account for the occurrence of artifact spectra. Dust particles or surface inhomogeneities caused approximately one in two hundred scans to be faulty at an aperture size of 20 μm x 20 μm. The resulting artifact spectra had extremely low signal intensities and an unusual baseline leading to invalid values during automatic peak integration. The capping step reliably excluded extreme amide/silicon peak ratios that were caused by the strongly aberrant artifact spectra.

Finally, the scanned grid was converted into a binary map using the calculated threshold value. Each pixel in the grid was assigned a value 1 or 0, depending on whether it had been evaluated as a location of increased lysozyme concentration or not. The resulting binary maps could then be evaluated for average cluster area and cluster density. Fig. 19 illustrates the influence of the threshold value on enzyme cluster analysis. A grid scan of a sample of 20 % (v/v) PTMS and 50 mg mL^{-1} lysozyme was analyzed and binary values assigned using threshold values of mean + 10 % (a), mean + 25 % (b) and mean + 40 % (c). It is apparent that as the threshold value is increased, the number and size of enzyme clusters decreases as anticipated.

3.3.4 Reproducibility

Although the choice of the aluminum material selected as the carrier was carefully made, inhomogeneities or surface features can affect signal intensity or signal quality when scans are conducted with an aperture as small as 20 μm x 20 μm. To assess variations in the signal for each of the three peak groups of interest, an area of 500 μm x 500 μm was scanned at an aperture of 20 μm x 20 μm on uncoated carriers. The integration functions were applied on each individual pixel of the grid to determine the areas of noise and error peaks in the respective groups of interest. The areas obtained in the absence of sol-gel thin films were used firstly to show the spatial distribution of signal variation of the errors and secondly to show the influence of the error on the silicon, amide and aliphatic signal. Fig. 20 shows the spatial distribution of the signal variation for the three peak groups investigated. White pixels represent areas of high signal deviation; black pixels represent areas without deviation from the background spectrum. The three plots show no pattern of signal variation, such as lines or clusters that could be related to the fabrication or preparation of the carrier. If the process of aluminum sheet fabrication by rolling lead to errors in the peaks analyzed these would be observable as parallel lines of signal variation.

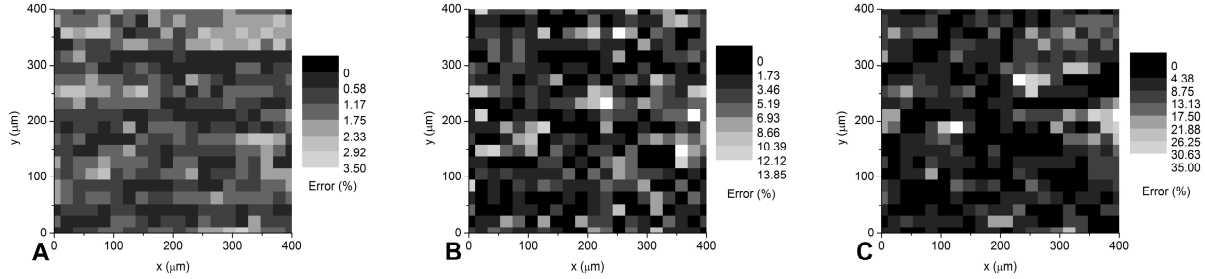

Fig. 20: Spatial Distribution of Error

The figure shows the spatial distribution of the error caused by environment and aluminum surface irregularities. Plots are shown for the silicon (a), aliphatic (b) and amide (c) peak groups.

In order to determine the influence of the error on the three signals analyzed, the area of each peak group (determined in the absence of the sol-gel thin film) was compared with the average area of the respective peak group in a sample containing 20 % (v/v) PTMS and 20 mg mL^{-1} lysozyme. For every pixel, the variation in areas was expressed as percentage and used to determine the cumulative distribution of the error intensities shown in Fig. 21. Negative areas were counted as their absolute value. The silicon peak group shows a distribution of errors with maximum values of 3 % of the average peak area. The background spectrum of aluminum shows a decrease in reflectance at wave numbers below 1600 cm^{-1}. The decrease was not completely constant in slope across the surface of the tested carriers, causing the observed error in the silicon signal. The aliphatic signal shows a wider range of error values than the silicon signal. The error was not caused by any overlapping peak, but by random spectral noise. The average area of the aliphatic signal was low, making the effect of spectral noise comparatively strong. Precautions were taken to reduce the spectral noise by avoiding air streaming through the IR beam and by working as dust-free as possible. The signal variation could, however not be reduced below the level reported here. The highest error values were observed for the amide peak. The error in the amide signal was mainly due to the neighboring H_2O peak which appeared in situations with normal ambient relative humidity (50-60 %) [17]. Errors are expressed as percent of the respective peak in a sample with the lowest lysozyme and PTMS concentrations used in this experiment. The majority of samples had a far smaller signal variation.

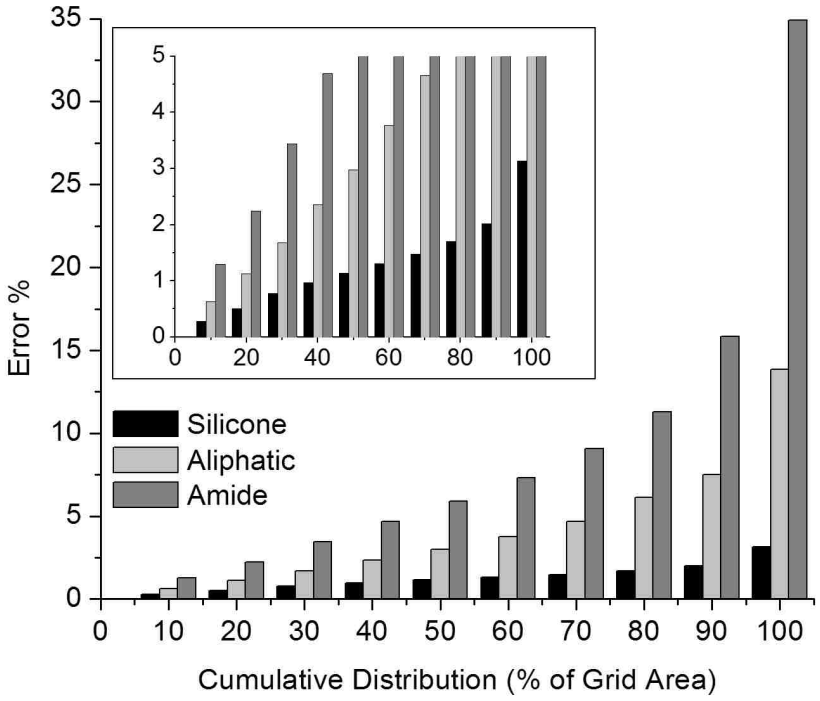

Fig. 21: Cumulative Error Distribution

The cumulative error distribution was calculated as percent of the average area of the silicon (a), aliphatic (b) or amide (c) range. The average area was determined in a sample with low lysozyme and low hydrophobic monomer content (20 % (v/v) PTMS, 20 mg mL^{-1} lysozyme) to give worst case error values. The scanned area was 500 μm x 500 μm at 20 μm square aperture and step width producing a grid of 25 x 25 (625 pixels).

To verify the reproducibility of this chemical mapping method, a sample containing 30 % (v/v) PTMS and 75 mg/mL lysozyme was studied. An automated grid scan was conducted twice on the same sample with a 10 min time interval between the two scans. The variation in the ratio of amide to silicon peak between two consecutive runs was calculated as the % error. The average error was 5.04 %, which is low considering that the FTIR measurements were not conducted in a dust-free environment and were conducted in a normal relative humidity environment (50 to 60 %) in which peaks of water slightly overlap with the amide signal. Fig. 22 shows the distribution of the error values obtained with 48 % of the pixels having an error smaller than 2 %, and 73 % of the pixels with errors smaller that 5 %. The two scans in the

distribution located at 20-50 % error and at >100 % error are attributed to dust particles. These two particular pixels with large errors had very low overall signal intensities and a baseline which was significantly shifted resulting in errors in the automatic peak integration.

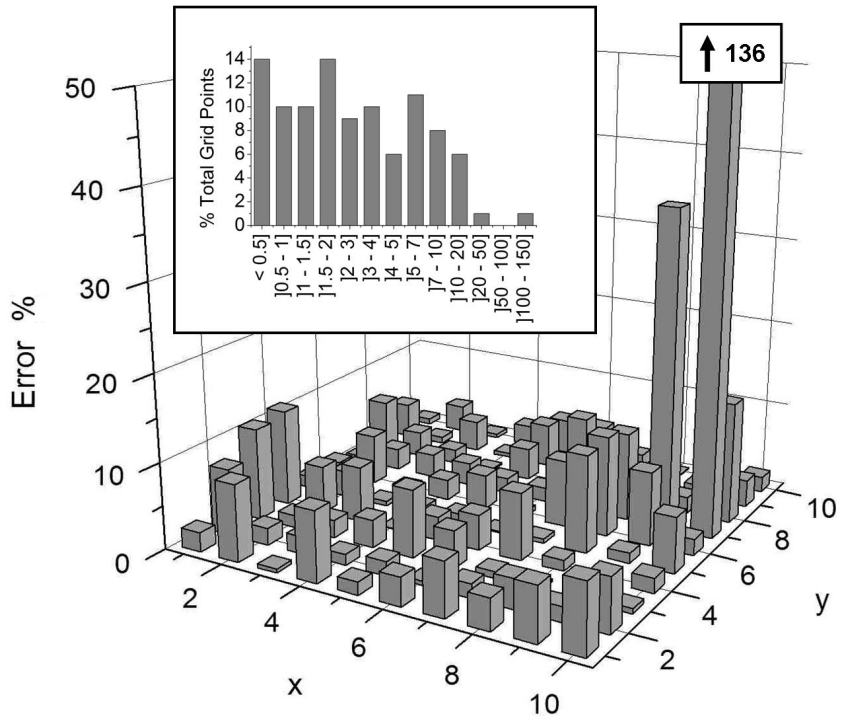

Fig. 22: Error Distribution in a Reproducibility Test

A sample coated with 30 % (v/v) PTMS and a lysozyme load of 75 mg mL^{-1} was scanned. The grid size was 200 μm x 200 μm at an aperture of 20 μm and a step width of 20 μm. The average error was 5.04 %.

3.4 Conclusion

Sol-gel thin films suitable for chemical mapping with FTIR and containing biological macromolecules like lysozyme can be prepared using spin coating. The chemical mapping procedure introduced here offers a noninvasive way of mapping concentrations of proteinaceous substances and organically modified monomers *in situ* with spatial resolution in such thin films. The availability of noninvasive method for semi-quantitative chemical mapping is an important prerequisite for research on the properties of biologically doped sol-gel thin films that could lead to industrial applications. The method proposed here allowed for the mapping of relative concentration differences of biomacromolecules and modified monomers. The technique of chemical mapping in sol-gel thin films will permit a wide range of investigations on the distribution of sol-gel components and immobilized biologicals as well as on the formation of microenvironments in sol-gel thin films.

3.5 References

[1] Drauz, K.; Waldmann, H. *Enzyme catalysis in organic synthesis*; Wiley-VCH: Weinheim, 2002.

[2] Clark, D. S. Can Immobilization Be Exploited to Modify Enzyme-Activity. *Trends in Biotechnology* **1994**, *12*, 439-443.

[3] Jürgen-Lohmann, D. L.; Legge, R. L. Immobilization of Bovine Catalase in Sol-Gels. *Enzyme Microb.Technol.* **2006**, *39*, 626-633.

[4] Gill, I.; Ballesteros, A. Bioencapsulation Within Synthetic Polymers (Part 1): Sol-Gel Encapsulated Biologicals. *Trends in Biotechnology* **2000**, *18*, 282-296.

[5] Jin, W.; Brennan, J. D. Properties and Applications of Proteins Encapsulated Within Sol-Gel Derived Materials. *Anal.Chim.Acta* **2002**, *461*, 1-36.

[6] Pierre, A. C. The Sol-Gel Encapsulation of Enzymes. *Biocatalysis and Biotransformation* **2004**, *22*, 145-170.

[7] Günzler, H.; Gremlich, H. U. *IR spectroscopy*; Wiley-VCH: Weinheim, 2002.

[8] Gremlich, H. U.; Yan, B. *Infrared and Raman spectroscopy of biological materials*; Marcel Dekker: New York, 2001.

[9] Schultz, C. P. Precision Infrared Spectroscopic Imaging: The Future of FT-IR Spectroscopy. *Spectroscopy* **2001**, *16*, 24-+.

[10] Mei, Y.; Miller, L.; Gao, W.; Gross, R. A. Imaging the Distribution and Secondary Structure of Immobilized Enzymes Using Infrared Microspectroscopy. *Biomacromolecules* **2003**, *4*, 70-74.

[11] Kistler, S. F.; Schweizer, P. M. *Liquid film coating*; Chapman & Hall: London, 1997.

[12] Huang, Y. Y.; Chou, K. S. Studies on the Spin Coating Process of Silica Films. *Ceramics International* **2003**, *29*, 485-493.

[13] Taylor, J. F. Spin Coating: An Overview. *Metal Finishing* **2001**, *99*, 16.

[14] Clifford, J. S.; Legge, R. L. Use of Water to Evaluate Hydrophobicity of Organically-Modified Xerogel Enzyme Supports. *Biotechnol.Bioeng.* **2005**, *92*, 231-237.

[15] Wetzel, D. L.; Striova, J.; Higgins, D. A.; Collinson, M. M. Synchrotron Infrared Micro Spectroscopy Reveals Localized Heterogeneities in an Organically Modified Silicate Film. *Vibrational Spectroscopy* **2004**, *35*, 153-158.

[16] Higgins, D. A.; Collinson, M. M. Gaining Insight into the Nanoscale Properties of Sol-Gel-Derived Silicate Thin Films by Single-Molecule Spectroscopy. *Langmuir* **2005**, *21*, 9023-9031.

[17] Durrani, C. M.; Donald, A. M. Compositional Mapping of Mixed Gels Using FTIR Microspectroscopy. *Carbohydr.Polym.* **1995**, *28*, 297-303.

Chapter 4

Distribution of Model Proteins in Organically Modified Sol-gel Thin Films

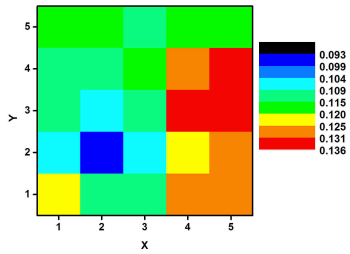

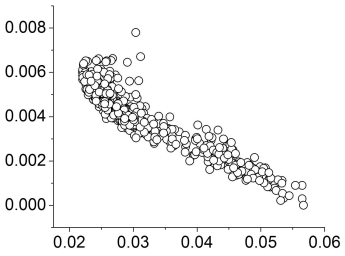

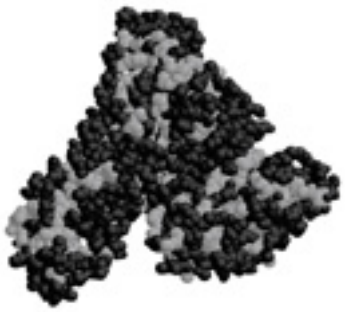

Preface

This chapter presents results from the use of the methodology developed in Chapter 3. Three model proteins immobilized in a range of four sol-gel compositions were studied. The proteins chosen were lysozyme, lipase and bovine serum albumin (BSA). Lysozyme has shown to be a good model protein as described earlier. In addition to being readily available, it also displays interesting properties in terms of protein distribution when entrapped in sol-gel thin films (Chapter 3). Lipase was selected as a model protein because it is well studied for sol-gel immobilization in general and lipase activity in sol-gels is largely dependent on the sol-gel formulation. In essence, gels with higher hydrophobicity display higher activity. It is generally believed that there is some interaction between the hydrophobic residues of the sol-gels and the lipase that causes an increase in enzymatic activity by mimicking the interfacial activation that is known to occur *in vivo*. Additionally, lipase was chosen as a replacement for hydroperoxide lyase (HPL), which had been initially selected as a model protein. HPL was also expected to interact with the hydrophobic residues of the sol-gel; however, as described in the preface to Chapter 2, a number of problems were encountered with sol-gel entrapped HPL. BSA was chosen because it is widely studied and to provide a larger protein for comparison. Size is expected as a factor in governing the distribution of protein throughout sol-gel thin films because it is generally believed that the entrapped species acts as a template during sol-gel formation.

Summary

The use of silica sol-gels for protein entrapment has been studied extensively over the past 15 years or so. However, the understanding of interactions between the immobilization matrix and the entrapped biomolecules is still relatively poor. Non-invasive *in situ* spectroscopic characterization is a promising approach to gain a better understanding of the fundamentals governing sol-gel immobilization. This work describes the application of Fourier transform infrared (FTIR) microscopy in measuring the distribution of three model proteins (lysozyme [E.C. 3.2.1.17], lipase [E.C. 3.1.1.3] and bovine serum albumin (BSA)) in silica sol-gel thin films containing various amounts of the organically modified precursor propyltrimethoxysilane (PTMS) resulting in a range of sol-gel hydrophobicity.

FTIR analysis of the overall immobilized protein distribution showed a general Gaussian type normal distribution. FTIR microscopic mapping, however, revealed the heterogeneous spatial protein distribution within the sol-gel thin films. When this positional information provided by FTIR microscopy was taken into account, areas of high protein concentration (clusters) were found and were not homogeneously distributed throughout the samples. The form of these clusters was found to depend on the type of protein entrapped, as well as on the composition of the sol-gel in some cases.

Positional analysis of the distribution of the organically modified precursor PTMS in correlation to the protein distribution was carried out. The localized concentration of PTMS was positively correlated with the protein concentration in the case of lipase and negatively correlated in the case of lysozyme and BSA. These results indicate that lysozyme and BSA concentration was higher in areas of low hydrophobicity, while lipase concentration was increased in areas of high hydrophobicity within the sol-gel. Additionally, a higher PTMS content seemed to have a conserving effect on protein structure in high concentration clusters for lipase, as indicated by peak shape analysis of the amide I peak. Lysozyme and BSA, on the other hand, seemed to retain their structures in high concentration clusters better at lower PTMS content. A hypothesis identifying hydrophobic interaction between lipase and PTMS as the reason for this behavioral difference between the model proteins is proposed.

4.1 Introduction

Although practiced for almost a century and demonstrating great potential, immobilized enzyme catalysis has not received the same amount of industrial attention as, for example, fermentation processes [1]. The transfer of enzyme catalyzed reactions from the laboratory to an industrial production scale is mainly hindered by the shortcomings of traditional enzyme immobilization, such as mass transfer limitations and enzyme inactivation [1]. Because enzymes are costly, the feasibility of an industrial enzymatic process is usually dependent on a highly active biocatalyst [1]. To improve the performance of immobilized enzymes, new immobilization materials, such as sol-gels, combined with new analysis techniques are emerging and are expected to significantly advance the understanding of immobilized enzyme systems [2-5].

The use of spectroscopic techniques for *in situ* characterization of immobilized proteins has seen a significant gain in attention recently [6,7]. Non-invasive spectroscopic methods allow for an assessment of the actual state the immobilized biomolecule is in. For example, Fourier transform infrared (FTIR) microscopy can link chemical features to positional information [8-10]. As described in Chapter 3, this method can be used to assess the distribution of proteins in sol-gel thin film systems. It was found in Chapter 3 that the distribution of lysozyme in sol-gel thin films was not homogeneous and was characterized by a clustering of areas of high protein concentration. In this chapter, the distribution of three model proteins - lysozyme, lipase and bovine serum albumin (BSA) in four different organically modified sol-gel thin films of varying propyltrimethoxysilane (PTMS) content (0, 10, 25 and 50 %) was assessed. The characteristic properties, such as hydrophobicity and pore size, of silica sol-gels can be controlled to a certain extent by varying the amount of modified precursor present. Protein distribution in immobilized systems has been described in the literature [11-14]. However, the work focuses on adsorbed protein or does not take into account the effects of matrix composition on protein distribution.

The heterogeneity of sol-gels was described by Higgins and Collinson [15] who identified organic- and inorganic rich domains in a thin film containing organically modified precursors. These findings were confirmed in Chapter 3 alongside with the heterogeneous distribution of the model protein lysozyme in sol-gel thin films.

In this chapter, the correlation between protein distribution and organic-rich domains was assessed. This correlation is particularly interesting in the case of lipase. Lipase activity in sol-gels is known to be composition dependent [16]. More specifically, gels with higher PTMS content display higher enzymatic activity. This phenomenon is generally attributed to matrix/enzyme interactions, mimicking the *in vivo* interfacial activation of lipase. The organic residues of PTMS containing sol-gels are believed to serve as a template for this activation phenomenon [16,17]. The direct association of lipase with these organic residues, however, has not been shown in the literature.

The distribution of BSA in sol-gels was described by Tran *et al.* using a near IR multispectral imaging technique [11]. It was found that BSA was heterogeneously distributed in pure tetramethoxysilane (TMOS) sol-gels. This heterogeneous distribution was attributed to matrix/protein interactions during the formation of the sol-gel, in which the entrapped molecule is thought to serve as a template [11]. The influence of matrix composition on BSA distribution, however, has not been discussed in the literature.

The influence of material properties of the immobilization support, as represented by the range in PTMS content, on the distribution of the three model proteins is characterized in this chapter. Furthermore, the implications of the localized protein concentration on the structure of the immobilized biomolecule are evaluated.

4.2 Materials and Methods

Some differences in the procedures for sample preparation and data analysis between Chapter 3 and this chapter should be noted. Firstly, a new aluminum carrier material was acquired; Anolux Miro IV (Anomet, Brampton, ON) reflective aluminum "lighting sheets" were found to provide a superior surface in terms of sol-gel thin film adhesion as well as infrared reflection. The sheets are finished by physical vapor deposition and covered with a protective polymer layer that can be removed prior to coating. Additional cleaning is therefore not necessary. The new carrier material allowed for a slightly larger range of PTMS content in the sol-gel thin films of up to 50 % PTMS compared to 40 % PTMS as described earlier (Chapter 3). Additionally, it was found that the correction function used in Chapter 3, to account for the contribution of protein to the PTMS quantification did not add any significant improvement of the quantification. The peak group around 2800 cm^{-1} was, therefore, solely attributed to PTMS content as an approximation.

4.2.1 Materials

Lysozyme [E.C. 3.2.1.17] (43,900 units/mg protein, 95 % purity) from chicken egg white, BSA (Fraction V, 98-99 % albumin) and lipase [E.C. 3.1.1.3] (4,000 units/mg protein, > 95 % purity) from *Mucor miehei* were obtained from Sigma (Oakville, ON) and used without further purification. Tetraethoxysilane (TEOS) (98%, Sigma, Oakville, ON), propyltrimethoxysilane (PTMS) (98%, Fluka Chemicals, Oakville, ON) and 2-amino-2-(hydroxymethyl)propane-1,3-diol (TRIS) (Baker Chemicals, Phillipsburg, NJ) were used as received. Aluminum carriers were cut into 1 x 1 cm^2 pieces out of Anolux Miro IV (Anomet, Brampton, ON) sheets with a sheet metal notcher.

4.2.2 Sol-gel Preparation

All liquid components were microfiltered using 0.2 μm Pall Gelman Laboratories Aerodisc syringe filters (Sigma, Oakville, ON) for particle removal. TEOS and PTMS were hydrolyzed separately by sonication for 2 h (TEOS) or 4 h (PTMS) in 1.67 mM HCl with a stoichiometric molar water to monomer ratio of 4:1. Hydrolyzed monomer batches were stored at -20 °C for a

maximum of one week. Ethanol was added at a concentration of 20 % (v/v) 10 min prior to coating to improve the coating properties. Polycondensation was initiated by mixing equal volumes of the hydrolyzed monomers with a starting buffer consisting of 10 mM TRIS at pH 7.2, 100 mM KCl and containing 50 mg mL^{-1} of protein.

4.2.3 Spin Coating

Samples were coated on a custom built spin coater with rotation speed control and vacuum chuck. Spin coating was conducted in a dust free environment to avoid contamination of the gel coat. Monomer hydrolysate and buffer solution were mixed directly before coating. A 100 μL sample was applied in a single step to the centre of the carrier rotating at 3000 rpm and spun for 60 sec. Coated samples were stored in dust free containers at ambient temperature.

4.2.4 FTIR Microscopy

FTIR microscopy was conducted using a Hyperion 2000 microscope and a Tensor 27 FTIR spectrometer (Bruker Optics, Milton, ON). Spectra acquisition and evaluation were performed with OPUS 4.2 software using the 3D and MAP packages (Bruker Optics, Milton, ON). Spectra were recorded at room temperature over a wavenumber range from 4000 cm^{-1} to 700 cm^{-1} at a resolution of 4 cm^{-1} in reflectance mode. Background and sample spectra were averaged from 64 scans. All grid scans were conducted with an aperture of 20 μm x 20 μm and a step width of 20 μm. The grid position was automatically controlled by a motorized stage with 1 μm resolution. The FTIR microscope was purged (75-45NA, Parker Balston, Haverhill, MA) with dry air at a flow rate of 7 L min^{-1} to ensure a constant atmosphere in the signal path.

4.2.5 Data Treatment

Integration of the significant peak regions was carried out using the OPUS 4.2 software. The integration boundaries were 1400-850 cm^{-1} for Si-O-Si and Si-OH signals, corresponding to the silica sol-gel, 1800-1500 cm^{-1} corresponding to the amide I and II, and 3000-2800 cm^{-1}, corresponding to the alkane peak group. Dimensionless peak ratios were calculated by division of the amide or alkane signal by the silica signal. For quantification, no manipulation of the spectra was performed prior to integration. For peak shape comparison, spectra were smoothed, baseline corrected and normalized.

4.3 Results and Discussion

4.3.1 Frequency Distribution of Model Proteins in Sol-gel Thin Films

In the previous chapter, a methodology for chemical mapping of sol-gel thin films containing proteins was described. This chapter applies this methodology to three model proteins (lysozyme, lipase and BSA) each immobilized in a set of sol-gel thin films of different composition and hydrophobicity (0, 10, 25 and 50 % PTMS content) resulting in 12 samples in total. A typical FTIR spectrum of a protein containing sol-gel thin film, coated on an aluminum carrier, is shown in Fig. 23. For the calculation of localized protein and PTMS content, three peak groups were quantified. The peak group corresponding to silica (1300 - 800 cm^{-1}), the amide I and II peak group (1700 - 1500 cm^{-1}) corresponding to protein content and the methyl and methylene stretching (~ 2800 cm^{-1}) corresponding to PTMS content [18,19].

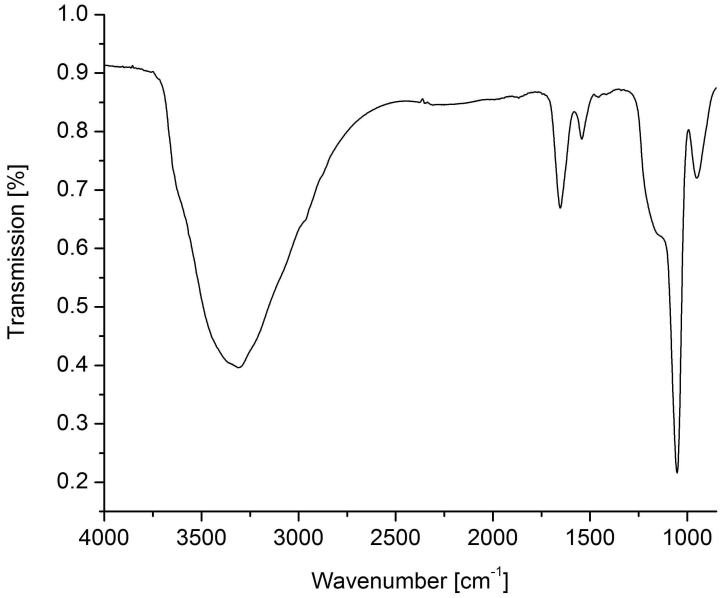

Fig. 23: Sample Spectrum of a Lysozyme Doped 10 % PTMS Sol-gel Thin Film

The spectrum with the four characteristic peak groups corresponding to Si-O-Si/Si-OH (1300 - 800 cm^{-1}), to the amide I and II signal (1700 - 1500 cm^{-1}), the methyl and methylene stretching (~2800 cm^{-1}) and the N-H stretching mode/O-H stretching (~3300 cm^{-1}). The spectrum was collected as an average of 64 scans with an aperture size of 100 x 100 μm.

All samples were scanned with an aperture size of 20 x 20 μm and a step size of 20 μm in an area of 25 x 25 sample points. The resulting scanned area is therefore 500 x 500 μm consisting of 625 data points. To gain a general understanding of the protein concentrations present in the samples, frequency histograms were created for all signal ratios amide/silica. These histograms are depicted in Fig. 24, Fig. 25 and Fig. 26.

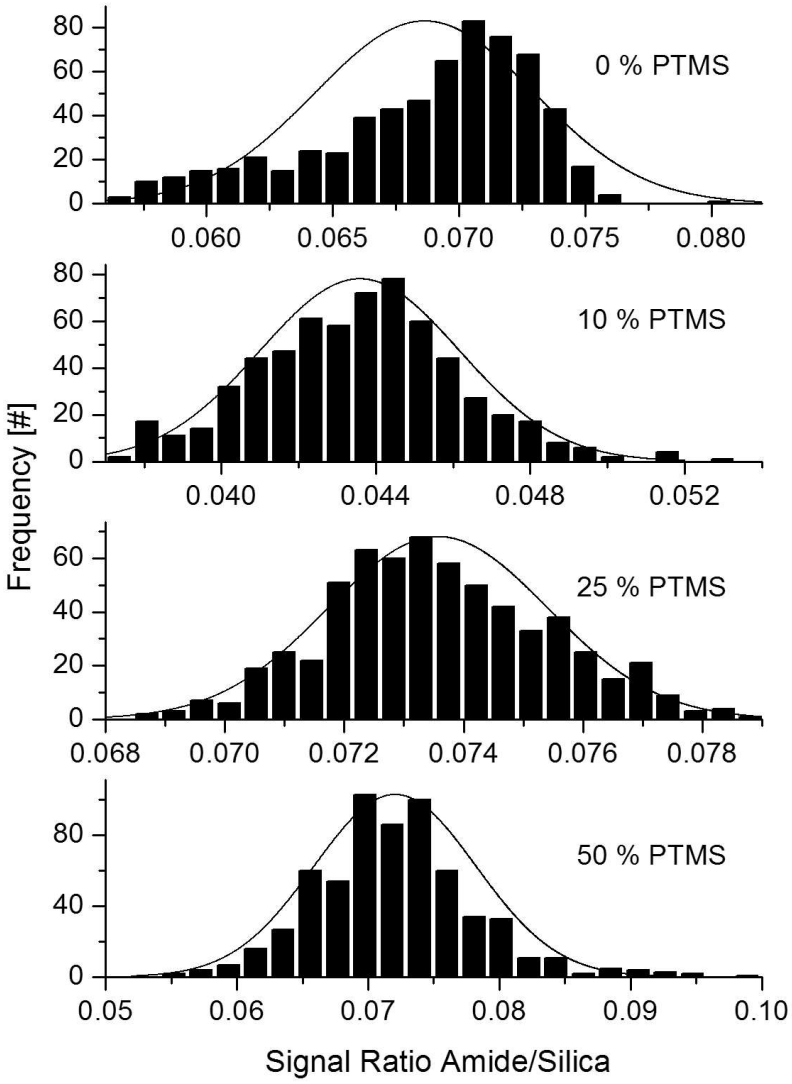

Fig. 24: Histogram of Lysozyme Concentrations in Sol-gel Thin Films

Lysozyme was entrapped in sol-gel thin films with four different PTMS contents (0, 10, 25 and 50 %). Each histogram contains the 625 data points of a 25x25 array.

A general observation from Fig. 24, Fig. 25 and Fig. 26, is that the protein concentrations in most of the 12 samples follow a normal Gaussian distribution reasonably well. More specifically, the lysozyme (Fig. 24) amide/silica signal ratio distributions are relatively narrow, spanning from 0.03 – 0.1. No clear trend is visible from the center points of the Gaussian distributions for lysozyme, located at around 0.07 (0, 25 and 50 % PTMS) and 0.045 (10 % PTMS). The 0 % PTMS sample, however, shows a somewhat skewed fronting distribution. It can therefore be concluded that the overall distribution of lysozyme concentrations in sol-gel thin films is apparently independent of the sol-gel composition within the tested range.

Lipase (Fig. 25), appears to behave differently, where the width of the concentration distribution changes, increasing with increasing PTMS content from 0.08 (0 and 10 % PTMS) to 0.14 (25 % PTMS) to 0.3 (50 % PTMS). The center of the distribution does not show an obvious trend, ranging from 0.04 to 0.1. From this data, it is suggested that higher PTMS content in a sol-gel thin film leads to a broader distribution of concentrations of lipase.

The distribution of concentrations for BSA (Fig. 26) displays a somewhat more complicated pattern. The width of the distributions spans from 0.06 (10 % PTMS) to 8 (50 % PTMS). The 0 % PTMS sample for BSA shows a distribution comparable to the lysozyme and lipase samples. However, it can be seen from Fig. 26 that there is a somewhat binomial distribution centered at 0.025 and 0.045 for the 10 % PTMS BSA sample. At higher PTMS concentrations (25 % and 50 %) the distribution significantly broadens. The higher PTMS content changes the concentration distribution characteristics of BSA in sol-gel thin films.

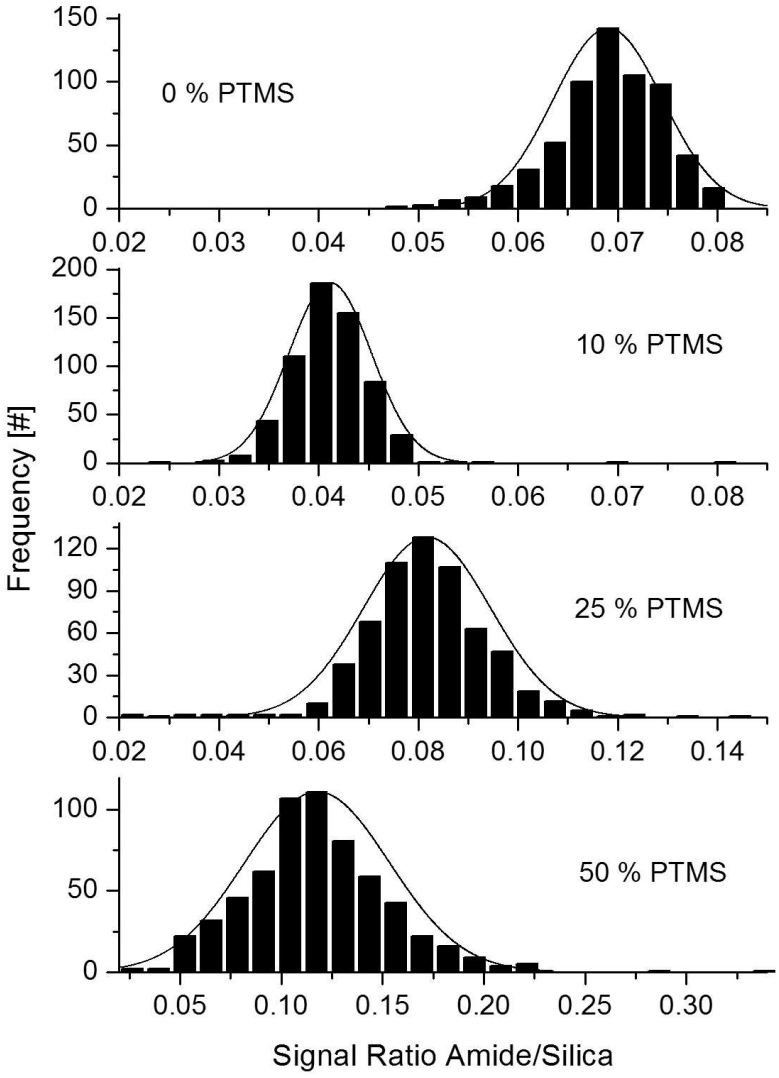

Fig. 25: Histogram of Lipase Concentrations in Sol-gel Thin Films

Lipase was entrapped in sol-gel thin films with four different PTMS contents (0, 10, 25 and 50 %). Each histogram contains the 625 data points of a 25x25 array. The distributions can be described reasonably well with a Gaussian normal distribution.

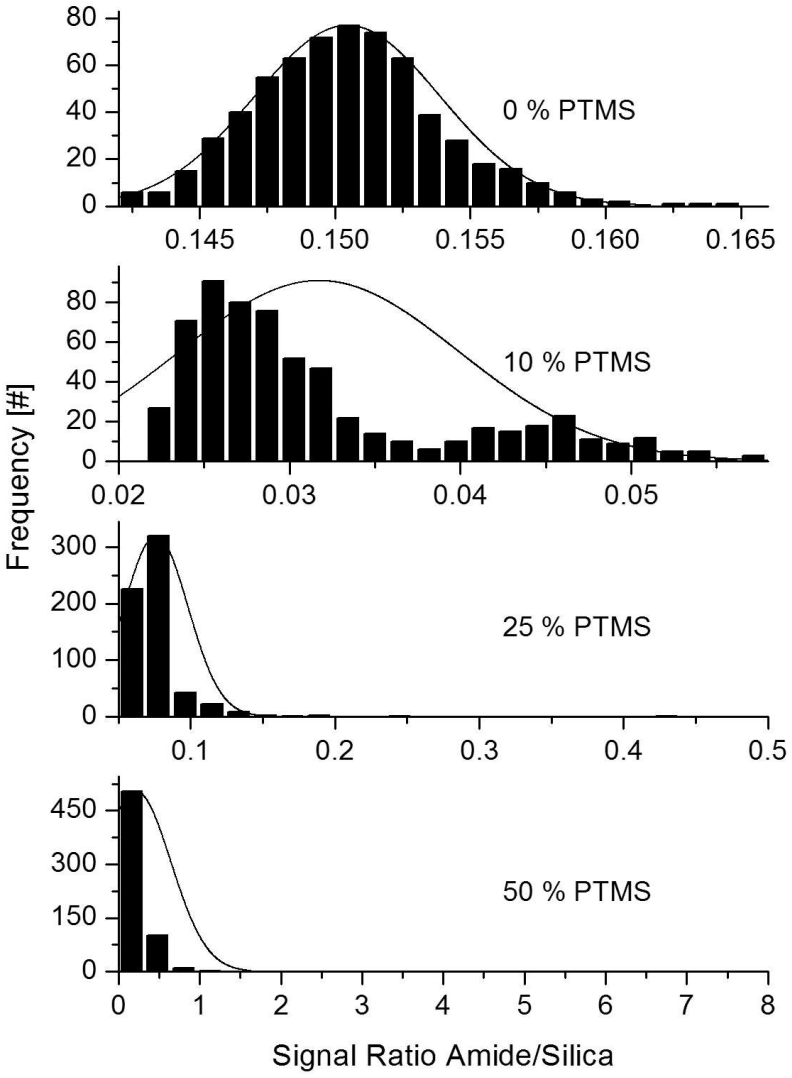

Fig. 26: Histogram of BSA Concentrations in Sol-gel Thin Films

BSA was entrapped in sol-gel thin films with four different PTMS contents (0, 10, 25 and 50 %). Each histogram contains the 625 data points of a 25x25 array. With the exception of the 10 % PTMS sample, the distributions can be described reasonably well with a Gaussian normal distribution.

4.3.2 Spatial Distribution of Model Proteins in Sol-gel Thin Films

As described in Chapter 3, FTIR microscopy can add spatial resolution to the analysis of immobilized protein. This spatial analysis can be used to infer the distribution of protein in an immobilized system and to identify areas of high protein concentration if they exist. These areas are chosen here as a representative feature of a heterogeneous distribution. It was previously shown in Chapter 3 that the high areas of high concentration of lysozyme or clusters were present in sol-gel thin films. This phenomenon is further studied here by comparing the distribution of three different proteins in sol-gel thin films of different compositions. To determine if the protein concentration was high, the same procedure as described earlier (Chapter 3) was used:

$$R > R_{MEDIAN} + \text{Threshold } (\%) \cdot (P0.99 - P0.01) \qquad (1)$$

where R is the measured amide/silica ratio, R_{MEDIAN} is the median amide/silica ratio for a given sample, P0.99 is the 99 % percentile of amide peak/silica peak ratios, and P0.01 is the 1 % percentile of amide peak/silica peak ratios. Amide concentration ratios calculated by (1) were classified as 1 for high concentration and 0 for low concentration. The cut-off values for the samples are given in Table 4.

Table 4: Cut-Off Values for Increased Protein Concentration

Protein	PTMS Content [%]	Cut Off Value
Lysozyme	0	0.073
	10	0.047
	25	0.076
	50	0.08
Lipase	0	0.076
	10	0.045
	25	0.10
	50	0.16
BSA	0	0.155
	10	0.04
	25	0.098
	50	0.435

The spatial distribution of the three model proteins in the different sol-gels is shown in Fig. 27, Fig. 28 and Fig. 29. The continuous maps, shown on the left of each figure (Fig. 27, Fig. 28 and Fig. 29) illustrate the heterogeneity of protein distribution in the samples. All continuous maps display a similar clustering of high concentration areas. These results are in accord with findings by Tran *et al.* who identified an inhomogeneous distribution of BSA in pure TMOS sol-gels with NIR spectroscopy [11]. To further investigate the clustering, the binary maps were generated, as shown on the right of Fig. 27, Fig. 28 and Fig. 29.

A description of the high concentration areas in the samples analyzed is given in Table 5. The data shows that high concentration positions account for 8-14 % of the total 625 points in all but two samples. One exception is BSA 10 % PTMS, showing 20 % occupation by high concentration samples. The explanation for this lies in the frequency distribution described above (Fig. 24, Fig. 25 and Fig. 26). Only the BSA 10 % PTMS sample displays a distribution that deviates from the normal Gaussian model and shows a somewhat bimodal behavior. The other exception, lipase 25 % PTMS, is reasonably close to the 95 % confidence level. These

results confirm the findings of the overall even distribution of protein concentration in most samples as described above.

Table 5: Cluster Features of the Immobilized Proteins

Protein	PTMS Content [%]	Positions with High Concentration [#]	Average and 95 % Confidence Interval [#]	Percentage of High Concentration Positions	
				[%]	Located in Clusters [%]
Lysozyme	0	73	72 ± 12	12	95
	10	67		11	97
	25	89		14	94
	50	59		9	88
Lipase	0	58	59 ± 14	9	88
	10	70		11	84
	25	39		6	79
	50	68		11	93
BSA	0	71	76 ± 36	11	97
	10	128		20	93
	25	47		8	55
	50	56		9	79

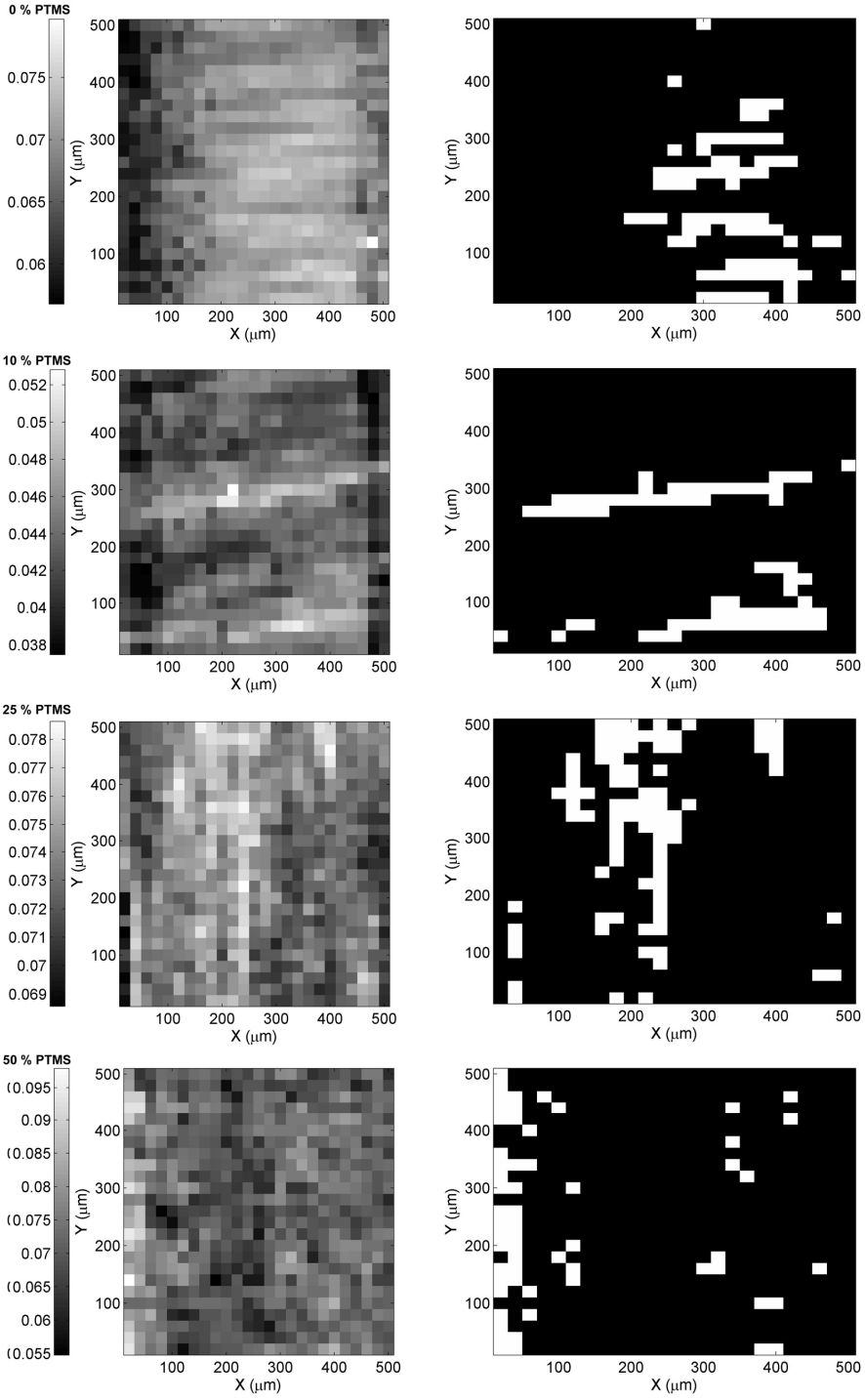

Fig. 27: Continuous and Binary Distribution Maps of Lysozyme in Sol-gel Thin Films

The continuous distribution of lysozyme in 0, 10, 25 and 50 % PTMS sol-gel thin films in the left column. The right column shows binary maps, generated from a cut off concentration value (1) above which the concentration is set to high (white) and below which the concentration is set to low (black).

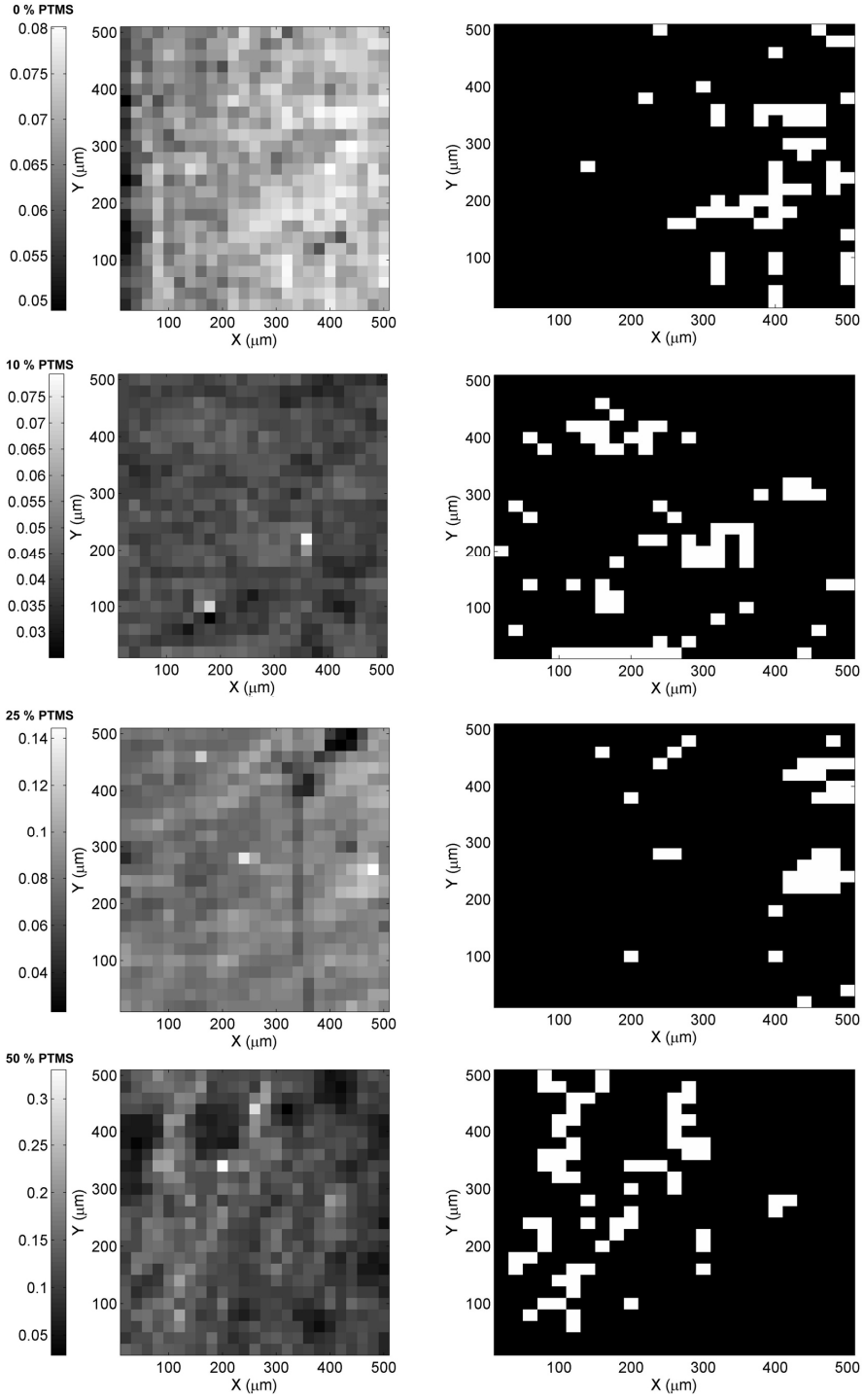

Fig. 28: Continuous and Binary Distribution Maps of Lipase in Sol-gel Thin Films

The continuous distribution of lipase in 0, 10, 25 and 50 % PTMS sol-gel thin films in the left column. The right column shows binary maps, generated from a cut off concentration value (1) above which the concentration is set to high (white) and below which the concentration is set to low (black).

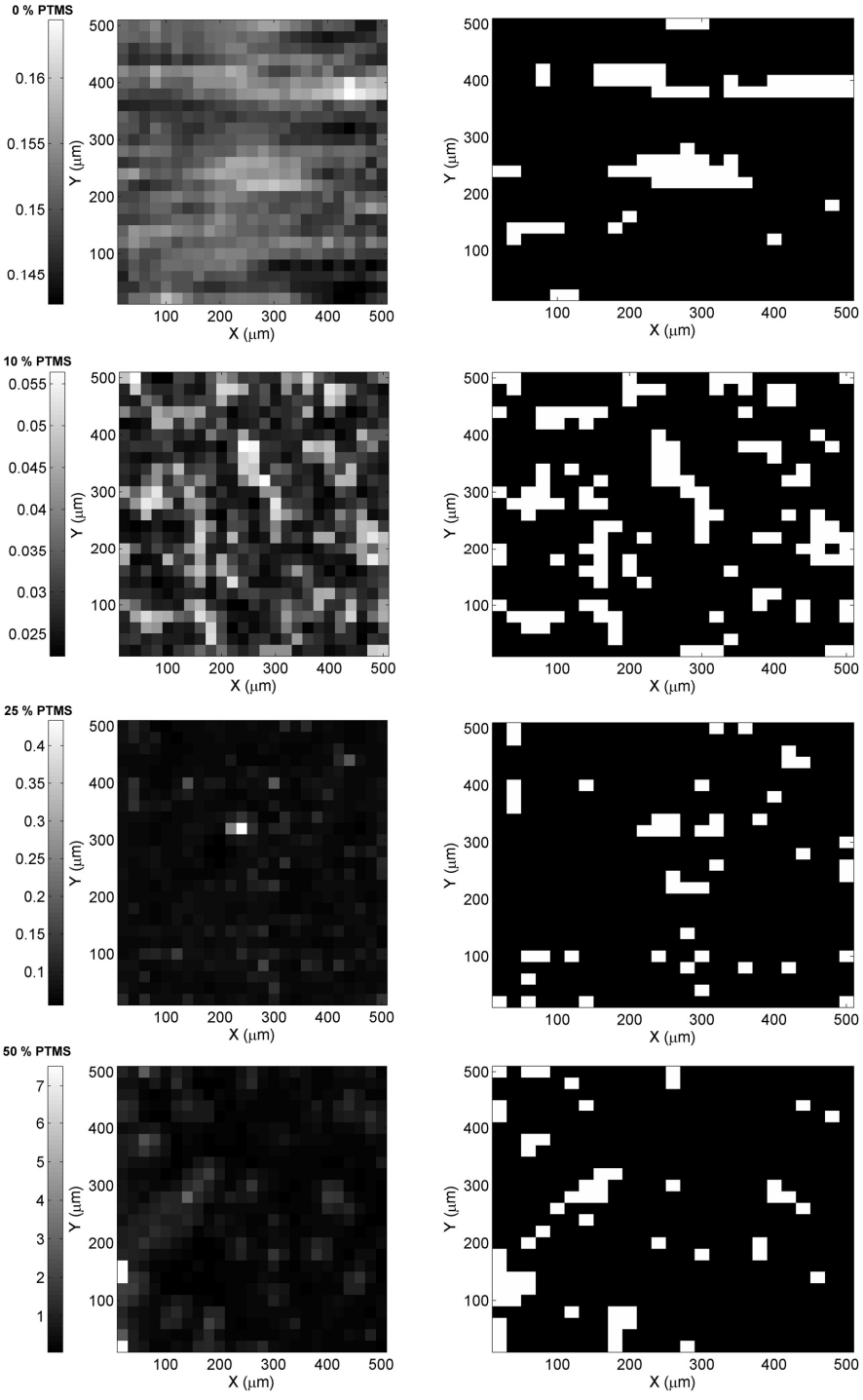

Fig. 29: Continuous and Binary Distribution Maps of BSA in Sol-gel Thin Films

The continuous distribution of BSA in 0, 10, 25 and 50 % PTMS sol-gel thin films in the left column. The right column shows binary maps, generated from a cut off concentration value (1) above which the concentration is set to high (white) and below which the concentration is set to low (black).

In all cases except for lysozyme in 25 % PTMS and BSA in 25 and 50 % PTMS, the percentage of high concentration areas being located beside each other, i.e. in a cluster, is higher than 80 %. When interpreting the cluster form as depicted in the right column of Fig. 27, Fig. 28 and Fig. 29, there appears to be a difference in size and shape of connected clusters. Lysozyme (Fig. 27) seems to arrange in extended clusters while lipase (Fig. 28) clusters appear to be more rectangular in shape. The cluster shape seems to be independent of the sol-gel composition in the case of both enzymes.

BSA (Fig. 29) on the other hand shows a lysozyme-like pattern for 0 % PTMS and a lipase like pattern for 10 % PTMS. For 25 and 50 % PTMS the cluster number seems to decrease in favor of isolated data points with increased protein content. This is also indicated by the relatively low percentage of high concentration areas being in a cluster (55 and 79 %, Table 5) for these two samples. It should be noted that the interpretation of cluster shape is purely descriptive and the statistical significance is difficult to assess. However, the observations are consistent with the results of the frequency distributions that show PTMS content independent behavior for lysozyme and lipase, but PTMS dependence for immobilized BSA.

4.3.3 Correlation between PTMS and Protein Localization in Sol-gel Thin Films

To further assess the distribution behavior of the three different model proteins, the correlation between localized PTMS content and localized protein content was investigated. The correlations for lysozyme, lipase and BSA can be seen in Fig. 30, Fig. 31 and Fig. 32.

A negative correlation between lysozyme and PTMS content, as indicated by a negative slope, is apparent for all three PTMS concentrations investigated as shown in Fig. 30. Lipase (Fig. 31) shows a negative correlation for 10 % PTMS but positive correlation for 25 and 50 % PTMS. This positive correlation is indicated for higher PTMS values in the 10 % PTMS sample.

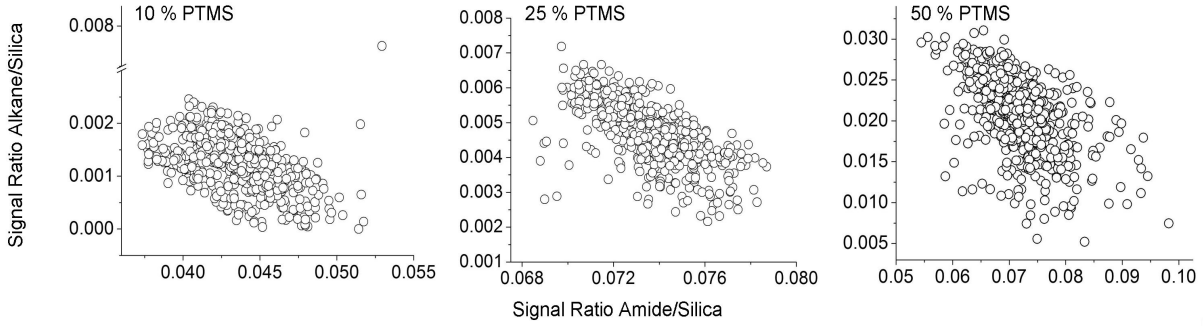

Fig. 30: Correlation between Localized PTMS and Lysozyme Concentration

Each plot contains the 625 data points of a 25x25 array.

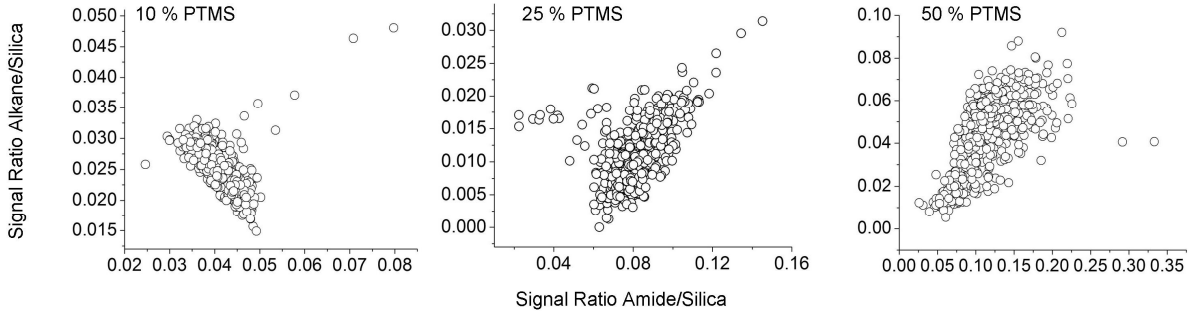

Fig. 31: Correlation between Localized PTMS and Lipase Concentration

Each plot contains the 625 data points of a 25x25 array.

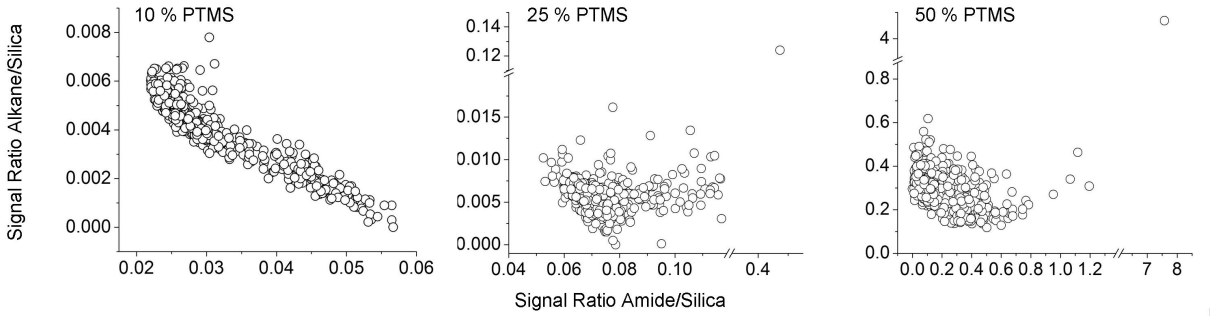

Fig. 32: Correlation between Localized PTMS and BSA Concentration

Each plot contains the 625 data points of a 25x25 array.

The correlations for BSA (Fig. 32) show a clear negative trend for 10 % PTMS and an apparent independent behavior for 25 and 50 % PTMS. A formal regression analysis was performed on all samples and the results are compiled in Table 6.

Table 6: Regression Analysis on the Correlation of Protein and PTMS content

Protein	PTMS Content [%]	Slope and Standard Error	Sample Size [#]	P
Lysozyme	10	-0.097 ± 0.007	624	<0.0001
	25	-0.303 ± 0.014	625	<0.0001
	50	-0.388 ± 0.035	625	<0.0001
Lipase	10	-0.614 ± 0.025	620	<0.0001
	25	0.297 ± 0.014	625	<0.0001
	50	0.168 ± 0.012	625	<0.0001
BSA	10	-0.149 ± 0.003	625	<0.0001
	25	0.016 ± 0.005	619	0.00305
	50	-0.202 ± 0.015	622	<0.0001

The regression analysis shown in Table 6 confirms the qualitative description of the correlation between protein and PTMS content. A negative correlation can be found for all lysozyme preparations, lipase in 10 % PTMS and BSA in 10 and 25 % PTMS. Lipase in 25 and 50 % PTMS show a positive correlation, while BSA 25 % shows a positive correlation with a significantly smaller slope compared to the other samples. The slopes are significant at a 99.605 % confidence level for BSA 25 % PTMS and on a 99.99 % confidence level in all other cases. A maximum of 6 leverage points was omitted from the regression analyses. The data points are, however, included in Fig. 30, Fig. 31 and Fig. 32.

The literature is in agreement that proteins can serve as a template around which the porous sol-gel is formed during gelation [3,5,11]. The size of the protein is usually identified as the main influence on this templating process. However, the data presented here, suggests that besides the size of the protein, the surface characteristics, might play an important role as well. Lipase (40 kDa) shows a positive correlation with PTMS at higher PTMS concentrations; all other samples show a negative correlation. Lipase is suspected to interact with hydrophobic residues upon sol-gel immobilization, resulting in an activation of the enzyme [16,17,20]. A certain PTMS content in the sol-gel is necessary for immobilized lipases in sol-gels to be active. From the correlation analysis presented here, it can be assumed, that interaction of lipase with the PTMS residues as early as during the templating process of the sol-gel, localizes the enzyme close to the organic residue. A direct interaction of these organic residues with the enzyme can therefore be assumed. This process can be envisioned to have similarities to self assembled systems driven by, e.g. hydrophobic interaction.

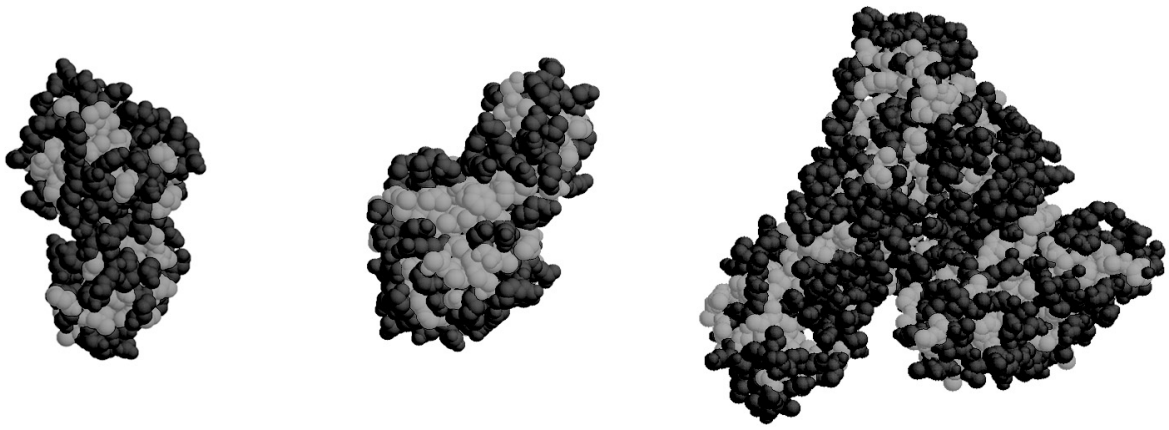

Fig. 33: Protein Surface Models for Lysozyme, Lipase and HSA

The 3D protein models for lysozyme (right), lipase (center) and HSA (right) are colored to show hydrophilic (dark) and hydrophobic (light) regions. Lipase is characterized by a large hydrophobic patch. HSA was used as a model for BSA. The 3D models are not to scale [21]. The PDB codes used are 2vb1 (Lysozyme), 3tgl (Lipase) and 1bm0 (HSA).

Lysozyme (14 kDa) and BSA (69 kDa) show a negative or absence of correlation with the PTMS content of the sol-gel. Comparing the surface characteristics of the three enzymes (Fig. 33) it can be seen that lipase has a large hydrophobic patch on its surface, while lysozyme and HSA/BSA show a mixed surface hydrophobicity.[4] The negative correlation with PTMS in the cases of lysozyme and BSA may be explained by a repulsion of the proteins from hydrophobic regions during phase separation upon gelation or by an affinity of these proteins to free silanol groups during gel formation [11]. These results are in agreement with findings about the heterogeneous BSA distribution in pure TMOS sol-gels as described by Tran *et al.* [11].

[4] Human serum albumin (HSA) was used as a model for BSA, since no crystal structure is available for BSA.

4.3.4 Implications on Protein Structure in Regions of High Protein Concentration

Areas of high concentration protein were taken as a feature to interpret the microscopic heterogeneity in sol-gel thin film systems. The localized information provided by FTIR microscopy can be used to compare the spectrum of a protein for an average concentration data point with the spectrum in a high concentration cluster. FTIR spectroscopy is known to be sensitive to protein secondary structure. Therefore, structural differences between proteins in average and high concentration areas might be determined [11]. The data points selected for spectral comparison between average and high protein concentration are summarized in Table 7.

In order to compare the spectra for the samples analyzed at average and high protein concentrations, the amide I bands were extracted from each original spectrum at every given position in the scanned grid (Table 7). Because of the small aperture used during mapping, the signal intensity and also the spectrum quality is relatively poor, and represents a compromise between reliable quantification and high spatial resolution. It was shown in Chapter 3 that the quality of the spectra is sufficient for reliable integration of the key peak areas; however, the raw spectra were not suitable for direct comparison of the peak shape. The data was therefore smoothed, baseline corrected and normalized. This procedure allows for a comparison between average and high concentration spectra of data points from a given sample. It is not intended to be used to derive specific protein structure motifs, but rather to determine if a change in structure is present between average and high concentrations in the same sample. The spectra will, therefore, be classified as "change present" or "no change present" between average and high concentration of every given sample.

Table 7: Data Points of Average and High Concentration Used for Spectral Comparison

Protein	PTMS Content [%]	X, Y [µm, µm] Average Concentration	X, Y [µm, µm] High Concentration
Lysozyme	0	100, 20	440, 60
	10	460, 20	320, 60
	25	120, 20	160, 0
	50	200, 20	20, 40
Lipase	0	160, 20	320, 80
	10	240, 20	360, 200
	25	120, 80	480, 240
	50	300, 160	120, 80
BSA	0	300, 20	100, 20
	10	200, 0	60, 80
	25	500, 420	240, 320
	50	340, 60	300, 480

The manipulated spectra for average and high concentrations of the analyzed samples are depicted in Fig. 34. In the case of lysozyme, there is no change present between average and high concentrations of the protein for 0, 10 and 25 % PTMS. For 50 % PTMS, a slight peak shift to higher wavenumbers can be seen for the high concentration sample. Lipase shows an opposite trend with a change present for high concentrations in the case of 0 and 10 % PTMS, while the higher PTMS content gels do not show a significant difference in the spectra. The BSA samples display no change for the 0 % PTMS sample, while a shift for higher PTMS contents is evident. A shift of the amide I peak to higher wavenumbers is usually an indication of the formation of an unordered structure, as e.g. upon unfolding of the protein [11,22,23].

The data compiled in Fig. 34 is in agreement with the correlation results described earlier. Lysozyme and BSA react differently to higher PTMS concentrations than lipase. In the case of lysozyme and BSA, the areas of high concentration may contain structurally intact protein for lower PTMS content, while there is a structural change at a higher PTMS content. The result for BSA is in agreement with the literature [11], where it was found that BSA structure was intact throughout a protein concentration range for TMOS gels. As can be seen in Fig. 34, the addition of an organically modified precursor results in a change in BSA structure at high BSA concentrations. It can be speculated, that the presence of organic residues in combination with high protein concentration may lead to an aggregation and/or partial denaturation of the protein through hydrophobic interaction. Lipase, however, seems to exhibit a structural change at lower PTMS contents. This observation can help to explain the lack of lipase activity in lower PTMS content sol-gels [16]. At 25 and 50 % PTMS no change is obvious for lipase, which is in agreement with the presumption that PTMS is able to provide some stabilizing and activating effects on immobilized lipase.

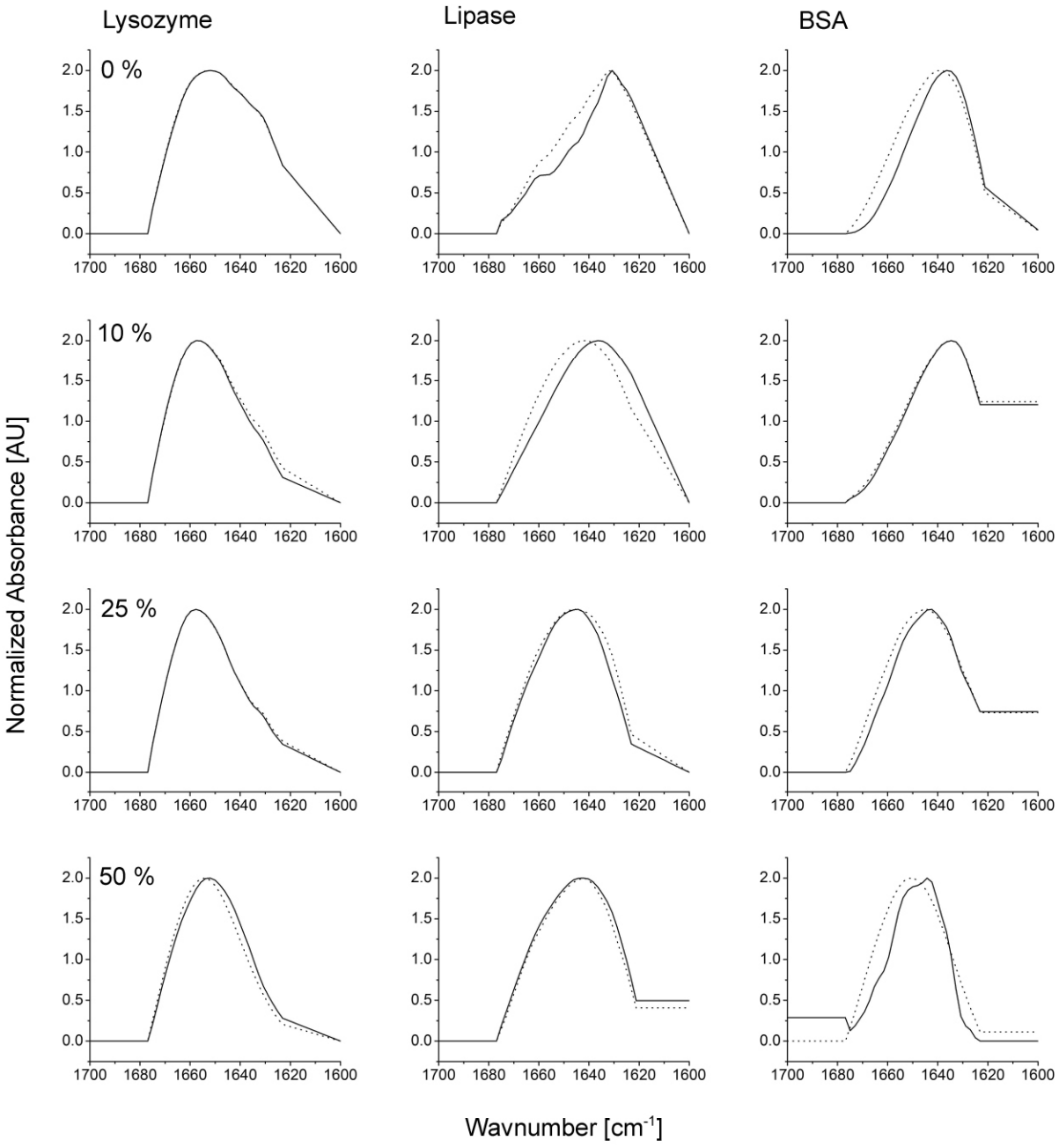

Fig. 34: Comparison of Amide I Peak for Average and High Concentrations of Protein

The smoothed, baseline corrected and normalized amide I peaks for average concentration data points (—) and high concentration data points (---) are compared for each sample. Data was collected for lysozyme, lipase and BSA entrapped in 0, 10, 25 and 50 % PTMS sol-gel thin films.

4.4 Conclusion

The scope of this chapter was to apply the methodology introduced in Chapter 3 to three model proteins immobilized in a set of sol-gels of varying PTMS content. It was found that the frequency distribution of lysozyme, lipase and BSA followed a normal Gaussian distribution in most cases. The spatial distribution characteristics of the model proteins in different immobilization matrices, however, differed depending on the nature of the protein and the sol-gel composition. These differences could be in part attributed to the surface characteristics of the model proteins. Additionally, the interaction of PTMS and lipase during the formation of the sol-gel is possible as a positive correlation of the positional information for the hydrophobic residues in the sol-gel thin films with lipase concentration was observed. On the other hand, a negative or no correlation between localized PTMS content and protein concentration could be observed for lysozyme and BSA. Moreover, implications on the changes in structure of the three model proteins in areas of high concentration, and in connection with PTMS content of the sol-gel, could be identified. These results represent a step forward in the understanding of biologically doped sol-gel systems and may aid in the explanation of some of the phenomena described in the literature, such as the activation of lipase in organically modified sol-gels.

4.5 References

[1] Drauz, K.; Waldmann, H. *Enzyme catalysis in organic synthesis*; Wiley-VCH: Weinheim, 2002.

[2] Clark, D. S. Can Immobilization Be Exploited to Modify Enzyme-Activity. *Trends in Biotechnology* **1994**, *12*, 439-443.

[3] Pierre, A. C. The Sol-Gel Encapsulation of Enzymes. *Biocatalysis and Biotransformation* **2004**, *22*, 145-170.

[4] Gupta, R.; Chaudhury, N. K. Entrapment of Biomolecules in Sol-Gel Matrix for Applications in Biosensors: Problems and Future Prospects. *Biosensors & Bioelectronics* **2007**, *22*, 2387-2399.

[5] Gill, I.; Ballesteros, A. Bioencapsulation Within Synthetic Polymers (Part 1): Sol-Gel Encapsulated Biologicals. *Trends in Biotechnology* **2000**, *18*, 282-296.

[6] Jin, W.; Brennan, J. D. Properties and Applications of Proteins Encapsulated Within Sol-Gel Derived Materials. *Anal.Chim.Acta* **2002**, *461*, 1-36.

[7] Jürgen-Lohmann, D. L.; Legge, R. L. Immobilization of Bovine Catalase in Sol-Gels. *Enzyme Microb.Technol.* **2006**, *39*, 626-633.

[8] Wetzel, D. L.; Striova, J.; Higgins, D. A.; Collinson, M. M. Synchrotron Infrared Micro Spectroscopy Reveals Localized Heterogeneities in an Organically Modified Silicate Film. *Vibrational Spectroscopy* **2004**, *35*, 153-158.

[9] Durrani, C. M.; Donald, A. M. Compositional Mapping of Mixed Gels Using FTIR Microspectroscopy. *Carbohydr.Polym.* **1995**, *28*, 297-303.

[10] Schultz, C. P. Precision Infrared Spectroscopic Imaging: The Future of FT-IR Spectroscopy. *Spectroscopy* **2001**, *16*, 24-+.

[11] Tran, C. D.; Ilieva, D.; Challa, S. Inhomogeneity in Distribution and Conformation of Bovine Serum Albumin in Sol-Gel: A Closer Look With a Near-Infrared Multispectral Imaging Technique. *Journal of Sol-Gel Science and Technology* **2004**, *32*, 207-217.

[12] Chen, B.; Miller, M. E.; Gross, R. A. Effects of Porous Polystyrene Resin Parameters on Candida Antarctica Lipase B Adsorption, Distribution, and Polyester Synthesis Activity. *Langmuir* **2007**, *23*, 6467-6474.

[13] Chen, B.; Miller, E. M.; Miller, L.; Maikner, J. J.; Gross, R. A. Effects of Macroporous Resin Size on Candida Antarctica Lipase B Adsorption, Fraction of Active Molecules, and Catalytic Activity for Polyester Synthesis. *Langmuir* **2007**, *23*, 1381-1387.

[14] Mei, Y.; Miller, L.; Gao, W.; Gross, R. A. Imaging the Distribution and Secondary Structure of Immobilized Enzymes Using Infrared Microspectroscopy. *Biomacromolecules* **2003**, *4*, 70-74.

[15] Higgins, D. A.; Collinson, M. M. Gaining Insight into the Nanoscale Properties of Sol-Gel-Derived Silicate Thin Films by Single-Molecule Spectroscopy. *Langmuir* **2005**, *21*, 9023-9031.

[16] Aucoin, M. G.; Erhardt, F. A.; Legge, R. L. Hyperactivation of Rhizomucor Miehei Lipase by Hydrophobic Xerogels. *Biotechnol.Bioeng.* **2004**, *85*, 647-655.

[17] Verger, R. 'Interfacial Activation' of Lipases: Facts and Artifacts. *Trends in Biotechnology* **1997**, *15*, 32-38.

[18] Günzler, H.; Gremlich, H. U. *IR spectroscopy*; Wiley-VCH: Weinheim, 2002.

[19] Gremlich, H. U.; Yan, B. *Infrared and Raman spectroscopy of biological materials*; Marcel Dekker: New York, 2001.

[20] Clifford, J. S.; Legge, R. L. Use of Water to Evaluate Hydrophobicity of Organically-Modified Xerogel Enzyme Supports. *Biotechnol.Bioeng.* **2005**, *92*, 231-237.

[21] www.proteinexplorer.org. Protein Explorer. 2007.

[22] Luft, M.; Boese, M. Untersuchung der Protein-Konformation mit FTIR. *Biospektrum* **2004**, *10*, 341-342.

[23] Perez, C.; Griebenow, K. Fourier-Transform Infrared Spectroscopic Investigation of the Thermal Denaturation of Hen Egg-White Lysozyme Dissolved in Aqueous Buffer and Glycerol. *Biotechnol.Lett.* **2000**, *22*, 1899-1905.

Chapter 5

Temperature Dependent Fluorescence and IR Spectroscopy of Model Proteins Immobilized in Sol-gel Thin Films

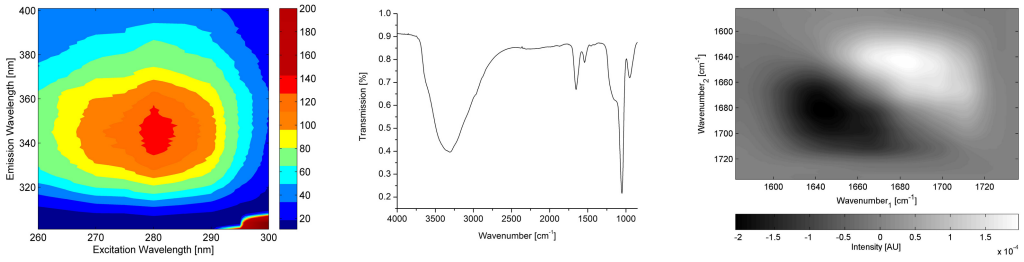

Preface

The effect of temperature on proteins immobilized in sol-gels is assessed by use of fluorescence and infrared spectroscopy in this chapter. For the same reasons outlined earlier, the proteins lysozyme, lipase and bovine serum albumin (BSA) were used as models for sol-gel immobilization. To gain an understanding of the stability of the immobilized biomolecules, they were subjected to a range of temperatures. Temperature was chosen for destabilization over chemical agents, such as urea, for practical reasons and to eliminate the influence of diffusion of a denaturant through the sol-gel matrix.

It should be noted at this point, that the spectroscopy in this chapter was performed without spatial resolution. In light of the results in Chapter 3 and 4, a given measurement can be seen as an average of a given sample, keeping in mind the heterogeneity present in sol-gel thin films.

Summary

Although the use of enzymes for industrial applications show great potential, their implementation from a practical perspective is still somewhat limited by various shortcomings in the area of enzyme immobilization. New characterization methods paired with new materials can help gain better insights into immobilized enzyme systems and provide information to improve their engineering and facilitate their industrial application.

Three model proteins (lysozyme [E.C. 3.2.1.17], lipase [E.C. 3.1.1.3] and bovine serum albumin (BSA)) were selected for various reasons and immobilized in sol-gel thin films. The physical characteristics of the sol-gels were modified by varying the amounts of the hydrophobic precursor propyltrimethoxysilane (PTMS) during synthesis. Fluorescence and Fourier transform infrared (FTIR) spectroscopy approaches were developed and then used to determine if there was a relationship between the physical properties of the sol-gels in relation to the characteristics of the selected model proteins. It was found that the PTMS content of the sol-gels had a direct effect on the physical properties of the immobilized proteins as evidenced by a blue shift of the intrinsic tryptophan (TRP) fluorescence. Temperature-dependent fluorescence spectroscopy revealed that the amount of TRP quenching was inversely proportional to the PTMS content of the sol-gel, suggesting that there were varying amounts of water available for quenching in the different immobilized enzyme systems in relation to the hydrophobicity of the support. Analysis of the sol-gels by 2D FTIR spectroscopy with a focus on the amide A region using Gaussian peak deconvolution revealed that for the 50 % PTMS thin film sol-gels with BSA that two different species of water could be identified; fully and not fully H-bonded. It was also found that these species of water showed different temperature dependent removal profiles. In addition, 2D FTIR of the amide I region followed by absorbance difference spectrum evaluation, revealed that the temperature stability of the three model proteins was sol-gel composition dependent. A hypothesis that the surface characteristics of the proteins determine the nature of the composition dependence is presented.

5.1 Introduction

The use of enzymes as efficient biocatalysts or in biosensors almost exclusively relies on immobilization [1]. Whereas the general knowledge about protein structure and chemistry as well as enzymatic reaction mechanisms has increased vastly over the past few decades, our fundamental understanding of immobilized enzyme systems is still relatively poor. As a result of this, the number of established enzymatic bioprocesses is still small compared to the variety of naturally occurring enzymatic reactions [1]. Recently, the understanding of immobilized enzyme systems on a molecular/microscopic level has improved significantly by using non-invasive spectroscopic measurements to characterize immobilized biomolecules [2-4]. Likewise, the availability of new materials with predefined properties, such as silica sol-gels, has renewed the interest in putting additional emphasis on engineering the immobilization support to enhance enzyme activity [5,6].

This chapter describes the use of temperature-dependent fluorescence and Fourier transform infrared (FTIR) spectroscopy to characterize sol-gel thin films containing immobilized lysozyme, lipase and bovine serum albumin (BSA). In particular, this work aims at identifying the influence of different immobilization matrices, represented by varying sol-gel compositions, on these three model proteins. In addition to their non-invasive nature, fluorescence and FTIR spectroscopy utilize responses generated from intrinsic properties of the materials, such as tryptophan fluorescence and amide absorption in the IR band [7-9]; as a result additional labeling, e.g. with fluorescent probes is not necessary. Both techniques are also sensitive to the presence of water, in this case allowing for a characterization of the sol-gel materials in terms of the amount and species of water present [7,10,11]. This is important, as water plays a special role in enzyme immobilization and enzyme functionality. Usually, a certain amount of water is necessary for the enzyme to retain activity [12]. Additionally, water content in an immobilization matrix can have an effect on mass transfer of substrate(s) and product(s) between the matrix and the bulk solution. In some reactions, e.g. ester hydrolysis, water might be a reactant [13] and so this relationship between the support matrix and water plays an additional role.

Fluorescence spectroscopy has been used to characterize sol-gels as an immobilization matrix, however, most of the current work has focused on the use of small reporter molecules or labeled proteins [2,14,15]. There has also been little focus on the influence of the sol-gel matrix composition on the immobilized species. 2D FTIR spectroscopy is a relatively new analysis method [16-18], that has not yet been applied to sol-gel entrapped proteins. It has been shown that 2D FTIR spectroscopy is a powerful tool and has been used to describe protein-doped Langmuir-Schaefer films in terms of water and protein properties [19]. A similar approach was adapted here and applied to sol-gel thin films containing various proteins and represents a significant step forward in the use of spectroscopy for *in situ* characterization of immobilized enzyme systems.

5.2 Materials and Methods

5.2.1 Materials

Lysozyme [E.C. 3.2.1.17] (43,900 units/mg protein, 95 % purity) from chicken egg white, BSA (Fraction V, 98-99 % albumin) and lipase [E.C. 3.1.1.3] (4,000 units/mg protein, > 95 % purity) from *Mucor miehei* were obtained from Sigma (Oakville, ON) and used without further purification. Tetraethoxysilane (TEOS) (98%, Sigma, Oakville, ON), propyltrimethoxysilane (PTMS) (98%, Fluka Chemicals, Oakville, ON) and 2-amino-2-(hydroxymethyl)propane-1,3-diol (TRIS) (Baker Chemicals, Phillipsburg, NJ) were used as received. Microscope glass cover slips were from Fisher Scientific (Ottawa, ON) and used without further preparation. Aluminum carriers were cut into 1 x 1 cm^2 pieces out of Anolux Miro IV (Anomet, Brampton, ON) sheets with a sheet metal notcher.

5.2.2 Sol-gel Preparation and Spin Coating

Sol-gel preparation and spin coating were performed as previously described (Chapter 4). Additionally, thin films were spin coated on microscope glass cover slips for fluorescence spectroscopy analysis. Cover slips were used without any treatment prior to the coating process and cut to size after coating with a diamond scribe.

5.2.3 Fluorescence Spectroscopy

Fluorescence spectroscopy was performed on a Cary Eclipse (Varian, Mississauga, ON) spectrofluorometer equipped with a temperature controlled multi-cell holder. Free proteins in solution were analyzed in quartz cuvettes, while immobilized proteins were fixed on a custom made sample holder (Fig. 35). Fluorescence maps were recorded in the excitation wavelength range from 260 – 300 nm and in the emission wavelength range from 300 – 400 nm. Scans were conducted at 280 nm excitation wavelengths and 300 – 400 nm emission wavelengths. In both cases, the slit width was set to 10 nm and the detector voltage was adjusted to account for the protein concentration present in each given sample.

Temperature dependent fluorescence spectroscopy was conducted at a constant detector voltage to allow for quantitative comparison of the results. A Cary Temperature Controller (Varian, Mississauga, ON) was used and profiles were programmed to start at 4 °C and ramp up to 84 °C with measurements every 5 °C after a 10 min equilibration time. The excitation wavelength was fixed at 280 nm while the emission was recorded at 310, 320, 330, 340, 350 and 360 nm at a slit width of 10 nm. The respective peak maximum emission wavelength was selected for each sample for temperature course analysis.

Sol-gel thin films were equilibrated to two different relative (rel.) humidity levels of 32.7 and 84.2 % at room temperature. Saturated salt solutions in desiccators were used to provide a controlled environment for equilibration. The higher humidity level was established with a KCl solution, while $MgCl_2 \cdot 6H_2O$ was used for the lower humidity level [20]. The actual humidity in the desiccators was verified and monitored using a hygrometer and was found to be within ± 5 % rel. humidity of the target value.

5.2.4 FTIR Spectroscopy

FTIR spectroscopy was conducted using a Hyperion 2000 microscope and a Tensor 27 FTIR spectrometer (Bruker Optics, Milton, ON). Spectral acquisition and evaluation were performed with OPUS 4.2 software (Bruker Optics, Milton, ON). Spectra were recorded over a wavenumber range from 4000 cm^{-1} to 500 cm^{-1} at a resolution of 4 cm^{-1} in reflectance mode. The aperture size was fixed at 100 μm x 100 μm for all measurements. A temperature controlled sample holder (Bruker Optics, Milton, ON) was used for all FTIR measurements. All spectra were averaged from 128 scans.

5.2.5 2D FTIR Spectroscopy

2D FTIR spectroscopy was performed on a Hyperion 2000 microscope and a Tensor 27 FTIR spectrometer (Bruker Optics, Milton, ON) using temperature as the perturbation parameter. Samples were equilibrated at 30 ^{o}C and the initial spectrum was recorded with the same instrument parameters as described above. The temperature was increased in 10 ^{0}C steps from 30 ^{o}C to 110 ^{o}C and spectra were collected for each temperature after a 10 min equilibration period.

Asynchronous 2D FTIR correlation was performed on the amide A (~3300 cm^{-1}) and the amide I (~1650 cm^{-1}) regions using OPUS 4.2 software (Bruker Optics, Milton, ON). A smoothing algorithm (15 points) was applied in some cases to improve the spectrum quality. Gaussian deconvolution was calculated with Origin Pro 7.5 (Origin Lab, Northampton, MA) software. Absorbance difference spectra were calculated using the initial spectrum at 30 ^{o}C as a reference.

5.3 Results and Discussion

5.3.1 Fluorescence Spectroscopy

Fluorescence spectroscopy is a very attractive technique for protein analysis. The fact that most proteins/enzymes contain the amino acid TRP allows characterization of the biomolecule of interest without the need for labeling [7]. Compared to UV/vis spectroscopy, fluorescence is very sensitive, making *in situ* detection of the immobilized protein possible [14]. Sol-gels - and especially thin films - as an immobilization matrix are unique in that they can provide an optically transparent material, which is compatible with light in the excitation/emission wavelengths of TRP [2,15].

Standard microscope cover slips were used as a carrier material for the sol-gel coatings. To account for the perpendicular orientation of the fluorometer excitation source and emission detector, a sample holder was constructed (Fig. 35).

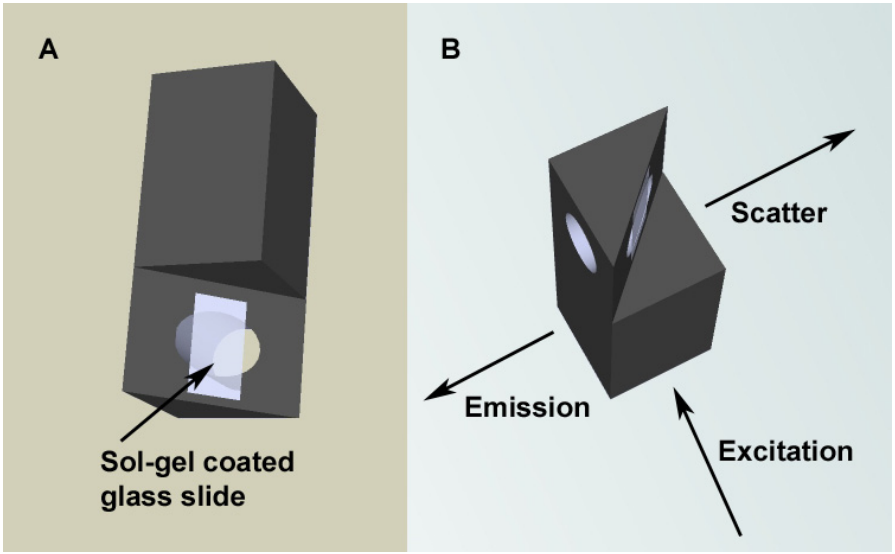

Fig. 35: Sample Holder for Fluorescence Spectroscopy of Sol-gel Thin Films

Illustration of the aluminum sample holder used for fluorescence spectroscopy. The coated microscope cover slide was held in place with an elastic rubber band (not shown) (A). The sample was fixed at a 45° angle to minimize scattering off the glass slide.

The sample holder minimized reflections off the sample into the detector by fixing the coated cover slip at a 45° angle. The sample holder was machined to fit snugly into the temperature controlled fluorometer cell holder to ensure heat transfer to the sample. The *in situ* detection of lysozyme in a 0 % PTMS sol-gel is shown as an example in Fig. 36. A blank sol-gel was also analyzed and did not show any significant background fluorescence in the relevant range. However, some background scattering in the emission range from 360 to 400 nm can be observed. The TRP signal is centered at 280 nm excitation and 345 nm emission wavelengths. This corresponds with the excitation and emission wavelengths of free lysozyme as reported in the literature [21], indicating that there are no dramatic changes in protein structure upon immobilization at least based on this TRP signal.

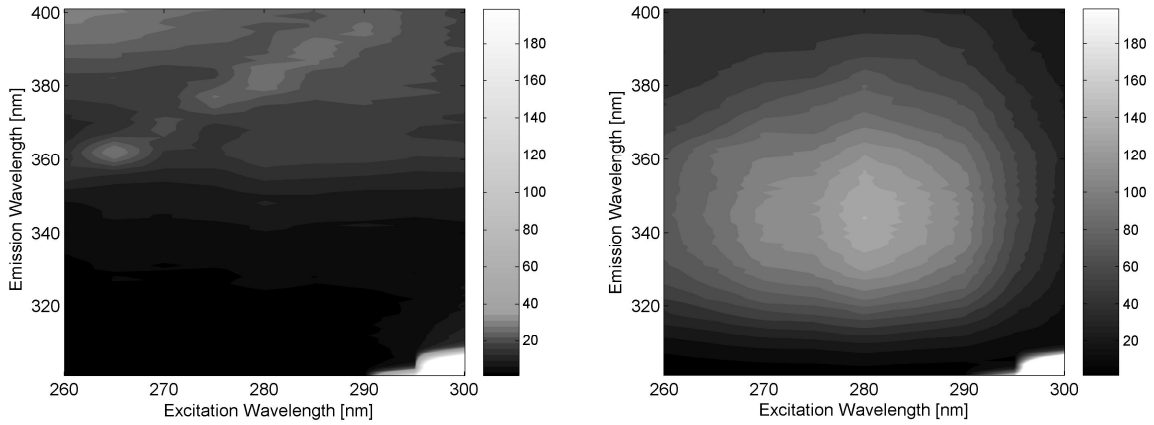

Fig. 36: Fluorescence Map of a Blank and Lysozyme Doped 0 % PTMS Thin Film

The fluorescence map of a blank 0 % PTMS film (left) shows no significant fluorescence. The sample containing immobilized lysozyme (right) shows the typical TRP fluorescence at 280 nm as the excitation wavelength and 345 nm as the emission wavelength.

It should be noted that the intrinsic fluorescence can only give information on the environment of the three TRP residues; therefore, no absolute conclusion on protein structure can be drawn from this. The signal strength obtained from the immobilized protein proved to be strong enough to ensure reliable detection.

Lysozyme, lipase and BSA were entrapped in sol-gel thin films with 0, 10, 25 and 50 % PTMS content. The different sol-gel materials are known to have different properties e.g. in terms of

pore size and hydrophobicity [3,13,22]. It is not well understood, however, if a change in material properties influences the immobilized protein directly. TRP fluorescence is sensitive to the hydrophobicity of its environment and can therefore serve as an intrinsic probe. The fluorescence of the three proteins immobilized in the different sol-gel materials can be seen in Fig. 37.

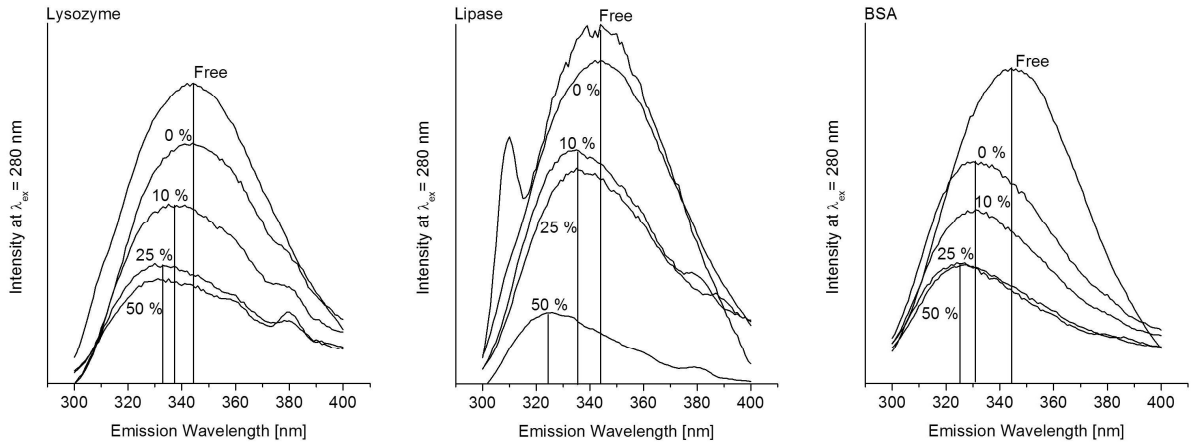

Fig. 37: TRP Fluorescence of Free and Immobilized Lysozyme, Lipase and BSA

Fluorescence spectra for lysozyme (left), lipase (center) and BSA (right). For the sol-gel thin film immobilized samples, the PTMS content is indicated with each respective curve. The spectra have been scaled to allow a better visualization of the blue shift phenomenon.

A blue shift of the TRP emission wavelength indicates a more hydrophobic environment [7]. As a general trend it can be seen from Fig. 37 that a blue shift occurs for all immobilized proteins as the hydrophobicity, i.e. the PTMS content of the immobilization matrix, was increased. However, the extent and the movement of the shift varied depending on the protein. Results are summarized in Table 8.

Table 8: TRP Fluorescence Emission Wavelength Maxima of the Three Model Proteins

Protein	Sol-gel	TRP Emission Wavelength [nm]	Magnitude of Blue Shift [nm]
Lysozyme	Free	345	-
	0 %	345	0
	10 %	337	7
	25 %	333	12
	50 %	333	12
Lipase	Free	345	-
	0 %	345	0
	10 %	335	10
	25 %	335	10
	50 %	325	20
BSA	Free	345	-
	0 %	331	14
	10 %	331	14
	25 %	325	20
	50 %	325	20

The differences in the blue shifts for the different proteins are likely caused by a combination of factors. All three proteins contain multiple TRP residues (lysozyme: 3, lipase: 4, BSA: 3). The TRP residues may be more or less exposed on the protein surface, depending on the tertiary structure.

Lysozyme and lipase show a similar trend, with the 0 % PTMS sol-gel leading to a TRP signal comparable to that of the free enzyme. The fact that lipase in a 0 % PTMS gel shows no TRP shift is in agreement with the literature that suggests that lipase is only active in sol-gels that

contain some PTMS as a precursor [6,13]. Lipase may require some hydrophobicity in the gel to cause the activation of the enzyme, which is accompanied by a change in the lid structure covering the active site [23].

BSA, however, shows a change in the TRP fluorescence upon immobilization, even for a 0 % PTMS gel. It can be, therefore, speculated that immobilization of BSA in sol-gels *per se* causes a subtle change of the protein. BSA is a plasma protein that has a number of functions *in vivo*, such as conserving the osmotic blood pressure and the transport of a range of molecules (fatty acids, steroid hormones, inorganic ions) [24]. BSA, therefore, has a variety of hydrophobic as well as ionic binding sites [24] and non-specific protein matrix interactions over a variety of sol-gel compositions are expected.

The various (12) immobilized protein samples were equilibrated at two different humidity levels of 32.7 % (low) and 84.2 % (high) rel. humidity [20]. A TRP fluorescence profile over a temperature range of 4 to 85 °C was recorded. A typical normalized fluorescence response of TRP to an increase in temperature shows a constant baseline slope at low temperatures, followed by a steeper slope and a gentle slope in the high temperature range [25]. The steep slope corresponds to a major structural change as the protein unfolds [25] exposing the TRP and changing the fluorescence intensity. When the TRP residue is exposed to water upon unfolding of the protein, the fluorescence intensity is quenched [7,25].

The TRP fluorescence of the sol-gel immobilized proteins upon temperature treatment is shown in Fig. 38, Fig. 39 and Fig. 40. The typical response as described above was not seen in any of the figures. This is most likely due to the presence of multiple TRP residues, the case for all three proteins, which are quenched to different degrees at different temperatures. Additionally, immobilized proteins usually exist in a number of subpopulations with slightly different thermostability [26]. Therefore, no obvious temperature could be identified that correlated with a major structural change in the immobilized protein. However, the ability of the different sol-gel materials and humidity levels to quench the TRP fluorescence can be compared providing insight into the amount of water present in the different sol-gel materials.

As a general trend in all cases it can be seen that the high humidity samples displayed a greater degree of quenching compared to the low humidity samples. The 0 % PTMS sol-gel, the most

hydrophilic of the immobilization matrices, shows the greatest extent of quenching in all cases. Also, in all cases the high humidity samples show a greater difference between the different sol-gel compositions than the low humidity samples. This is expected, since exposure to a higher humidity enables a 0 % PTMS gel to take up more water than a hydrophobic gel. The difference between high and low humidity for a 50 % PTMS gel, or strongly hydrophobic matrix, should be marginal (Fig. 38, Fig. 39 and Fig. 40). These results confirm the previous findings [13] with regards to water content and the hydrophobicity of sol-gel bulk materials, demonstrating that this also applies at least qualitatively to sol-gel thin films.

The relationship between the amount of PTMS and the extent of quenching was generally consistent for all three immobilized proteins. For example, lysozyme shows a clear distinction between 0 % PTMS and the other compositions at high humidity, while the fluorescence quenching for low humidity is virtually indistinguishable (Fig. 38). Lipase on the other hand, shows similar decreases in fluorescence for 0, 10 and 25 % PTMS with only the 50 % PTMS gel displaying a significantly reduced quenching for high and low humidity (Fig. 39). BSA consistently shows less quenching with each increase in PTMS content for both humidity levels (Fig. 40).

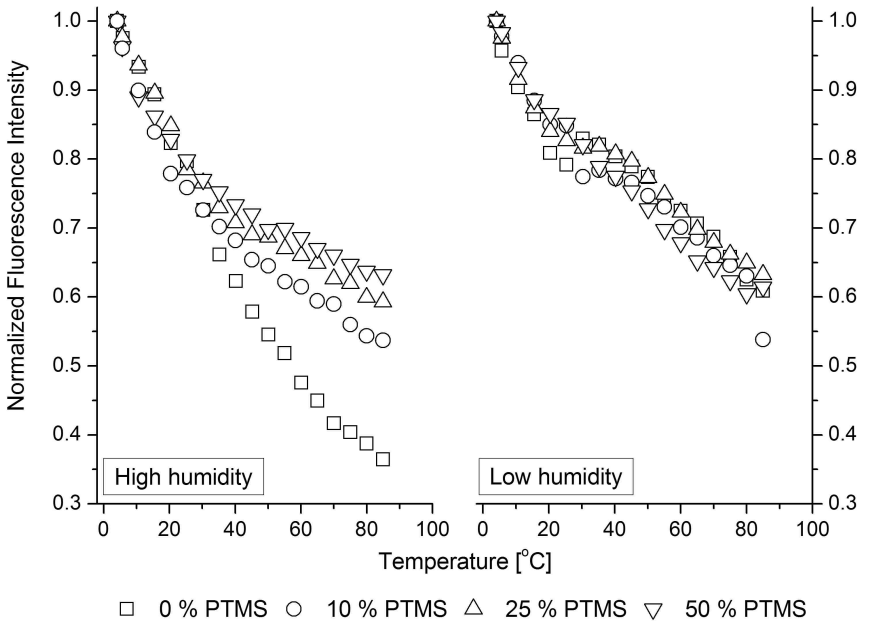

Fig. 38: TRP Fluorescence Quenching for Immobilized Lysozyme

Temperature course of TRP fluorescence for immobilized lysozyme for different sol-gel compositions and different humidity levels.

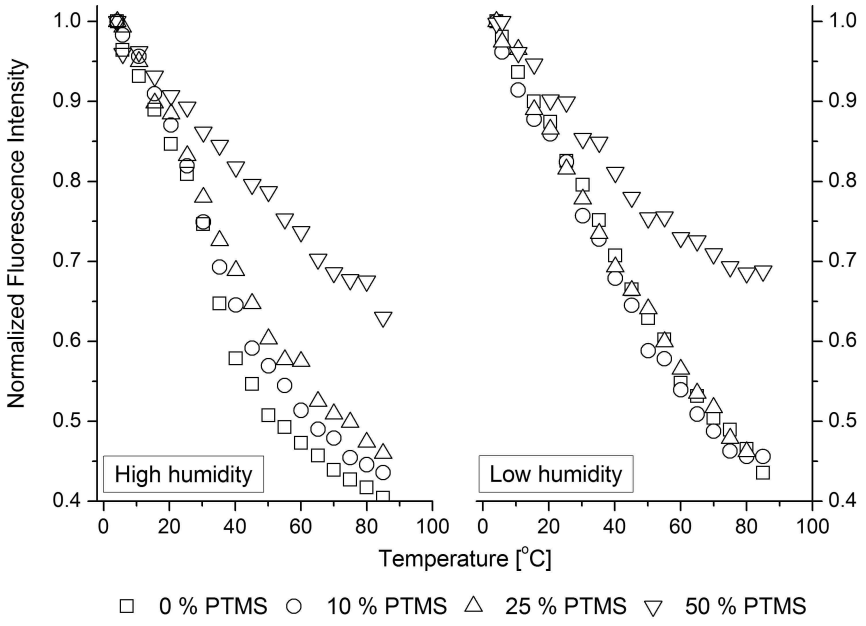

Fig. 39: TRP Fluorescence Quenching for Immobilized Lipase

Temperature course of TRP fluorescence for immobilized lipase for different sol-gel compositions and different humidity levels.

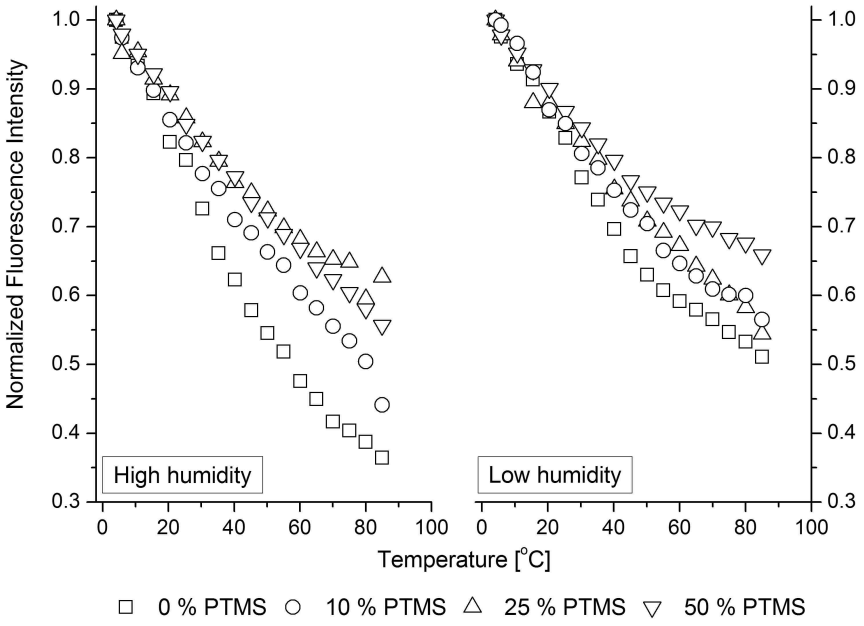

Fig. 40: TRP Fluorescence Quenching for Immobilized BSA

Temperature course of the TRP fluorescence for immobilized BSA for different sol-gel compositions and humidity levels.

The differences in trends for the different enzymes, matrix compositions and environmental conditions are most likely a combination of the quenching of multiple TRP residues, different unfolding steps and unfolding temperatures of the immobilized species and also different stabilizing effects of the immobilization matrix on the proteins. The complexity of the scenario does not allow for a distinction between these effects with the data obtained.

The previously described general trend that more hydrophobic sol-gel leads to a blue shift in the TRP fluorescence is valid for all three model proteins studied. These results indicate a direct influence of the immobilization material on the immobilized protein. If a sol-gel immobilized enzyme is characterized for its activity, it is, therefore, important to take direct effects of the sol-gel on the enzyme into consideration. These have to be combined with the physical effects of the immobilization material in the reaction system to obtain a complete picture.

5.3.2 FTIR Spectroscopy

FTIR spectroscopy was performed for the three model proteins for the four different sol-gel compositions. As described in Chapter 3 and 4, a coating procedure was developed to generate sol-gel thin films on aluminum carriers that were suitable for analysis by FTIR microscopy in reflectance mode. A sample FTIR spectrum of lysozyme immobilized in 0 % PTMS sol-gel thin film is given in Fig. 41.

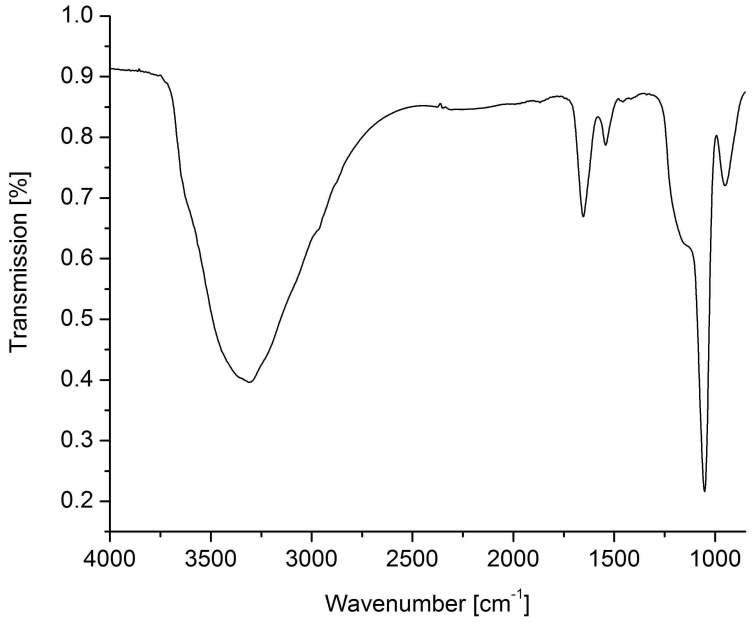

Fig. 41: Sample FTIR Spectrum of Lysozyme in 0 % PTMS Sol-gel Thin Film

Three characteristic peak groups corresponding to Si-O-Si/Si-OH (~800 to 1300 cm^{-1}), to the amide I and II signal(~1500 to 1700 cm^{-1}) and the N-H stretching mode/O-H stretching (~3300 cm^{-1}) are evident [8].

Three characteristic regions can be identified in Fig. 41. The peak group corresponding to Si-O-Si and Si-OH bonds from ~800 to 1300 cm^{-1} [8], the amide I and II group from ~1500 to 1700 cm^{-1} [9] and a broad peak centered at around 3300 cm^{-1}. This broad peak is the summation of several signals in this region. It contains the signal for ethylene stretching at ~2800 cm^{-1}, which is difficult to make out in a 0 % PTMS gel [8]. It also contains the amide A band (N-H stretching mode) [11], corresponding to the immobilized protein and the peaks corresponding to

H_2O in different H-bonding states, fully and not-fully H-bonded [10]. This peak decreases significantly upon thermal treatment. It is not evident, however, from the general FTIR spectrum which of the three chemical species, i.e. amide A, fully or not-fully H-bonded water, decreases at which temperature. 2D FTIR can give an insight into these phenomena.

5.3.3 2D FTIR of the Amide A Region

In order to identify the processes taking place in the immobilized protein system upon thermal treatment, the asynchronous 2D FTIR spectrum of the amide A region (3000 – 4000 cm^{-1}) of the BSA in 50 % PTMS was generated from 9 spectra collected at temperatures from 30 °C to 110 °C. The asynchronous spectrum generated is given in Fig. 42 [16].

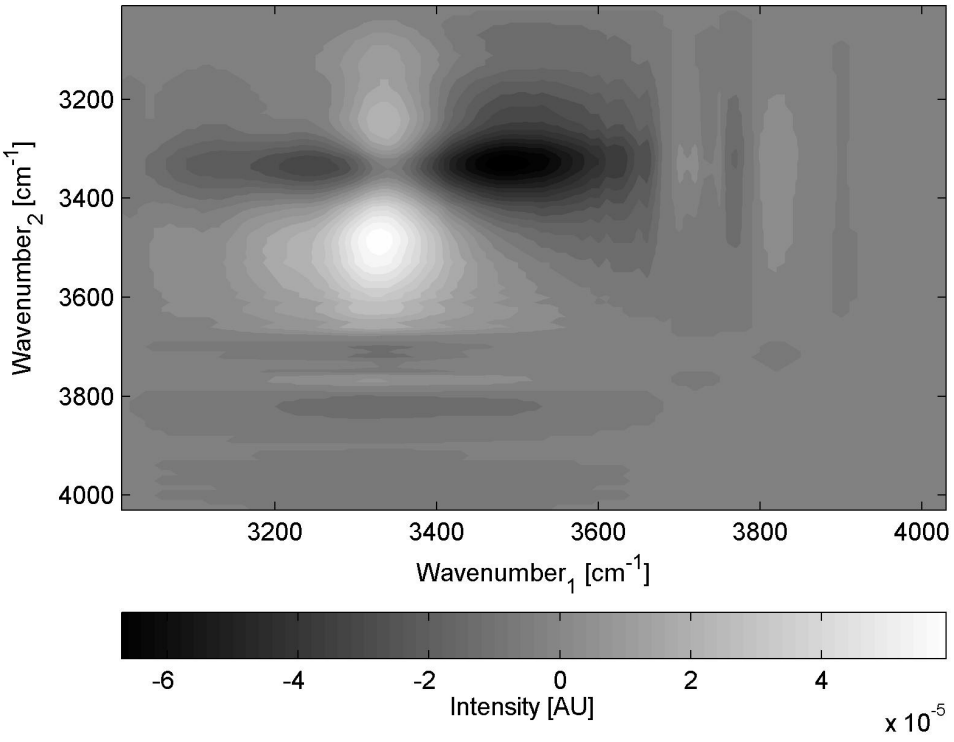

Fig. 42: Asynchronous 2D FTIR Map of the Broad Peak of a 50 % PTMS Thin Film containing BSA

Two correlation squares can be built from the positive cross peak at 3330 cm^{-1} to the negative cross peak at 3250 cm^{-1} and the negative cross peak at 3500 cm^{-1} [17].

Two correlation squares can be identified in Fig. 42. The first square is between the positive peak at 3330 cm^{-1} and the negative peak at 3500 cm^{-1}. The second square can be built from the positive peak at 3330 cm^{-1} and the negative peak at 3250 cm^{-1}. The peaks can be assigned to the amide A N-H stretching mode at 3330 cm^{-1}, to O-H stretching in a fully H-bonded environment (3250 cm^{-1}) and O-H stretching in a not fully H-bonded environment (3500 cm^{-1}) [10]. From Fig. 42 it can be concluded that the two O-H stretching bands are asynchronously correlated with the amide A band and sensitive to a change in temperature. The broad peak centered at around 3300 cm^{-1} was deconvoluted into the three components (3250 cm^{-1}, 3330 cm^{-1} and 3500 cm^{-1}) for each of the 9 temperatures investigated to track the change with temperature in the three chemical species. The deconvolution is shown in Fig. 43 and the parameters of the deconvolution into three Gaussian components are summarized in Table 9.

Table 9: Parameters of the Deconvolution of the Amide A Region

Temperature [^oC]	Area 3250 cm^{-1} [counts]	Area 3330 cm^{-1} [counts]	Area 3500 cm^{-1} [counts]	R^2
30	11.5	4	20.3	0.998
40	18.4	3.3	8.9	0.998
50	13.6	3.2	10	0.998
60*	17.2	3.2	3.4	0.997
70	11.2	3.1	7.4	0.997
80	11	3	5.6	0.996
90	9.6	2.8	4.6	0.997
100	7.9	2.7	4.3	0.996
110	0.7	4.3	7.2	0.993

**The 60 ^oC value was classified as an outlier.*

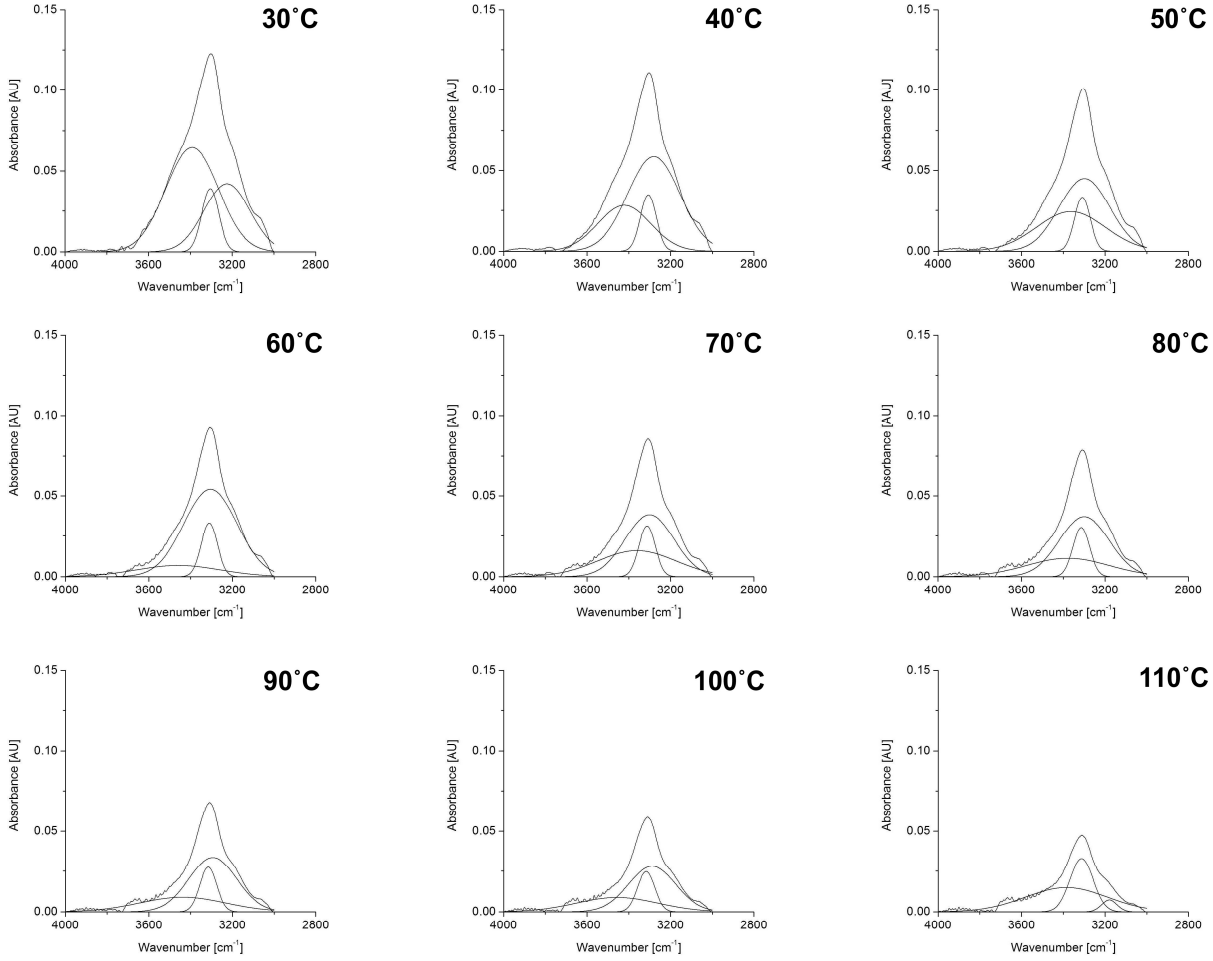

Fig. 43: Deconvolution of the Broad Peak Region for a BSA 50 % PTMS Sol-gel Thin Film

The broad peak region at different temperatures is depicted. The large main peak at 3300 cm^{-1} is a superposition of three smaller peaks at 3250 cm^{-1} (O-H stretching in fully H-bonded environment), 3500 cm^{-1} (O-H stretching in not fully H-bonded environment) and 3330 cm^{-1} (N-H stretching mode). The N-H stretching mode signal stays relatively constant, while the two O-H stretching signals and the superimposed peak decrease.

It can be seen that the signal for O-H stretching in a not fully H-bonded environment (3500 cm^{-1}) decreases steadily until about 60 °C when it becomes constant. The peak corresponding to O-H stretching in a fully H-bonded environment remains somewhat constant until about 80 °C

and then starts to decrease rapidly. This result is expected as fully H-bonded water is more tightly bound in the system. The N-H stretching mode signal remains relatively constant throughout the whole temperature range. This is also expected since no decomposition of the protein should take place for the chosen temperatures. The temperature courses of the three peaks are summarized in Fig. 44. It should be noted that the values for 60 °C were not included as these values were considered outliers as they do not fit the general trend very well.

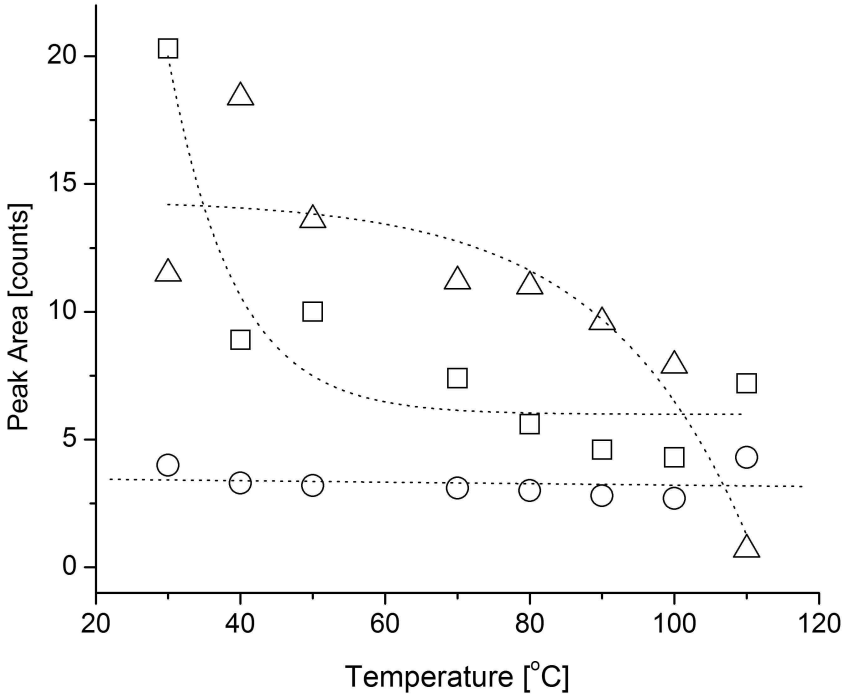

Fig. 44: Temperature Course of the Three Components of the Broad Peak Region for a BSA 50 % PTMS Sol-gel Thin Film

The temperature course for the N-H stretching mode (○) shows no significant temperature dependence. The O-H stretching in a not fully H-bonded environment (□) decreases rapidly to about 60 °C and remains relatively constant at higher temperatures. The O-H stretching in a fully H-bonded environment (Δ) remains relatively constant to about 80 °C and decreases rapidly at higher temperatures. The dotted lines are intended as a visual aid and do not represent a temperature course model.

The results obtained here are in excellent agreement with the literature. A similar system with lysozyme in Langmuir-Schaefer films obtained by Pechkova *et al.* [19] was found to retain fully H-bonded water up to temperatures of 100 °C while the protein signal was stable up to 200 °C. The deconvolution of the broad peak centered at 3300 cm^{-1} requires excellent quality spectra. Out of the 12 samples investigated, only the BSA in 50 % PTMS provided the required quality. For the lysozyme and lipase samples, the peaks at 3330 cm^{-1} and 3250 cm^{-1} could not be distinguished by deconvolution, even though their presence could be verified by asynchronous 2D FTIR analysis. A possible reason for this is the complexity of the doped sol-gel thin film system that results in a very broad peak centered at 3300 cm^{-1} that often stretches down to 2600 cm^{-1}. It is therefore consistent that lower water content sol-gels (such as 50 % PTMS) are more likely to be suitable for peak deconvolution as they exhibit a smaller peak in the 3300 cm^{-1} region. This analysis nevertheless presents a powerful method to further explain the role of water in sol-gel immobilization systems.

5.3.4 2D FTIR of the Amide I Band

As shown above, the signal intensity corresponding to immobilized protein remains constant over the selected temperature range. It can, however, be assumed that the immobilized biomolecules undergo significant changes in structure within this temperature range [27]. Protein structure can to a certain extent be deducted from the peak shape of the amide I peak (~ 1650 cm^{-1}). To identify the major components of this peak that are changing within the selected temperature range, an asynchronous 2D FTIR map of the amide I region was constructed for all 12 samples. A typical 2D FTIR map of this region is given in Fig. 45.

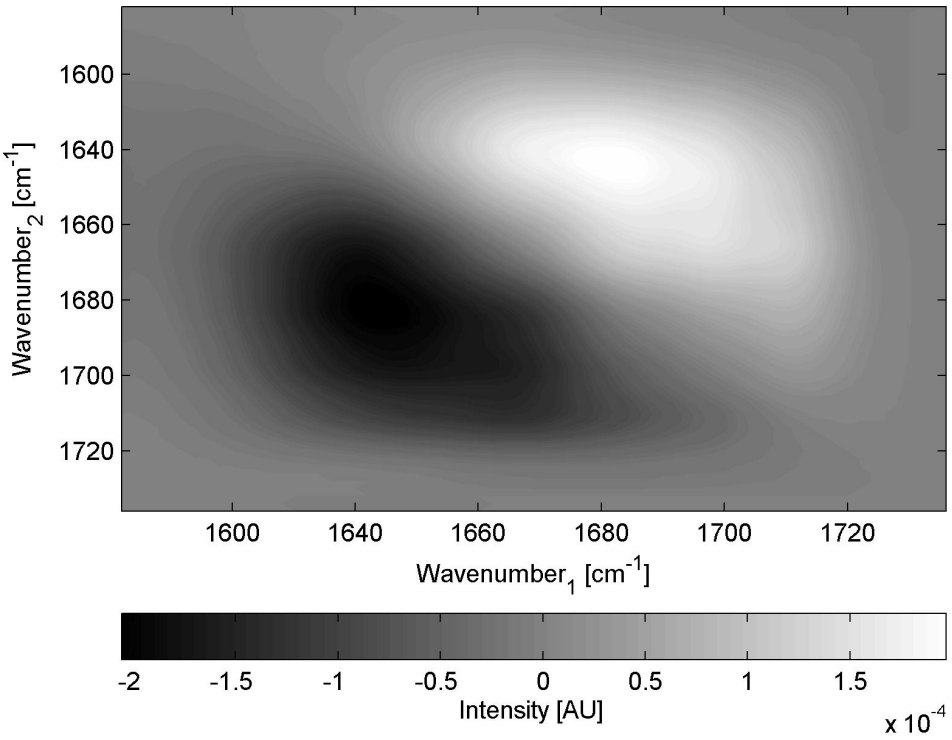

Fig. 45: Sample Asynchronous 2D FTIR Map of the Amide I Region of a BSA 50 % PTMS Sol-gel Thin Film

A correlation square can be built between the positive cross peak at 1680 cm^{-1} and the negative cross peak at 1640 cm^{-1}. The peaks represent the formation of an unstructured conformation and the unfolding of a β-sheet, respectively [17].

A correlation square can be constructed from the negative cross peak at 1640 cm^{-1} and the positive cross peak at 1680 cm^{-1} [16]. As described above, suitable spectra are required for a full deconvolution of superimposed peaks. The data collected was not sufficient for this analysis method; however, difference spectra could be obtained, taking the 30 °C spectrum as a reference. A sample difference spectrum is given in Fig. 46.

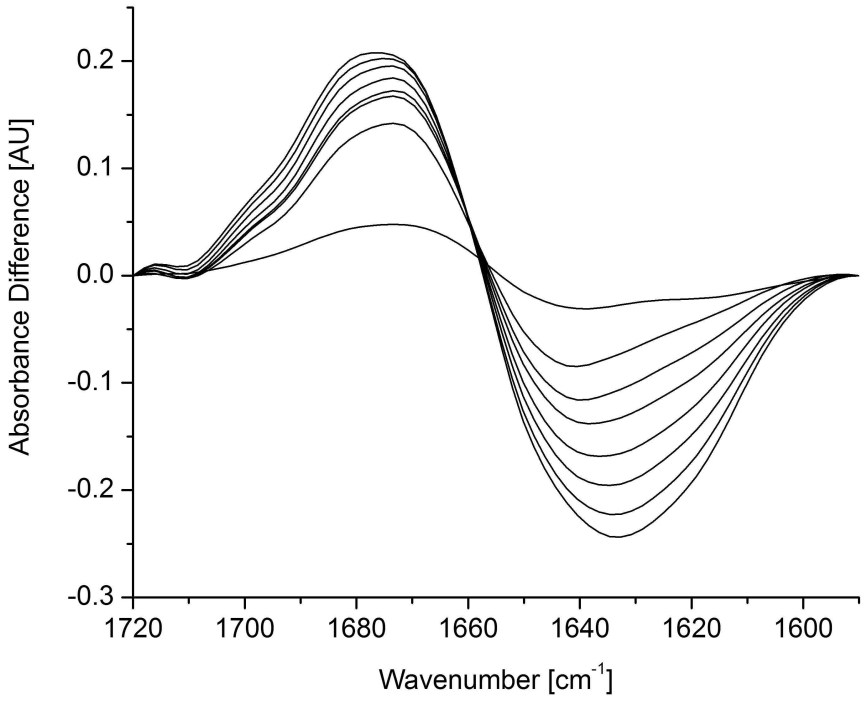

Fig. 46: Sample Difference Spectrum of the Amide I Region of a Lysozyme 0 % PTMS Sol-gel Thin Film

The spectra represent the difference between the recorded signal for 30 °C and 40, 50, 60, 70, 80, 90, 100, 110 °C respectively. With increasing temperature, an increase in the difference at 1680 cm^{-1} can be observed, while the difference at 1640 cm^{-1} is decreasing.

Fig. 46 shows that an increase in the difference absorbance at 1680 cm^{-1} and a decrease in difference absorbance at 1640 cm^{-1} occur with increasing temperature. An increasing absorbance at 1680 cm^{-1} corresponds to the formation of an unstructured protein conformation, whereas a decrease at 1640 cm^{-1} corresponds to the unfolding of a β-sheet [28]. Using FTIR spectroscopy, these two characteristics are the most prominently detected ones. Correct protein structure is a feature generally required for correct protein function. The unfolding of β-sheets and the formation of an unordered conformation can represent a change that is synonymous with a decrease or even loss in protein function.

Amide I difference spectra were calculated for 10 samples (spectra for lysozyme and lipase in 10 % PTMS could not be obtained) and the difference absorbance at 1640 and 1680 cm^{-1} plotted (Fig. 47, Fig. 48 and Fig. 49). The original difference absorbance spectra can be found in the Appendix (B).

Immobilized lysozyme (Fig. 47) showed a relatively steady increase at 1680 cm^{-1} and decrease at 1640 cm^{-1} in the difference spectrum over the temperature range investigated. It can be seen from Fig. 47 that the structural change in the enzyme is most prominent for the 0 % PTMS sol-gel and least prominent for the 50 % PTMS sol-gel. The top branch in Fig. 47, corresponding to the formation of an unstructured protein conformation, shows the largest increase for the 0 % PTMS sol-gel and the least increase for the 50 % PTMS sol-gel. Similarly, the bottom branch, corresponding to the unfolding of a β-sheet structure, shows the largest decrease in difference absorbance at 1640 cm^{-1} for the 0 % PTMS composition. The differences, however, are not as pronounced as for the formation of an unordered structure.

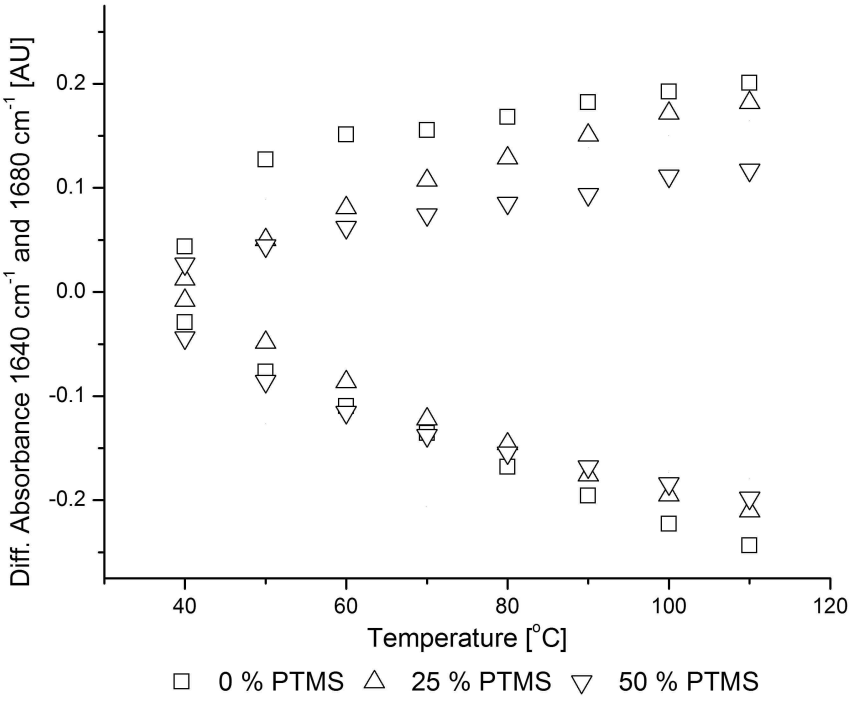

Fig. 47: Temperature Course for the Difference Absorbance for Immobilized Lysozyme

Sol-gel thin film immobilized lysozyme shows the best thermal stability when immobilized in 50 % PTMS followed by 25 % PTMS and 0 % PTMS. The top branch of the graph corresponds to the formation of an unstructured protein conformation (1680 cm^{-1}) while the bottom branch corresponds to the unfolding of a β-sheet structure (1640 cm^{-1}).

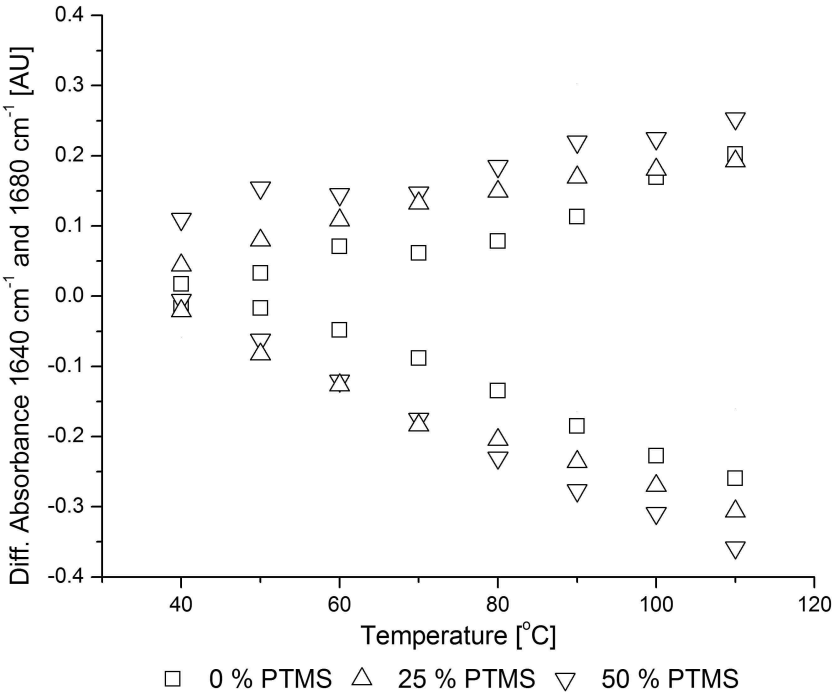

Fig. 48: Temperature Course for the Difference Absorbance for Immobilized Lipase

Sol-gel thin film immobilized lipase shows the best thermal stability when immobilized in 0 % PTMS followed by 25 % PTMS and 50 % PTMS. The top branch of the graph corresponds to the formation of an unstructured protein conformation (1680 cm^{-1}) while the bottom branch corresponds to the unfolding of a β-sheet structure (1640 cm^{-1}).

Similar to lysozyme, BSA (Fig. 49) is most stable in a 50 % PTMS sol-gel and least stable in a 0 % PTMS gel. The formation of an unordered structure is significantly more pronounced for 0 and 10 % PTMS gels as indicated by the top branch in Fig. 49. The unfolding of β-sheet structures, is least prominent for 50 % PTMS, while the 10 and 25 % PTMS samples show similar temperature stability (Fig. 49). The 0 % PTMS composition displays the least thermal stability towards unfolding of β-sheets. In contrast to lysozyme, however, BSA seems to display somewhat of a common thermostability of all preparations up to about 60 °C.

Lipase (Fig. 48) on the other hand, displays a reversed behavior in terms of thermostability of the different preparations. The 50 % PTMS preparation is least stable, whereas the 0 % PTMS

sol-gel shows the best stability. A similar magnitude of difference between the compositions can be seen for both features evaluated, the formation of unstructured protein (top branch, Fig. 48) and the unfolding of β-sheets (bottom branch, Fig. 48.).

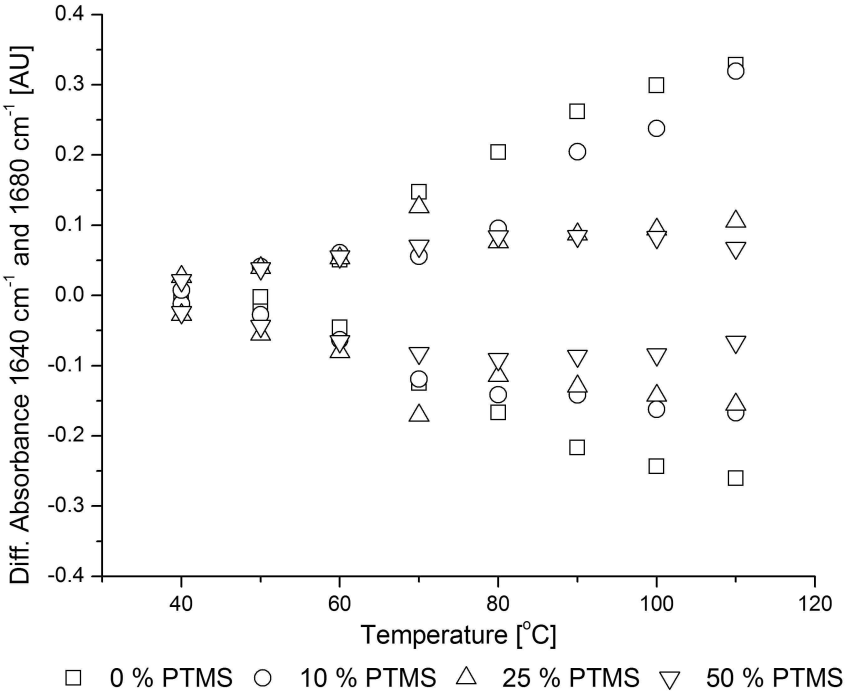

Fig. 49: Temperature Course for the Difference Absorbance for Immobilized BSA

Sol-gel thin film immobilized BSA shows the best thermal stability when immobilized in 50 % PTMS followed by 25 % PTMS, 10 % PTMS and 0 % PTMS. The top branch of the graph corresponds to the formation of an unstructured protein conformation (1680 cm^{-1}) while the bottom branch corresponds to the unfolding of a β-sheet structure (1640 cm^{-1}).

To interpret these phenomena, the three model proteins were compared in terms of their size and surface hydrophobicity (Fig. 50). Lysozyme is a relative small protein (15 kDa) and shows a mixed surface hydrophobicity. Lipase on the other hand is somewhat larger (40 kDa) and shows significant hydrophobic patches on the surface. Because the crystal structure of BSA is not available, HSA (human serum albumin) was taken as a representative model instead. BSA is a relatively large protein (69 kDa) and the HSA model displays a mixed surface hydrophobicity [29].

The different sol-gel materials are presumed to vary predominantly in hydrophobicity and in pore size, with 50 % PTMS being the most hydrophobic and having the largest pores [3,22]. If the difference in thermostability of the different proteins was due mainly to the size of the protein, a similar behavior of lysozyme and lipase would be expected, while BSA would be expected to behave differently. However, it was shown that lysozyme and BSA have similar preferential sol-gel compositions for highest stability (Fig. 47 and Fig. 49), while lipase displays a different preference (Fig. 48).

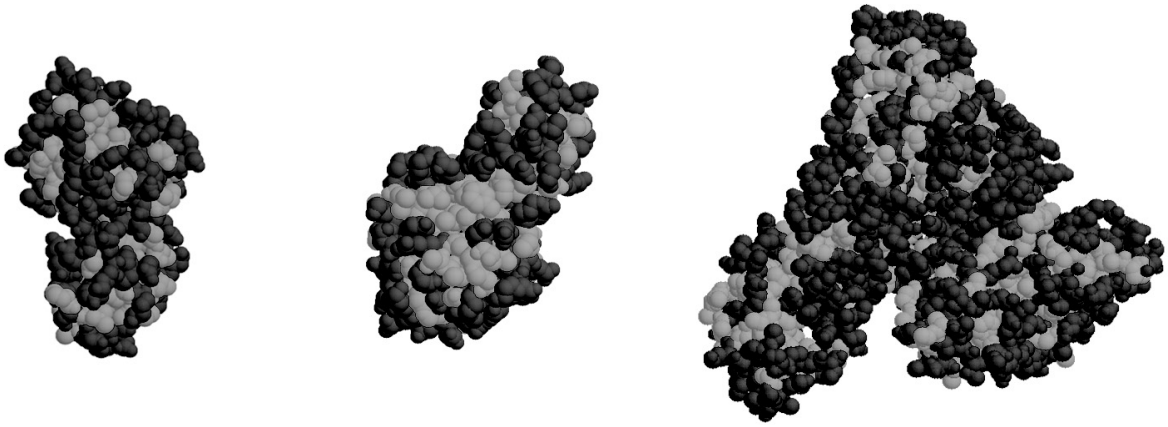

Fig. 50: Protein Surface Models for Lysozyme, Lipase and HSA

3D protein models for lysozyme (right), lipase (center) and HSA (right) are colored to show hydrophilic (dark) and hydrophobic (light) regions. Lipase is characterized by a large hydrophobic patch. HSA was used as a model for BSA. The 3D models are not to scale [29]. The PDB codes used are 2vb1 (Lysozyme), 3tgl (Lipase) and 1bm0 (HSA).

BSA and lysozyme show similar surface characteristics and similar preferential sol-gel compositions for increased thermostability. Both proteins show mixed surface hydrophobicity (Fig. 50) and displayed the best thermostability in 50 % PTMS sol-gels (Fig. 47 and Fig. 49). Lipase on the other hand has different surface characteristics with large hydrophobic patches (Fig. 50) and shows a different preferential sol-gel composition; it is most stable in a 0 % PTMS sol-gel (Fig. 48). It can therefore be assumed that the surface characteristics of a sol-gel immobilized protein are the dominant factor over the protein size to determine the thermostability of different sol-gel compositions. Further research, characterizing the thermostability of sol-gel immobilized proteins in terms of activity is needed to confirm this assumption.

5.4 Conclusion

The work described here represents a significant step forward in spectroscopic *in situ* characterization of sol-gel immobilized protein systems. It was shown with fluorescence spectroscopy that the varying hydrophobicity of different sol-gel compositions has a direct effect on the entrapped biomolecules. The three model proteins tested, lysozyme, lipase and BSA, were affected to a varying degree by the composition of the entrapment matrix. Fluorescence spectroscopy also confirmed that previous findings about the hydrophobicity/water content of sol-gel bulk material apply qualitatively to thin films. Higher PTMS content in a sol-gel thin film resulted in a reduction in TRP fluorescence quenching through a reduction in available water.

Additionally, the application of 2D FTIR spectroscopy helped to gain valuable insight into the chemical complexity of a doped sol-gel system. It was found that predominantly two species of water are present in the sol-gel, fully H-bonded and not fully H-bonded. Further, it was shown through peak deconvolution that not fully H-bonded water is removed prior to fully H-bonded water over the course of a temperature increase, while no protein decomposition could be observed. This powerful analysis method, however, was limited by the selection of suitable samples and may require further refinement to be utilized to its full potential.

Lastly, it was shown that protein surface characteristics rather than protein size seem to play an important role in determining how different sol-gel compositions affect the thermostability of the entrapped biomolecule. Lysozyme and BSA, which both display a mixed surface hydrophobicity, showed similar preferential sol-gel compositions, i.e. higher PTMS content, for increased structural thermal stability. Lipase, on the other hand, which is similar in size to lysozyme, but displays patches of surface hydrophobicity, was most stable in pure TMOS sol-gels. It is recommended that these findings be verified by activity measurements.

5.5 References

[1] Drauz, K.; Waldmann, H. *Enzyme catalysis in organic synthesis*; Wiley-VCH: Weinheim, 2002.

[2] Jin, W.; Brennan, J. D. Properties and Applications of Proteins Encapsulated Within Sol-Gel Derived Materials. *Anal.Chim.Acta* **2002**, *461*, 1-36.

[3] Pierre, A. C. The Sol-Gel Encapsulation of Enzymes. *Biocatalysis and Biotransformation* **2004**, *22*, 145-170.

[4] Jürgen-Lohmann, D. L.; Legge, R. L. Immobilization of Bovine Catalase in Sol-Gels. *Enzyme Microb.Technol.* **2006**, *39*, 626-633.

[5] Clark, D. S. Can Immobilization Be Exploited to Modify Enzyme-Activity. *Trends in Biotechnology* **1994**, *12*, 439-443.

[6] Aucoin, M. G.; Erhardt, F. A.; Legge, R. L. Hyperactivation of Rhizomucor Miehei Lipase by Hydrophobic Xerogels. *Biotechnol.Bioeng.* **2004**, *85*, 647-655.

[7] Lakowicz, J. R. *Principles of fluorescence spectroscopy*; Kluwer Academic/Plenum: New York, 1999.

[8] Günzler, H.; Gremlich, H. U. *IR spectroscopy*; Wiley-VCH: Weinheim, 2002.

[9] Gremlich, H. U.; Yan, B. *Infrared and Raman spectroscopy of biological materials*; Marcel Dekker: New York, 2001.

[10] Bayly, J. G.; Kartha, V. B.; Stevens, W. H. The Absorption Spectra of Liquid Phase H_2O, HDO and D_2O From 0.7 Um to 10 Um. *Infrared Phys.* **1963**, *3*, 211-222.

[11] Liu, Y. L.; Cho, R. K.; Sakurai, K.; Miura, T.; Ozaki, Y. Studies on Spectra-Structure Correlations in Near-Infrared Spectra of Proteins and Polypeptides .1. A Marker Band for Hydrogen-Bonds. *Appl.Spectrosc.* **1994**, *48*, 1249-1254.

[12] Zaks, A.; Klibanov, A. M. The Effect of Water on Enzyme Action in Organic Media. *J.Biol.Chem.* **1988**, *263*, 8017-8021.

[13] Clifford, J. S.; Legge, R. L. Use of Water to Evaluate Hydrophobicity of Organically-Modified Xerogel Enzyme Supports. *Biotechnol.Bioeng.* **2005**, *92*, 231-237.

[14] Goring, G. L. G.; Brennan, J. D. Fluorescence and Physical Characterization of Sol-Gel-Derived Nanocomposite Films Suitable for the Entrapment of Biomolecules. *J.Mater.Chem.* **2002**, *12*, 3400-3406.

[15] Gulcev, M. D.; Goring, G. L. G.; Rakic, M.; Brennan, J. D. Reagentless PH-Based Biosensing Using a Fluorescently-Labelled Dextran Co-Entrapped With a Hydrolytic Enzyme in Sol-Gel Derived Nanocomposite Films. *Anal.Chim.Acta* **2002**, *457*, 47-59.

[16] Noda, I. 2-Dimensional Infrared (2D Ir) Spectroscopy - Theory and Applications. *Appl.Spectrosc.* **1990**, *44*, 550-561.

[17] Noda, I.; Dowrey, A. E.; Marcott, C. Recent Developments in 2-Dimensional Infrared (2D-Ir) Correlation Spectroscopy. *Appl.Spectrosc.* **1993**, *47*, 1317-1323.

[18] Noda, I. Progress in Two-Dimensional (2D) Correlation Spectroscopy. *J.Mol.Struct.* **2006**, *799*, 2-15.

[19] Pechkova, E.; Innocenzi, P.; Malfatti, L.; Kidchob, T.; Gaspa, L.; Nicolini, C. Thermal Stability of Lysozyme Langmuir-Schaefer Films by FTIR Spectroscopy. *Langmuir* **2007**, *23*, 1147-1151.

[20] Young, J. F. Humidity Control in Laboratory Using Salt Solutions - A Review. *Journal of Applied Chemistry of the Ussr* **1967**, *17*, 241-&.

[21] Lu, X. M.; Figueroa, A.; Karger, B. L. Intrinsic Fluorescence and Hplc Measurement of the Surface Dynamics of Lysozyme Adsorbed on Hydrophobic Silica. *J.Am.Chem.Soc.* **1988**, *110*, 1978-1979.

[22] Gill, I.; Ballesteros, A. Bioencapsulation Within Synthetic Polymers (Part 1): Sol-Gel Encapsulated Biologicals. *Trends in Biotechnology* **2000**, *18*, 282-296.

[23] Verger, R. 'Interfacial Activation' of Lipases: Facts and Artifacts. *Trends in Biotechnology* **1997**, *15*, 32-38.

[24] Koolman, J.; Roehm, K. Gewebe und Organe; In *Taschenatlas der Biochemie*; Thieme: Stuttgart, 1998.

[25] Eftink, M. R. The Use of Fluorescence Methods to Monitor Unfolding Transitions in Proteins. *Biophys.J.* **1994**, *66*, 482-501.

[26] Ulbrich, R.; Schellenberger, A.; Damerau, W. Studies on the Thermal Inactivation of Immobilized Enzymes. *Biotechnol.Bioeng.* **1986**, *28*, 511-522.

[27] Fersht, A. Protein Stability; In *Structure and Mechanism in Protein Science*; W. H. Freeman and Company: 1999; pp 508-539.

[28] Luft, M.; Boese, M. Untersuchung der Protein-Konformation mit FTIR. *Biospektrum* **2004**, *10*, 341-342.

[29] www.proteinexplorer.org. Protein Explorer. 2007.

Chapter 6
Overall Conclusion and Recommendations

The objective of this work was to use non invasive spectroscopic techniques to gain a better understanding of the phenomena governing the immobilization of proteins in sol-gels. In order to achieve this, several model proteins were selected and immobilized in sol-gel thin films of different compositions using a thin film technique that was amenable to various spectroscopic techniques.

The enzyme hydroperoxide lyase (HPL), which was intended to serve as a model for sol-gel immobilization, was characterized with regards to its activity under aqueous and micro-aqueous conditions in Chapter 2. A better understanding of the factors which modulate HPL activity was garnered by using novel reaction media and substrates. HPL activities under micro-aqueous conditions and with the novel substrate LS-OOH were described for the first time. The effect of salt, surfactant, solvent and substrate on HPL activity was assessed by means of experimental design. It was found that HPL activity is maximal at high salt and low surfactant concentrations under aqueous conditions with LA-OOH as a substrate. Furthermore, an influence of the surfactant Triton X-100 on solubility properties of the system and resulting HPL activity were identified. The interaction of different effects was found to be significant and the complexity of the investigated effects, were revealed through the use of experimental design.

A methodology for spin coating of sol-gel thin films and subsequent analysis by FTIR microscopy was described in Chapter 3. The chemical mapping procedure introduced offers a noninvasive way of mapping concentrations of proteinaceous substances and organically modified monomers *in situ* with spatial resolution. This methodology was applied to a set of three model proteins (lysozyme, lipase and BSA) immobilized in a range of sol-gel compositions (0 - 50 % PTMS content) in Chapter 4. It was found that the frequency distribution of lysozyme, lipase and BSA followed a normal Gaussian distribution in most cases. The spatial distribution characteristics of the model proteins in different immobilization matrices, however, differed depending on the nature of the protein and the sol-gel composition. These differences could be in part attributed to the surface characteristics of the model proteins. Additionally, an interaction of PTMS and lipase during the formation of the sol-gel is possible, as a positive correlation of

the positional information for the hydrophobic residues in the sol-gel thin films with lipase concentration was observed. On the other hand, a negative or no correlation between localized PTMS content and protein concentration could be observed for lysozyme and BSA. Moreover, implications on the changes in structure of the three model proteins in areas of high concentration, and in connection with PTMS content of the sol-gel, could be identified.

Fluorescence spectroscopy showed that the varying hydrophobicity of different sol-gel compositions has a direct effect on the entrapped biomolecules (Chapter 5). The three model proteins examined, lysozyme, lipase and BSA, were affected to varying degrees by the composition of the entrapment matrix. Fluorescence spectroscopy confirmed previous findings regarding the hydrophobicity/water content of sol-gel bulk material and were found to be qualitatively similar based on sol-gel composition to thin films. Higher PTMS content in a sol-gel thin film resulted in a reduction in TRP fluorescence quenching through a reduction in available water. Additionally, the application of 2D FTIR spectroscopy provided insight into the chemical complexity of a doped sol-gel system. It was found that predominantly two species of water are present in the sol-gel, fully H-bonded and not fully H-bonded. It was shown through peak deconvolution that not fully H-bonded water is removed prior to fully H-bonded water over the course of a temperature increase, while no protein decomposition could be observed. It was also shown that protein surface characteristics rather than protein size appear to play an important role in determining how different sol-gel compositions affect the thermostability of the entrapped biomolecule. Lysozyme and BSA, which both display a mixed surface hydrophobicity, showed similar preferential sol-gel compositions, i.e. higher PTMS content, for increased structural thermal stability. Lipase, on the other hand, which is similar in size to lysozyme, but displays patches of surface hydrophobicity, was most stable in pure TMOS sol-gels.

The work presented here clearly shows the usefulness of non-invasive *in situ* spectroscopic characterization to explain the complex phenomena governing sol-gel bioimmobilization. The techniques that have been developed can help to identify problems in protein immobilization systems, facilitate the design of immobilization supports that are tailor made for a specific application and, ultimately aid in the generation of better biocatalysts.

Recommendations for future work:

1. Development of a suitable immobilization support for HPL: If sol-gels are chosen, an interesting route could be the use of glycerol substituted precursors that have been demonstrated to provide an even more biocompatible support. Alternatively, the pre-entrapment of HPL in, e.g. a lipid bilayer structure, prior to a more rigid immobilization could be investigated.

2. Correlation with activity measurements: In the case of lysozyme and lipase, the activity of sol-gel thin film immobilized enzymes should be characterized. The composition dependent activity could then be compared to distribution, structure and stability. The activity of thin films should be compared to bulk sol-gel material to investigate the potential advantages of a reduction in internal mass transfer resistance through diffusion path length reduction.

3. Assessment of diffusion through sol-gel thin films: The spatial resolution provided by FTIR microscopy in combination with time dependent measurements could be used to determine the matrix composition dependent diffusion of tracer substances through sol-gel thin films. Tracer substances could be chosen to mimic enzymatic substrates. The results of these studies could help to identify problems associated with substrate/product/matrix interactions and aid in the improvement of sol-gel support materials.

4. *In situ* monitoring of immobilized enzyme activity: The advantage of *in situ* spectroscopic characterization of immobilized enzymes could be used to measure the activity of these enzymes directly. A suitable system would have to provide a substrate and/or product that can be easily identified and quantified by FTIR. A process can be envisioned, where the complete reaction of an immobilized enzyme, from the diffusion of the substrate through the matrix to the turnover at the active site to the diffusion of the product back into the bulk solution could be monitored and characterized.

5. Transfer of sol-gel thin film characterization to other spectroscopic techniques: The optical transparency of sol-gel thin films could allow for an easy transition of the methodologies described here to other spectroscopic techniques, such as fluorescence microscopy or circular dichroism. The additional information available through these techniques could confirm the findings described here and add new insights to the understanding of sol-gel immobilized protein systems.

Appendices

Appendix A

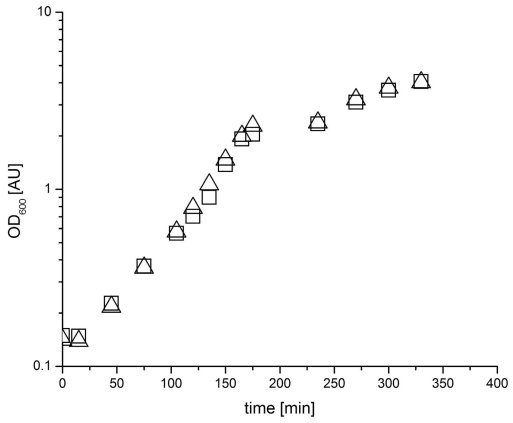

Fig. 51: Growth Curve for E. coli M15

The growth curve for cultures grown at 37 °C and 280 rpm. Logarithmic growth occurs between 50 and 200 min for M15 *E. coli* transformed with 9-HPL (Δ) and 13-HPL (□).

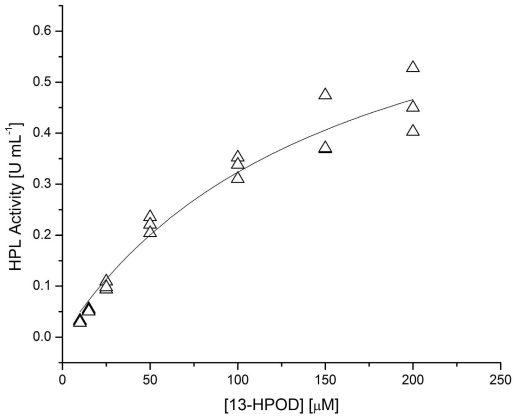

Fig. 52: Kinetics of 13-HPL

The diagram shows the dependence of 13-HPL activity on substrate concentration (Δ) determined by triplicate analysis. The solid line represents a non-linear regression according to the Michaelis Menten model. Non linear regression yields a K_M value of 160 ± 36 μM and v_{max} = 0.83 ± 0.1 U mL^{-1}. 1 U being the amount of enzyme reducing the absorbance at 234 nm for 0.1 AU in 1 min.

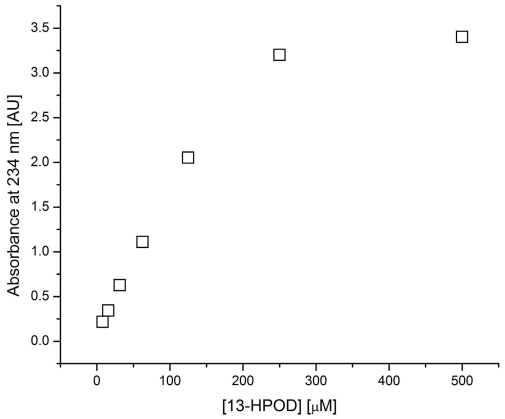

Fig. 53: Linearity of Absorbance of LA-OOH

The figure illustrates the relationship between LA-OOH concentration and absorbance at 234 nm. The linear range extends to a concentration of about 200 μM.

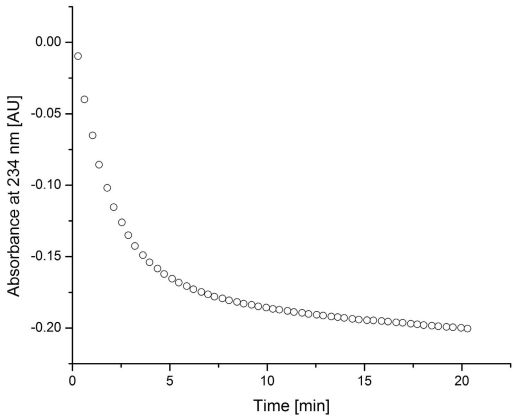

Fig. 54: LS-OOH Activity of 13-HPL

The figure shows the time course of absorbance at 234 nm.

Table 10: Activity Data HPL Aqueous Conditions

Standard Order	Run Order	Surfactant [%]	Salt [M]	Substrate	Activity [μmol min^{-1} mg^{-1}]
3	1	0	0	COOH	3.487805
18	2	0.01	0	SO4	1.317073
21	3	0	1.5	SO4	3.47561
12	4	0.01	1.5	COOH	4.018293
11	5	0.01	1.5	COOH	5.640244
10	6	0.01	1.5	COOH	6.853659
9	7	0	1.5	COOH	3.695122
8	8	0	1.5	COOH	8.932927
23	9	0.01	1.5	SO4	2.920732
2	10	0	0	COOH	3.564024
7	11	0	1.5	COOH	8.731707
14	12	0	0	SO4	1.030488
16	13	0.01	0	SO4	1.237805
6	14	0.01	0	COOH	7.597561
26	15	0.005	0.75	SO4	2.042683
1	16	0	0	COOH	3.335366
28	17	0.005	0.75	SO4	2.170732
22	18	0.01	1.5	SO4	2.847561
15	19	0	0	SO4	1.012195
27	20	0.005	0.75	COOH	6.841463
20	21	0	1.5	SO4	3.810976
4	22	0.01	0	COOH	7.384146
19	23	0	1.5	SO4	3.865854
5	24	0.01	0	COOH	7.390244
17	25	0.01	0	SO4	1.140244
25	26	0.005	0.75	COOH	6.841463
13	27	0	0	SO4	0.926829
24	28	0.01	1.5	SO4	2.853659

Standard order is the order laid out by the experimental design; run order is the order in which the experiments were performed; COOH: linoleic acid hydroperoxide; SO4: linoleyl sulfate hydroperoxide.

Table 11: Activity Data HPL Micro-Aqueous Conditions

Standard Order	Run Order	Surfactant [%]	Salt [M]	Substrate	Activity [μmol min^{-1} mg^{-1}]
27	1	0.005	0.75	COOH	0.560976
17	2	0.01	0	SO4	2.006098
16	3	0.01	0	SO4	2.463415
15	4	0	0	SO4	0.670732
22	5	0.01	1.5	SO4	1.865854
8	6	0	1.5	COOH	0.146341
21	7	0	1.5	SO4	0.628049
26	8	0.005	0.75	SO4	1.45122
2	9	0	0	COOH	0.481707
9	10	0	1.5	COOH	0.195122
28	11	0.005	0.75	SO4	1.365854
1	12	0	0	COOH	0.378049
20	13	0	1.5	SO4	0.634146
25	14	0.005	0.75	COOH	0.567073
4	15	0.01	0	COOH	1.243902
10	16	0.01	1.5	COOH	0.676829
6	17	0.01	0	COOH	0.945122
12	18	0.01	1.5	COOH	0.689024
24	19	0.01	1.5	SO4	2.628049
19	20	0	1.5	SO4	0.579268
23	21	0.01	1.5	SO4	2.841463
3	22	0	0	COOH	0.408537
14	23	0	0	SO4	0.609756
11	24	0.01	1.5	COOH	0.963415
18	25	0.01	0	SO4	1.884146
5	26	0.01	0	COOH	1.262195
7	27	0	1.5	COOH	0.231707
13	28	0	0	SO4	0.609756

Standard order is the order laid out by the experimental design; run order is the order in which the experiments were performed; COOH: linoleic acid hydroperoxide; SO4: linoleyl sulfate hydroperoxide.

Appendix B

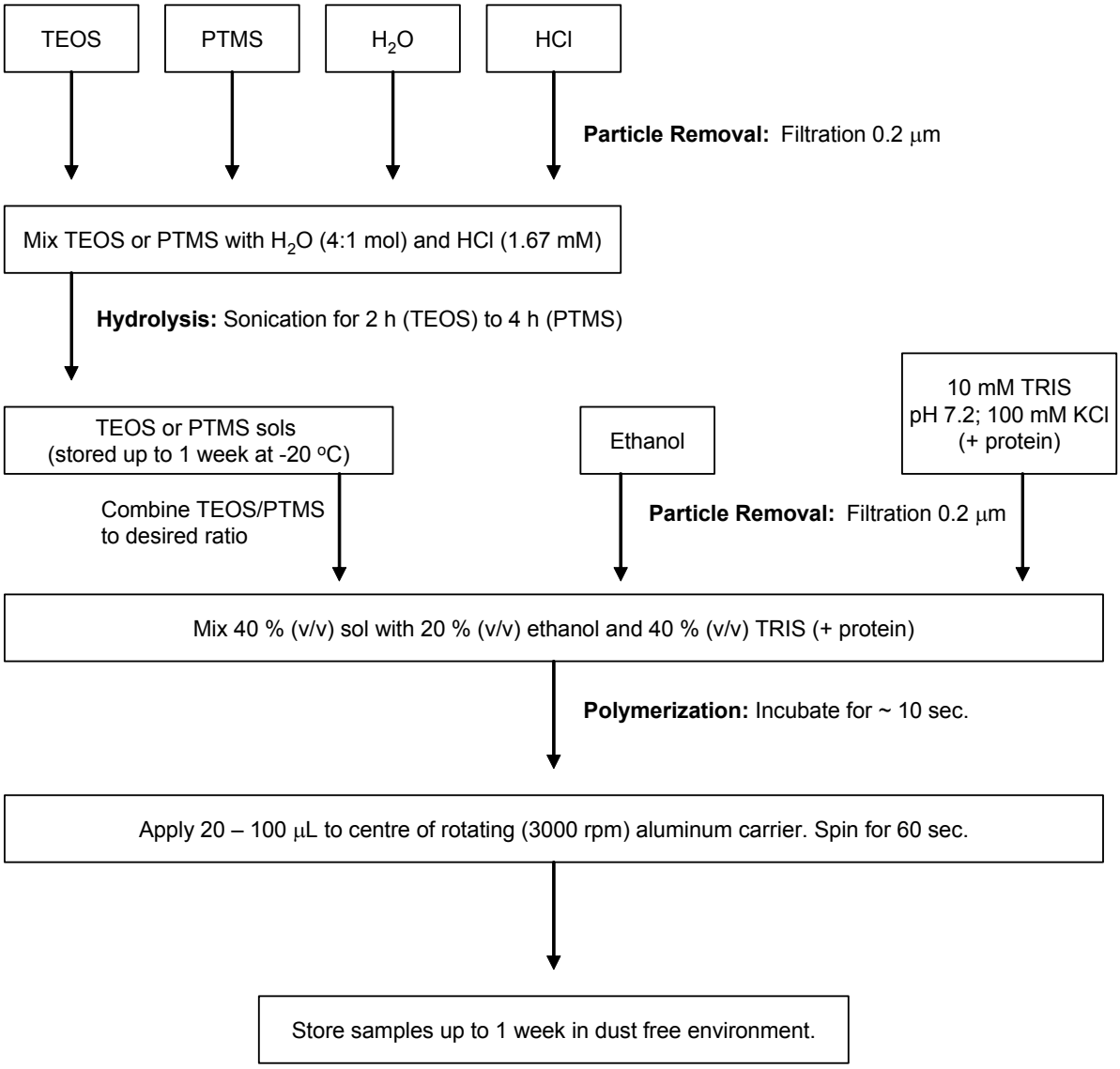

Fig. 55: Flowchart for Sol-gel Thin Film Spin Coating Process

Experimental Details on Spin Coating Process:

It should be noted that the nature of the spin coating process requires specific attention to experimental details to ensure thin film quality as well as reproducibility of the results.

- A dust free environment is necessary to produce high quality films. Also, all tubes, pipette tips, etc. should be dust free.
- Practical working volumes for the coating solution are 40 μL sol, 20 μL of ethanol, and 40 μL of buffer (+ protein). The components should be mixed in a microcentrifuge tube (1.5 mL) using a 100 μL pipette. Mixing should not take longer than 10 sec to avoid gelation before the coating process is started.
- 20-100 μL of coating solution should be applied for a carrier of 1 cm^2 size.
- FTIR analysis should be carried out in the center region of the carrier to avoid the influence of end effects.

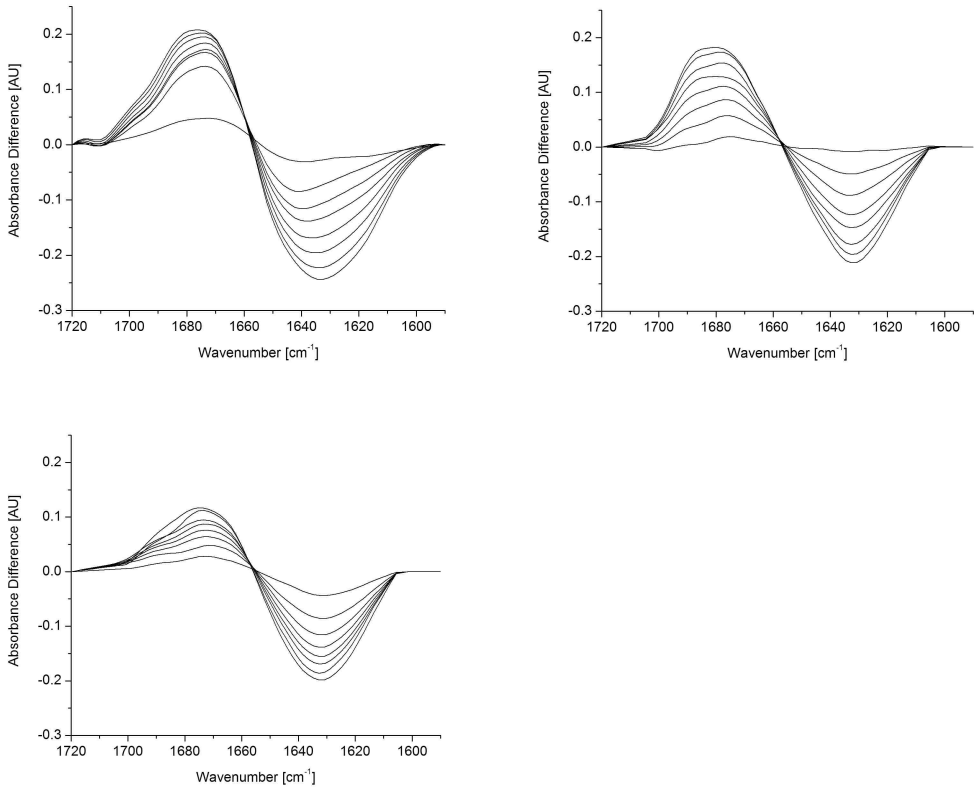

Fig. 56: Lysozyme Amide I Absorbance Difference Spectra

The spectra represent the difference between the recorded signal for 30 °C and 40, 50, 60, 70, 80, 90, 100, 110 °C respectively. With increasing temperature, an increase in the difference at 1680 cm^{-1} can be observed, while the difference at 1640 cm^{-1} is decreasing. The spectra were recorded for lysozyme 0 % (top left), 25 % (top right) and 50 % (bottom) PTMS sol-gel thin films.

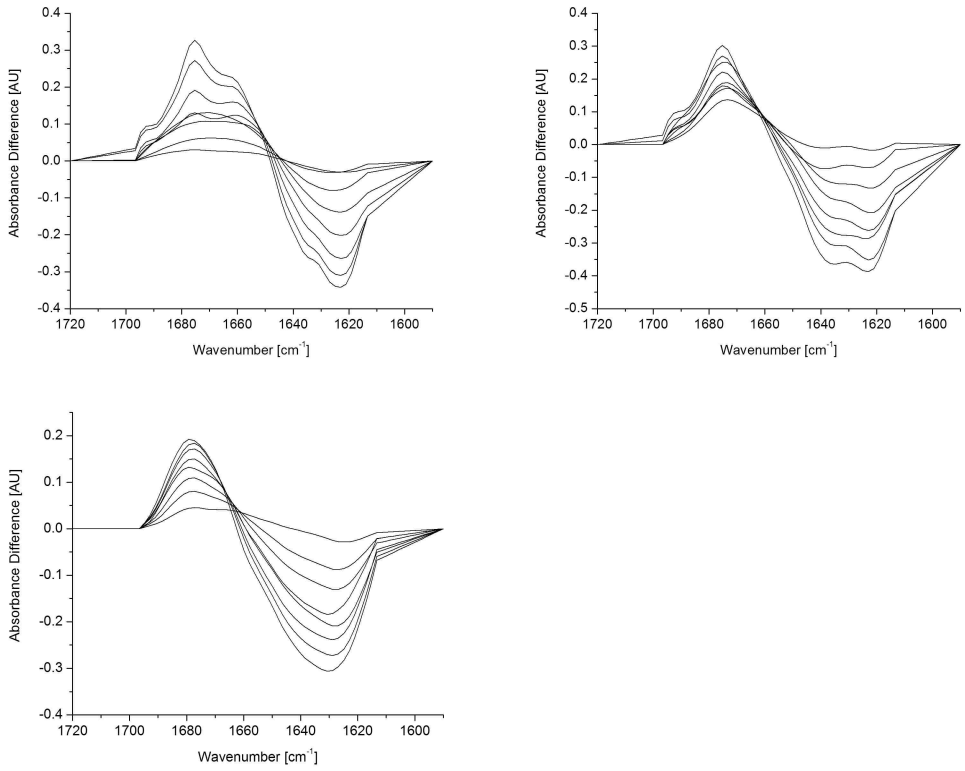

Fig. 57: Lipase Amide I Absorbance Difference Spectra

The spectra represent the difference between the recorded signal for 30 °C and 40, 50, 60, 70, 80, 90, 100, 110 °C respectively. With increasing temperature, an increase in the difference at 1680 cm^{-1} can be observed, while the difference at 1640 cm^{-1} is decreasing. The spectra were recorded for lipase 0 % (top left), 25 % (top right) and 50 % (bottom) PTMS sol-gel thin films.

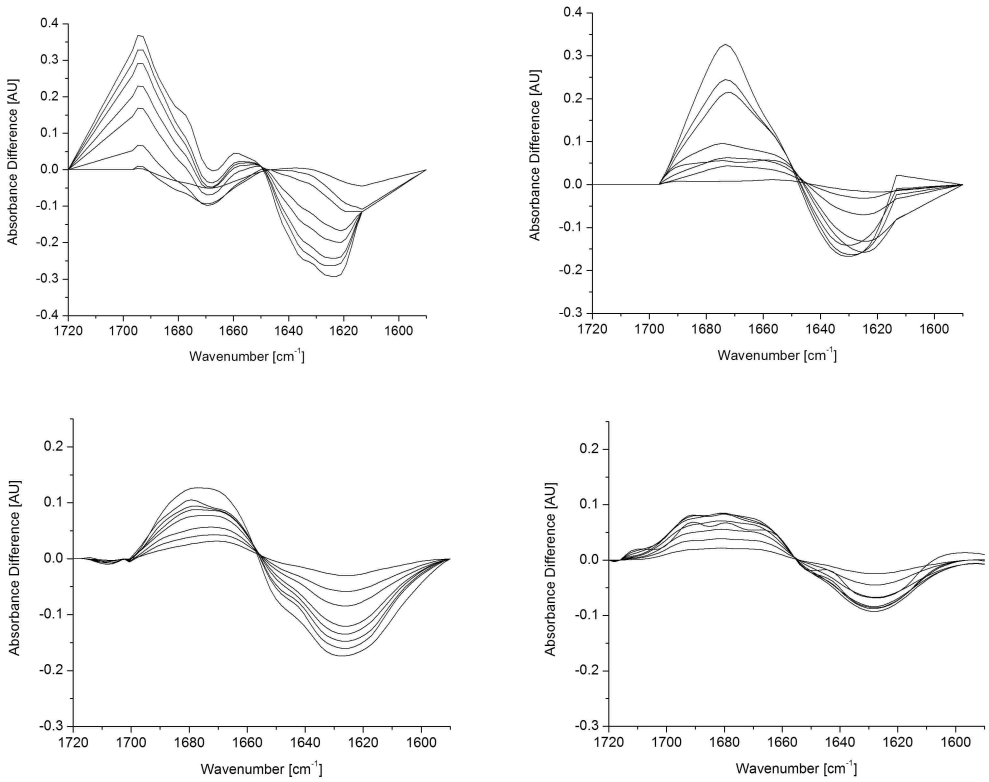

Fig. 58: BSA Amide I Absorbance Difference Spectra

The spectra represent the difference between the recorded signal for 30 °C and 40, 50, 60, 70, 80, 90, 100, 110 °C respectively. With increasing temperature, an increase in the difference at 1680 cm^{-1} can be observed, while the difference at 1640 cm^{-1} is decreasing. The spectra were recorded for BSA 0 % (top left), 10 % (top right) 25 % (bottom left) and 50 % (bottom right) PTMS sol-gel thin films.